PROCESS AND PRODUCT UNDERSTANDING OF RAPID AND CONTINUOUS WET GRANULATION

by Carlota Méndez Torrecillas

A thesis in fulfilment of the requirements for the degree of

Doctor of Philosophy

Strathclyde Institute of Pharmacy and Biomedical Sciences

University of Strathclyde, Glasgow

October, 2018

Declaration of authenticity and Author's rights ‘

This thesis is the result of the author’s original research. It has been composed by the author and has not been previously submitted for examination which has led to the award of a degree.’

Signed: Date:

A mis padres

Abstract

Wet granulation is a common industrial operation for particle size enlargement, which traditionally has been performed in batch-based operations. However, the potential advantages of continuous granulation such as improved quality, rapid API sparing development and greater flexibility have drawn attention to this technology.

One of the common equipment evaluated to perform continuous granulation is the twin-screw granulator (TSG). The advantage of this equipment is the flexibility offered from the high number of possible working environments achieved by changing different sections of the screw assembly, different segment geometries or feed port locations. However, the current state of art of this technology does not yet allow the implementation into the pharmaceutical process. The introduction of this technology requires an increased knowledge of the granules properties as well as the acceptable working limits of the TSG equipment. In this thesis, both issues have been addressed. On one side, a homogeneity factor to transform particle size distributions in a percentage easing the creation of design workspaces was developed. Also, the verification of the channel fill methodology to an 11 mm twin screw granulator and its relationship with another

process parameters was explored. Furthermore, a method to use microencapsulated sensors (CAMES) whose rupture is directly dependant on their experienced shear stress was developed for first time for TSG. On the other side, an algorithm to extract selected parts from inside the granule was developed and applied to granules obtained by both batch and continuous. In addition, the effect of the liquid availability and drying effect in the formation of granules was studied obtaining significant morphological differences depending on the temperature. Furthermore, it was found that nuclei obtained a different liquid to solid ratio were similar in size but different in number which suggest that the granules size is directly dependant on the liquid availability.

Acknowledgements

This PhD has been a long journey that fortunately I didn't make alone. I am so grateful to all the people who have helped me in a way or another to complete it. First of all, I want to thank both of my supervisors: Prof. Gavin Halbert and Dr. Dimitrios Lamprou. I am so pleased to have worked with both of them. They always helped me to "go for it" meanwhile they gave me the freedom and confidence necessary to finish this PhD. Also more a friend than a supervisor, I want to thank to Dr. Robertson for being a daily support in every aspect with our coffee gatherings.

A very special thanks to Dr. Thomas McGlone who is not only the best lab manager I had the opportunity to work with, he is also a great friend. I also want to thank to Dr. Deborah Bowering, Dr. Tariq Islam and Dr. Elke Prassad for always having a smile when they provided me training and support. I cannot forget to thank two of my PhD fellows: Fred Doerr and Lauren Connor who performed the NanoCT and STA analysis and with whom I really enjoyed to work with. Also, Bilal Ahmed for proofreading my work and avoid my Spanglish. In the computational part, I would like to thank Dr. Javier Cardona and Dr. Tony Vassileiou for helping me to go a step further with my codes and even more important for being great friends. A very special gratitude goes out to all down at CMAC for helping and providing the funding for my work. Also, I would like to thank R&D Platform Technology & Science GSK group in Ware and

especially to Richard Elks and Lee Gorringe for the opportunity of working with them during my placement.

Less related to my work but essential to my PhD journey, I want to thank my full coffee team: Alice, Arabella, Bruce and SJ with occasional appearances of Antonia and Mike. You have been my main reason to make it at a reasonable hour in the morning. Also, I am very happy to be part of the "Friday pints group" because in many ways you have made all these years full of crazy fun and good conversations. A special remark goes for three of my favourite drama people: Carla, Georgia and Scott.

There are some people who supported me all the way here. First of all, I want to thank my friends from Santiago (Lu, Ade, Quinte, Roi, Colo, Dibua, Mac y Lara). I hope we keep meeting for many years to come. Also, my friends from Allariz (Lore, Brais, Pau and Manza) who always 'confian' even if when I don't do it. A special remark goes to Maro and Vado who have been one of my main constant supports during this PhD never mind the 2500 km in the middle. Special mention to Rosa, my chemistry teacher who was the first one to introduce me her love for science.

And finally, last by no means least, to my family and especially to my parents who have been always a source of inspiration, love and support. I doubt you can be luckier than to be raised in a home so full of laughter and joy. I am quite certain I owe you any achievement I make, *os quiero muchisimo*. Also, to my *primi* who is more a sister than a cousin. Finally to Paul, who is the one who gave me the biggest encouragement in this PhD and to be fair, in my life in general, you are okay+, Polpol.

Table of contents

List of figures

List of tables

List of symbols

A_0	Area corresponding to the equivalent minimum homogeneity of PSD
A_{100}	Area corresponding to the equivalent maximum homogeneity of PSD
A_{PSD}	Area corresponding to the PSD
B%	Percentage of broken sensors
C_c	Final concentration of the solution
C_{eq}	Standardised concentration
C_i	Initial concentration
$C_{100\%}$	100% rupture of sensors concentration.
C_{stock}	Concentration of the stock solution
CAMES	Calibrated Microencapsulated sensors
CLAHE	Contrast-limited adaptive histogram equalization
CT	X-ray computerised tomography
D	Tablet diameter

d	Diameter
d_x	Intercept x of the cumulative volume
DoE	Design of experiments
DSC	Differential Scanning Calorimetry
EQPC	Equivalent diameter of a circle of equal projection area
F	Powder feedrate (kg/hr)
$F_{applied}$	Applied load
FH	Homogeneity factor
HSWG	High Shear Wet Granulator
k_1	Sorting factor parameter
k_2	Sorting factor parameter
L/D	Length to Diameter ratio
L/S	Liquid/Solid ratio
m_i	Sample mass (g)
$\dot{m}$	Powder flowrate
n	Number of repetitions

N	Screws velocity.
n_{interv}	Number of intervals
n_v	Volumetric efficiency of the conveyor
μ	Mean value
p	Percentage of the value of the population
PSD	Particle Size Distribution
QbD	Quality by Design
q_x	Density distribution
Q_x	Cumulative distribution
R2	Coefficient of determination
s	Sorting factor
SME	Specific Mechanical Energy
T	Torque
T_{tablet}	Tablet thickness.
$\Delta\Phi$	Difference of channel fill
Φ	Channel fill fraction

σ	Tensile stress of the tablet
σ_{CAMES}	Shear stress calculated for calibrated microencapsulated sensors
TSG	Twin-Screw Granulator
UV	Ultraviolet
V_c	Volume of the solution
V_F	Conveyor free volume
V_i	Sample volume (ml)
V_{stock}	Volume required of the stock solution
VMD	Volume mean diameter
w(d)	Weight distribution
w_{PSD}	Weight distribution corresponding to the particle size distribution
w_0	Weight distribution corresponding to the equivalent minimum homogeneity of PSD
w_{100}	Weight distribution corresponding to the equivalent maximum homogeneity of PSD
xm	Particle size
xm_0	Particle size of the first value

xm_{max}	Particle size of the maximum peak

Chapter 1

Introduction

Implementing new technologies in industry is always a challenging goal which offers a great opportunity but brings major challenges. Introducing continuous granulation in the pharmaceutical industry is no exception. It requires a common effort between industry and academia to be able to develop a feasible and well-understood process. The motivation of this thesis was to contribute to a certain extent part to this mutual effort.

The thesis was structured in five chapters although they could be seen as three main parts. In the first part and chapter, a literature review introducing gran-

ulation and some of the most interesting research performed to date was included. In the second part (chapters 3 and 4), two new computational techniques were developed. The first one involves a new technique to measure the homogeneity of particle size distributions. The aim behind this metrology was to be able to design workspaces and use it as starting point in the design of experiments. The second technique was an algorithm which is able to analyse the internal core of the granules and analyse the granule via the individual constituent pieces. Both techniques were used in different ways in the third part which involves a more detailed experimental look to twin screw granulation. In the fifth chapter, the effect of static drying was used to compare what happens to the granule depending of the liquid availability to form the solid bridges inside the granules. Furthermore, the sixth chapter studies the internal forces that the powder experiences inside a granulator as well as offering a global view of the equipment.

To sum up, the thesis has increased the knowledge of less studied topics in granulation in order to help in the feasibility of introducing TSG in the pharmaceutical process.

Chapter 2

Literature review

2.1 Continuous wet granulation in pharmaceutical process

Many products in everyday life in a wide range of industries are initially produced in powder and small hard particle form. However, their down-stream processing is limited due to fine powders, which do not flow uniformly, producing products without uniform dispersion in content and quality. In addition, fine powders complicate significantly the subsequent operations required to deliver the products to the market since they could lack content uniformity and segre-

gate (Parikh, 2009). Avoiding these issues has been overcome by industry increasing the size of these small particles through granulation. This predicament is especially sensitive for the pharmaceutical sector due to the liability of producing uniform and consistent products as required by the different pharmacopoeias (Litster et al., 2004, Miller, 1995, Nolte, 2010, Parikh, 2009).

The importance of the pharmaceutical sector is globally well-known, since it has contributed significantly to reducing mortality rates throughout the world, as well as increasing the quality of life and life expectancy of patients, especially during the last century. Consequently, the intrinsic goal of the pharmaceutical industry causes a conflict between the social and the industrial objectives of this sector. This results in a very complex market which is subject to many public interventions by government bodies which demand high quality standards. As such pharmaceutical companies are required to ensure the welfare of patients through cost-containment strategies at the same time as maintaining their own financial solvency with a high level of competitiveness and innovation (Jacobzone, 2000, Vervaet and Remon, 2005).

Unexpectedly, the current level of development and efficiency in production within the pharmaceutical sector is dramatically lower than other analogous processes. For instance, the capacity of a typical process at a chemical factory is

around 70 % of the theoretical maximum, which is significantly higher than that of the pharmaceutical industry that only reaches 30 % (Remington et al., 2006, Vervaet and Remon, 2005). This lack of efficiency leads to waste produced by lower yields as well as wastage of utilities such as water or energy, resulting in a direct environmental impact (Plumb, 2005, Taylor, 2015).

In the past decade, the pharmaceutical sector has focused on improving the synthesis routes for active pharmaceutical ingredients (API), however this has been detrimental to the rest of the production process as less attention has been applied to other areas. Observing the process, this is done in two principal stages, primary and secondary processing. From the first stage, the active ingredient is obtained and purified as figure 2.1 shows. However, after this stage, the active substance is not ready to be administered to the patient in an accurate dose and form. Hence, it should be processed further in the second stage to allow the drug to meet the required specifications. For instance, most new drugs require to increase their solubility or permeability before they can be administered orally (Saffoon et al., 2011). Furthermore, it was estimated that 40% of the new compounds of a pharmaceutical company have poor water solubility ($\leq$50 μg/mL)

and 30% have very poor water solubility (≤5 μg/mL) (Aungst, 2017). The industry costs for the second stage process are up to 40 % of the overall manufacturing costs (Nolte, 2010, Profiles, 1995).

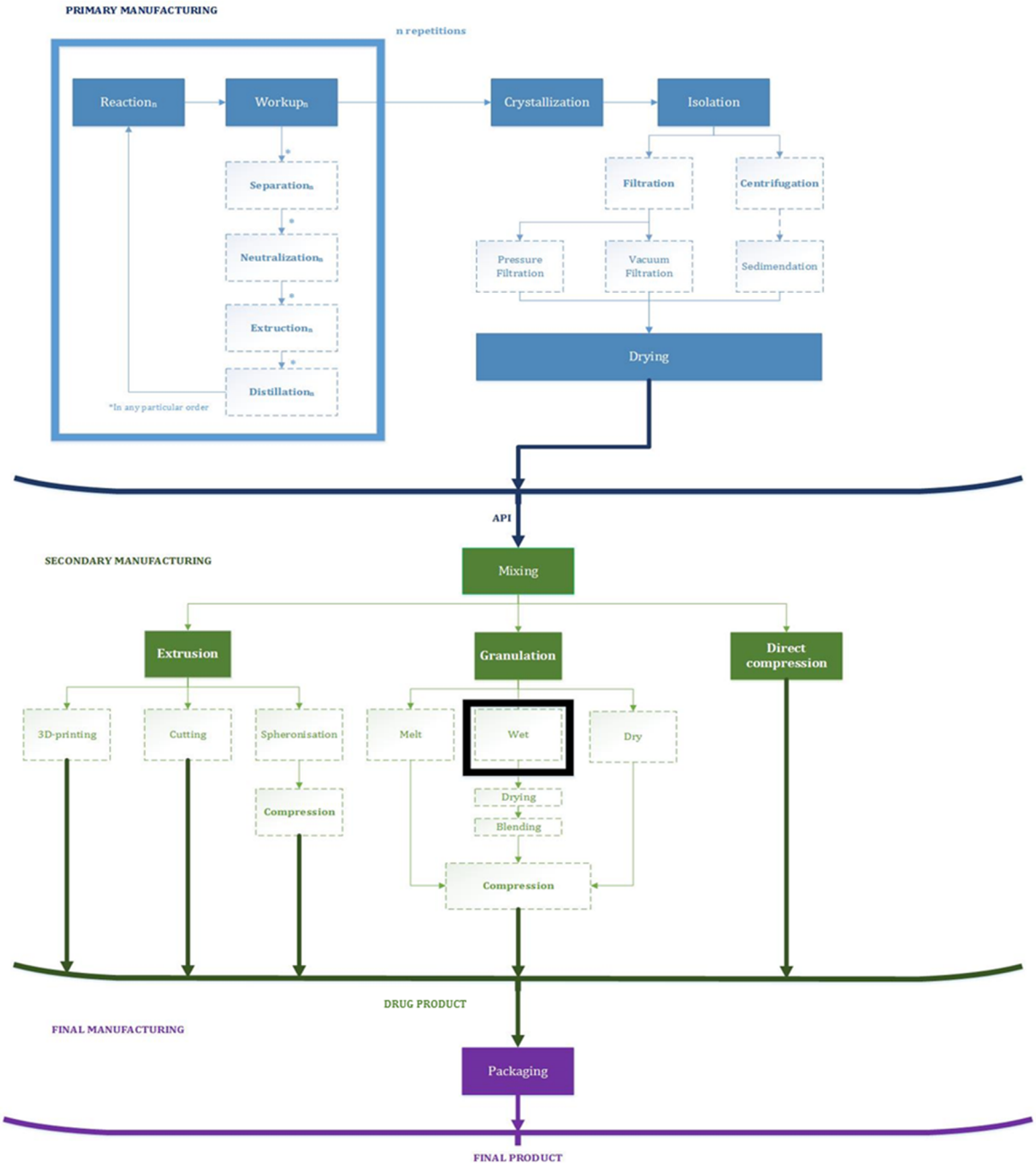

Figure 2.1 Typical process in the pharmaceutical industry. Adapted from "Continuous manufacturing of pharmaceuticals" (p. 6-7), (Kleinebudde et al., 2017).

One of the traditional strategies followed to innovate the manufacturing process is via the improvement of existing operations, and one of the suggestions is transformation of the traditional processes from batch into continuous. The possibility of reducing costs and the generation of novel processes and pathways have attracted the interest of academics and industrialists alike (Locke and Wellhausen, 2014, Mascia et al., 2013). The advantages of continuous processes are well-known in industry, from the economic side, the reduction of inventory, footprint or energy consumption, provides a lower cost of production and an increase of the sustainability of plants. From a security point of view, the continuous processing minimises the risks, increasing the process control and therefore, the potential exposition of the operator to hazardous agents. In addition, operating under continuous process has the potential of increasing the quality and the standardisation of the products (Plumb, 2005). Other great advantages offered by continuous processing is the introduction of the inline assessment of the products rather than the current analytical techniques which imply destruction of the sample analysed and which do not ensure a uniform product over time (Federsel, 2009, Jiménez-González et al., 2011, Mascia et al., 2013, Plumb, 2005). However, in the specific case of the pharmaceutical sector, the flexibility offered

by batch equipment can be an outstanding advantage. The biggest batch productions are around 1200 tonnes per year and the majority of products are in 100 – 1000 tonnes per year (Plumb, 2005) which does justify economy of scale. Also, the processes are liable to constant modifications due to changes in legislation, patent expiration or introducing into the market of newer effective drugs (Taylor, 2015). These factors could overshadow continuous processing due to its specific nature (Jiménez-González et al., 2011, Mascia et al., 2013). Within the pharmaceutical sector, that produces many concerns related to the lack of certainty that the continuous process will be delivering enough profit to compensate for the investment required and not all the operations would be liable to be transformed into a continuous process (Poechlauer et al., 2012). However, these concerns do not take into account some of the main problems associated with batch processes such as the difficulty to scale up production or manufacturing homogeneous products with lower quality than required (Plumb, 2005). Contrary to these issues, continuous process could offer a great flexibility in which a new output can be developed in a short period of time speeding up the supply chain and reducing floor space and investment costs up to 80% (Kleinebudde et al., 2017).

One of the operations that has been highlighted as a good candidate to improve the manufacturing process and its feasibility as a continuous operation is wet granulation (Kumar et al., 2017). Perry's Chemical Engineer's Handbook defines granulation as, "any process whereby small particles are gathered into larger, permanent masses in which the original particles can still be identified" (Perry, 1950). From this definition is obvious that the original particles do not suffer alterations which is an outstanding advantage due to the requirement of not modifying the original APIs. Furthermore, this operation shows many other advantages such as the reduction of the segregation of the blends, the porosity control and the improvement of the flow properties among others which can be seen in figure 2.2.

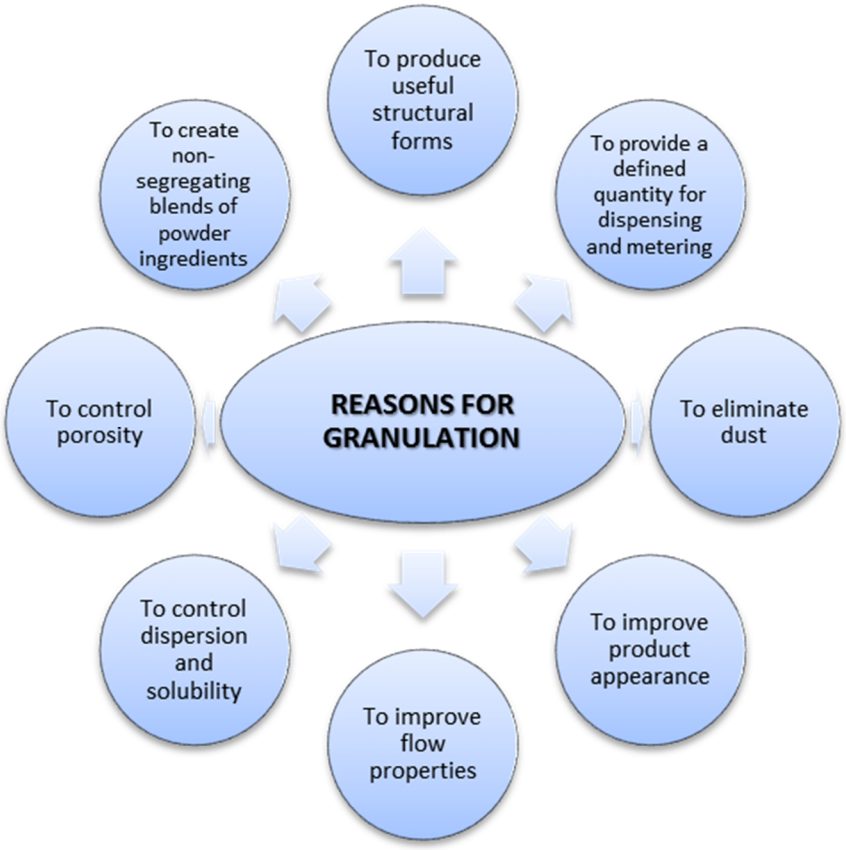

Figure 2.2 Reasons for granulation. Adapted from "The science and engineering of granulation processes" (p. 1), (Litster et al., 2004).

In addition, adequate equipment for granulation implies more flexibility in the need of new dosing and allows working with high value APIs which is more important than ever (Nolte, 2010).

Within granulation, there are two major methods to accomplish it based on if any liquid is used to bind the primary particles or not, which is called wet and dry granulation respectively (Parikh, 2005). Dry granulation has lower opera-

tional costs and easier methods of control than standard wet granulation methods and it is suitable for temperature sensitive or hydrolytically sensitive products (Korhonen, 2017). However, this process produces a higher amount of fines with lower flow properties (Šantl et al., 2011) and it cannot be used for low drug dosages or if precise tablet properties such as specific hardness or friability are required (Parikh, 2009). Wet granulation is applicable to a larger spectrum of drugs and it increases the probability of meeting the physical requirements for the production of suitable tablets downstream (Remington et al., 2006). However, this does not mean that wet granulation does not have some important disadvantages, for instance the benefit of content uniformity is not necessarily guaranteed for low dose drugs or there may be unwanted changes in the drug or excipients due to the added binder. Nevertheless, in many cases it is the only feasible way to granulate certain drugs (Durgin and Hanan, 2004). This process has been traditionally performed as a batch process although there are some specific examples where continuous granulation has been applied as a proof of concept of continuous manufacturing (Kleinebudde et al., 2017). This allowed to estimate that the transition from batch to continuous of wet granulation would reduce the amount of energy required from 14.0 kJ to 8 kJ per tablet (De Soete et al., 2013).

Although the transition from batch to continuous offers all the mentioned advantages, it has an important associated issue which is the lack of understanding of the theory behind the process. In this instance, batch granulation process doesn't waste material at the start and it offers a well-known mode of operation which does not require a wide knowledge of the mechanism. Contrary to batch, continuous which requires extensive knowledge to ensure robust and controlled state since shutdowns need to be minimised (Kleinebudde et al., 2017, Kumar et al., 2017, Leuenberger, 2001a, Leuenberger, 2001b, Wu et al., 2007).

2.2 Theory of wet granulation

The definition of granulation covers a wide range of techniques used to increase the size of the primary particles to a range from 100 µm to 20 mm. The majority of the granulation in the pharmaceutical sector has been done by wet granulation except in those cases where the nature and the drug's properties make dry methods feasible (Durgin and Hanan, 2004). However, the mechanisms and the underlying physics of wet granulation are still currently not completely understood and being actively researched. The associated problems to this lack of understanding is the difficulty to predict the behaviour of new formulations from their fundamental properties and the need of pilot scale experiments which frequently are not able to be reproduced in the large scale (Iveson et al., 2001).

Nevertheless, the understanding of wet granulation has had notable advances in the past twenty-five years since the macroscopic study of granulation was replaced by a microscopic study of the variables. This first study about the influence of the viscosity of the binder in the granulation highlighted the requirement to know the intrinsic nature of the process (Ennis et al., 1990). At that point, the previous traditional description of granulation was rejected and a modern approach was taken instead (Ennis and Litster, 1997). Figure 2.3 illustrates the change where the rate processes were: nucleation, coalescence, abrasion transfer, breakage, and snowballing (Sastry and Fuerstenau, 1973). In the traditional approach, the major contribution of the physical forces in the presence of a liquid which wets the particles, is due to the interfacial and capillary forces on the relative distribution and air phases in the porous agglomerate. It was remarked that the mechanical forces are required to bring the individual wetted particles in contact with one another, thereby producing the growth of the particles by coalescence. However, some of the results demonstrated that a deeper understanding was required since some phenomena could not be totally explained by this approach (Sastry and Fuerstenau, 1973). The next approach was based on three sets of rate processes and the possibility that they can occur simultaneously: wetting and nucleation, coalescence or growth, consolidation and attrition

and breakage (Iveson et al., 2001, Parikh, 2009). This theory is the most accepted one and it is considered the modern approach of wet granulation and therefore, the individual processes are explained in more detail in this section. However, with the introduction of continuous equipment, the lines of research started to consider a more fragmented study of the individual processes rather than a whole theory approach. In order to reproduce and model the full process, some authors had considered granulation as a set of possible jump events such as nucleation, particle collision (which may lead or not to coagulation and compaction), breakage and penetration (Braumann et al., 2010, Lee et al., 2015, McGuire et al., 2018). A schematic comparison of those approaches is presented in figure 2.3.

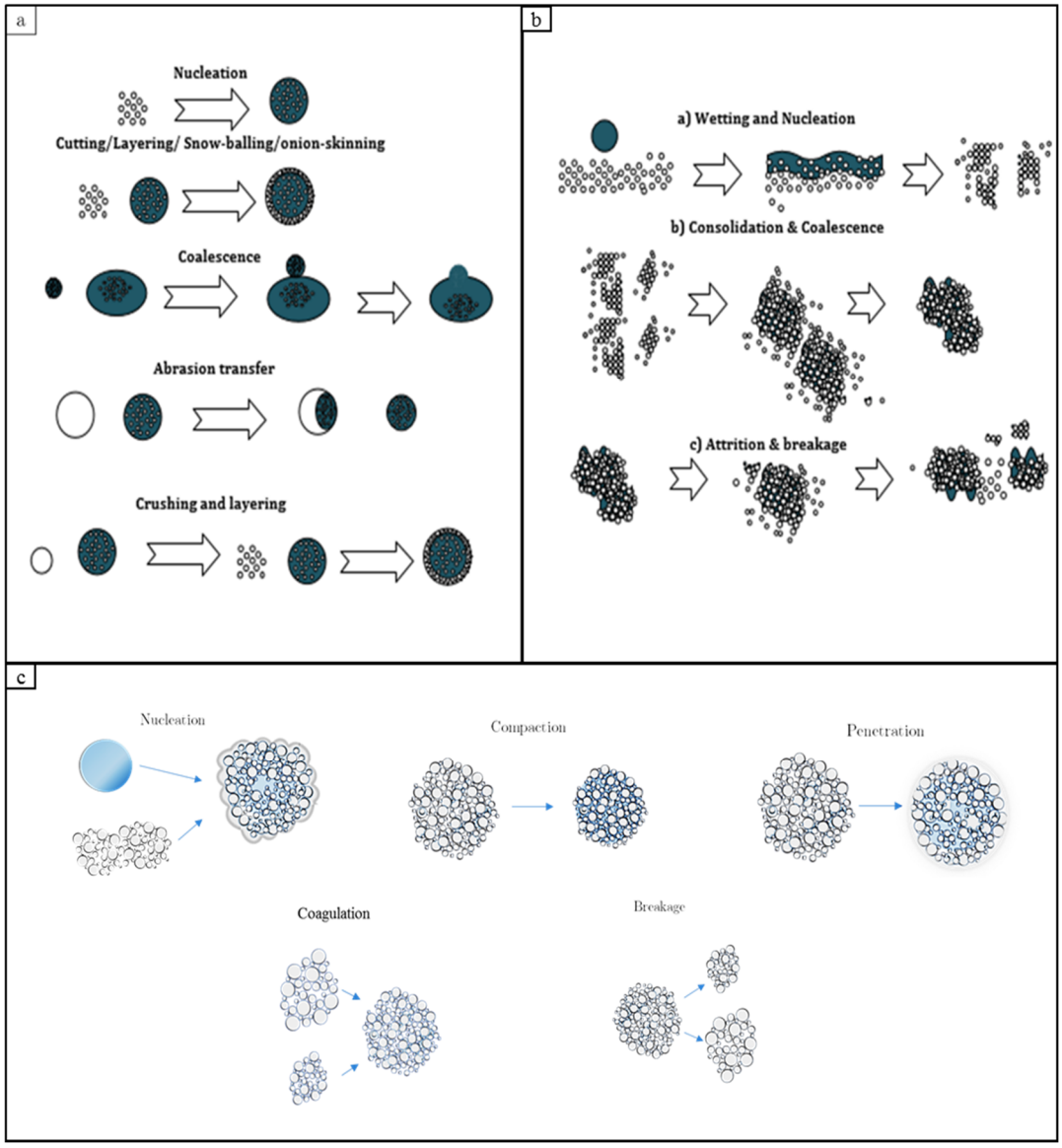

Figure 2.3 Rate processes on wet granulation: a) traditional adapted from "Mechanisms of agglomerate growth in green pelletization" (Sastry and Fuerstenau, 1973), b) modern approach adapted from "Nucleation, growth and breakage phenomena in agitated wet granulation processes: a review" (Iveson et al., 2001), c) and jump events adapted from "A high-dimensional, stochastic model for twin-screw granulation – Part 1: Model description" (McGuire et al., 2018).

2.2.1 Wetting and nucleation

In the first stage of wet granulation, the liquid is added to the powder and the initial contact takes place. Depending on the properties of both powder and liquid, the solid surface and the liquid drop will establish a contact angle which can be used to define the degree of wetting. This angle will be determined by the balance of the solid and liquid surface energies. The spreading will be favourable if the difference between the energy required to form a new interface between liquid and solid overcomes the energy required to destroy the individual interface of the material from itself.

Three types of spreading are possible depending on this relationship: creating a surface film where the liquid totally spreads, the solid adheres to the liquid (when solid movement is physically possible) and the solid-liquid interfacial area is minimised and the wetting does not occur (Aulton and Taylor, 2017, Hapgood, 2000). However, it has been reported extensively in literature that spreading is also function of the velocity and direction of both solid and liquid and therefore of the dynamic contact line between them (Blake and De Coninck, 2002, Dussan, 1979, Huh and Scriven, 1971). Yet there is still no agreement on how to integrate every aspect of dynamic wetting in a model (Cappelli et al., 2015). Furthermore, in some cases where the screws are not fully covered, liquid drops can strike the

surface of the screws before contact the powder. In those cases, the type of impact depends on their kinetic energy and drops can bounce, spread or splash (Figure 2.4) which could also change the contact surface between the liquid and the powder (Rein, 1993).

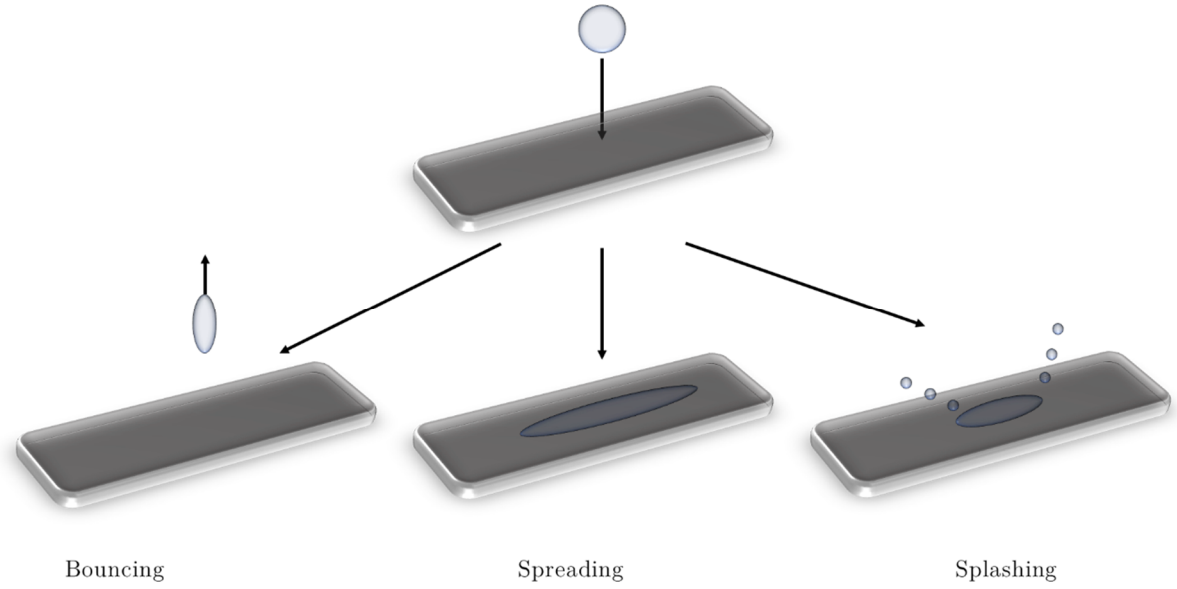

Figure 2.4 Impact of a drop on a solid surface (Rein, 1993)

Once the powder and liquid are in contact, the surface energy changes are directly related with the wetting. This changes can create three different scenarios for a non-porous cube solid: adhesional, immersional and spreading. When the particles are real with irregular surfaces and internal pores, the three stages are essentially the same, however the immersion is substituted for penetration. Liquid penetration in powder pores is driven by the capillary pressure difference and resisted by the fluid viscosity. The capillary pressure increases as the pore size

decreases allowing the liquid to penetrate further into a powder bed and creating a stronger liquid bridge (Iveson et al., 2001).

The liquid bridge is a critical parameter on granulation and even defines the nuclei morphology. Furthermore, the liquid bonding between particles can acquire different configurations depending on the amount of liquid as it can be seen in figure 2.5 (Parikh, 2009, Rhodes, 2013).

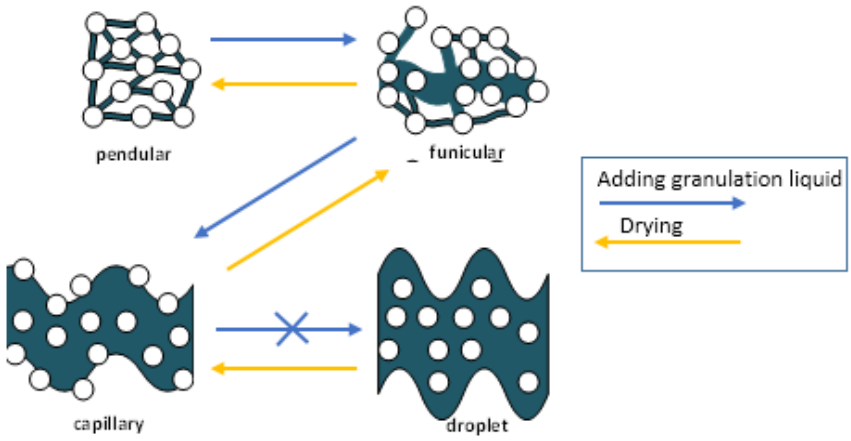

Figure 2.5 Liquid bonding between particles, adapted from "Introduction to particle technology" (section 13.2.3), (Rhodes, 2013)

The type and strength of the bonds and therefore of the nuclei and granules formed are completely related to the solid and liquid physical interaction. Hence, the method employed to incorporate the solid and liquid, viscosity of the binder, the length of the powder bed or the ability of the binder to fill the void spaces of the particle are key in the understanding of the granules formed (Parikh, 2009,

Rhodes, 2013) (Hapgood et al., 2003, Parikh, 2009). The most currently accepted methods are shown in figure 2.6.

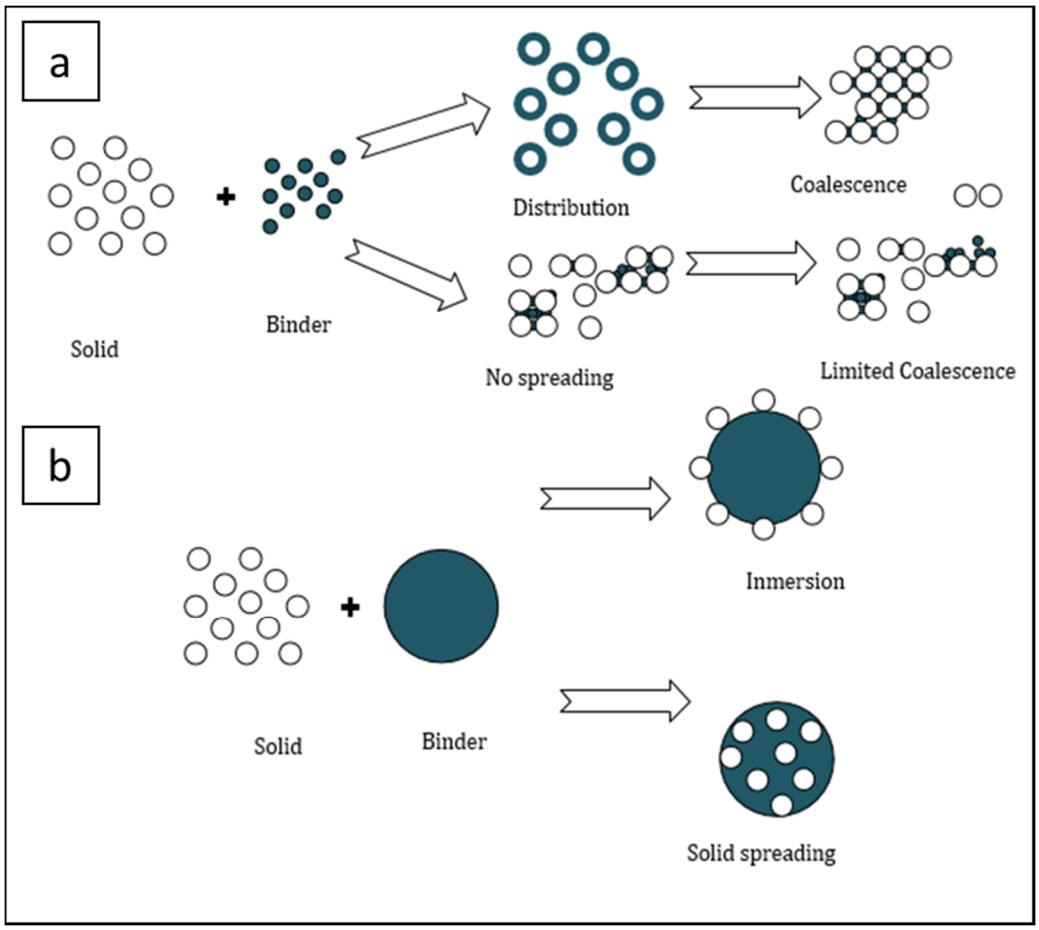

Figure 2.6. Nucleation when a) liquid droplet is smaller than particle and b) liquid droplet is larger than particle adapted from "Granulation Rates Processes" (Hapgood et al., 2007)

However, although there are multiple studies conducted of liquid bridge obtaining analytical models with good experimental agreement, most of those studies consider the liquid bridge as a static or equilibrium (Iveson et al., 2001, Lambert et al., 2008, Willett et al., 2000). However, when the dynamic liquid bridge has

been studied by simulations, the liquid bridge stability was dependant on the velocity of collision of the particles. It was found that at low velocities, the liquid bridge was stronger than at higher velocities (Kan et al., 2015). Also, studied was the case when multiple liquid bridges are formed at the same time, finding that for the same volume of liquid, the adhesion between particles increased when the size of droplet was decreased (Kan et al., 2017). Compared with the static liquid bridge which is highly dependent on the saturation level of the granules, the dynamic liquid bridge depends on the number of contact points between the moving particles and is independent of the liquid bridge volume after a minimum value. This dynamic liquid bridge has been related to the formation of the solid bridges between particle-particle during the drying which will determine the final breakage of the granules (Nieuwmeyer et al., 2007b). The solid bridges require a long time for their completion which can span from hours to even days to obtain the final structure (Farber et al., 2003, Farber et al., 2005).

One of the proposals to map the criteria which governs the nucleation and therefore the granules produced was elaborated by Hapgood and Litster (Figure 2.7) as a function of the spray flux of the liquid and time of penetration which depends of the binder and the solid. However, even if this tool could be useful and

it offers a route to scale up due to the use of dimensionless parameters, it should be applied carefully due to the fact it is based on estimates (Hapgood et al., 2003).

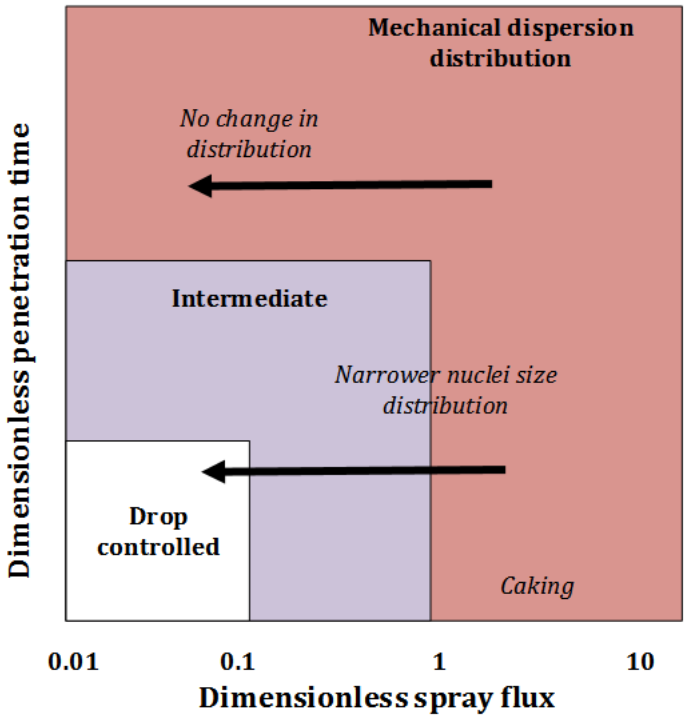

Figure 2.7. Nucleation regime map for this case adapted from "Granulation rate processes" (Hapgood et al., 2003)

2.2.2 Consolidation and coalescence

The granule growth process begins after wetting and nucleation i.e. when they start to form colloids with neighbouring particles and start to form larger granules. The driving force in this case is that the wet solid tends to reduce its surface free energy through forming liquid bridges. However, these forces should be large enough to overcome the external forces produced by the equipment.

Consequently, the nuclei formed in the first stage depend on and the external forces produced by the equipment. There are two fundamental different approaches to model coalescence depending on the importance of the elastic properties. When the elastic properties are considered highly relevant, it is assumed that the initial impact between particles is the one which will produce coalescence and the subsequent impacts will have no effect between the nuclei. Opposite to this, when elastic effects are considered negligible nuclei are in contact for a finite amount of time in which a bond is developed and depending on the strength of the bond, this will be permanent or not. The reality is believed to be a combination between these two approaches (Iveson et al., 2001, Parikh, 2009).

Different regime maps to measure growth have been proposed for different types of granulators (Dhenge et al., 2012b, Dhenge et al., 2013, Iveson et al., 2001). All of them classify the different granules in a full range of options from powder to over-wet mass. However, there is a difference between them since Dhenge et al. tied the rate processes of twin screw granulation to specific compartments and screw length (Dhenge et al., 2012b) which differs of Ivenson and al. which linked the growth to the pore saturation of the granule and deformation number (Iveson and Litster, 1998).

2.2.3 Attrition & breakage

Breakage of the granules can occur within or after the granulator. Breakage within the granulator is associated with the applied external energy. The growing of the granules is subjected to the adhesional forces as well as the agitation produced by the equipment (Iveson et al., 2001, Parikh, 2009). As the particle size is larger, it would be more difficult to grow these granules as a point can be reached where the adhesional forces are not enough to continue growing and breakage takes place. Also, in some granulators, there are some specific parts or locations which will apply stronger mechanical energies (Seem et al., 2015). When the breakage happens after the granulation has ended, it is called attrition and normally involves an uncontrolled size reduction which has been related with the evaporation of the water from the solid without the formation of the solid-solid bridges (Nieuwmeyer et al., 2007a, Nieuwmeyer et al., 2007b).

2.3 Overview of available techniques on granulation

Batch equipment has been widely used in wet granulation in industry, however, this equipment is difficult to design and scale up due to all the rate processes and the many variables in operation. Therefore, the new trend is continuous processing which offers several advantages where the typical barriers of adopting a new process are avoided. Figure 2.8 shows the most popular techniques in this field.

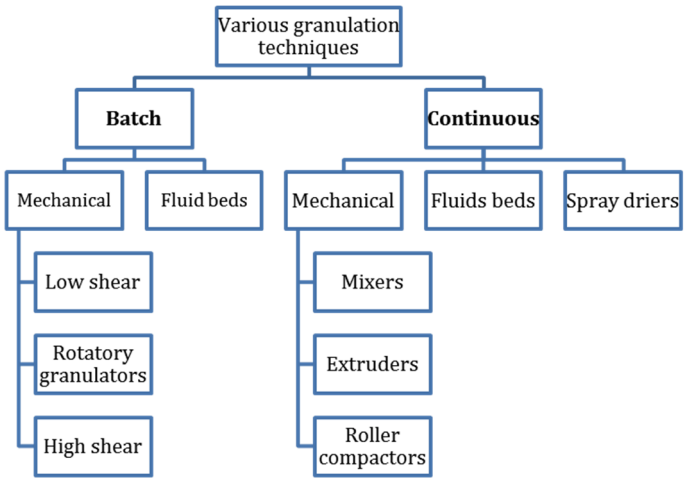

Figure 2.8 Various granulation techniques adapted from "Handbook of pharmaceutical granulation technology" (Parikh, 2009)

2.3.1 High shear granulators

The majority of the high-shear granulators have the following parts: a mixing bowl, a three-bladed impelled and an auxiliary chopper. The wet agglomeration

in a high-shear mixture involves typically three phases: dry powder mixing, liquid binder addition and wet massing. One of the main advantages of this equipment is the reproducibility of the granules with a uniform particle size distribution, however it offers other important advantages such as the short processing time, the lesser amount of binder required compared with fluid bed granulation and the possibility of granulating highly cohesive material (hydrophilic polymers). However, some disadvantages can be produced by this equipment since it can result in mechanical degradation of fragile particles, degradation of thermo sensitive material due to the increase of temperature and the risk of over wetting the granules can lead to the formation of large sized lumps (Agrawal and Naveen, 2011).

2.3.2 Fluid bed granulator

In the fluid bed granulation equipment, the granules are produced spraying a binder solution onto a fluidized powder bed. The material processed is flowing freely and homogenously through a current of air which directs it towards the spray. The main advantages of this process are the reduction of dust formation and product lost, however it is difficult to ensure reproducibility and the time of operation is greater than other available equipment. Furthermore, there are many energy costs related to the fluidisation of the different compounds.

2.3.4 Potential of continuous granulation

In order to be able of identify the potential of continuous wet granulation, the available technologies for particle enlargement were compared with twin screw granulation. Although there are many options with different levels of complexity, only the most common ones available in the market for production and research scale were compared in terms of active ingredient suitability (API), process capacity, and process control systems among others. It was concluded that the preferred systems for production scale are high shear granulator, fluid bed granulators and spray drying. On the other side, for research scale, the preferred systems are single pot processor, high shear granulation and fluid bed granulator. These technologies were compared with twin screw granulation (Aktiengesellschaft, 2015, Vervaet and Remon, 2005).

Table 2.1 .Comparison of available techniques for granulation in industrial scale (Aktiengesellschaft, 2015, Parikh, 2009, Vervaet and Remon, 2005)

	High shear granulators	**Fluid bed granulation**	**Spray drying**	**Twin screw granulation**
Volume (process capacity)	Up to 1800 litres	30 grams-2 tonnes	Defined by the container	Defined by the container
Mode of operation	Batch	Batch	Batch/ Continuous	Continuous
API suitability	Majority of API	PSD of raw materials should be similar	Suspended particles need to be smaller than 30 μm	Majority of API

	Not suitable for thermosensitive or fragile materials.		to promote the atomization	
Reproducibility	High	High	Very high	High
Energy required	0.25 kW/kg	0.37 kW/kg	7.5 kW/kg	0.25 kW/kg
Process control Strategy	End point	End point	Process control model	Process control model
Process control system safety	Off line systems and PAT Integration	Off line systems or PAT integration	Off line systems or PAT integration	PAT integration
Amount of granulation liquid required	Medium low	Medium	Very high	Low
Footprint	Large	Small	Large	Small
Number of operators required	Large	Large	Small	Small
Investment cost	Low	Low	High	High
Special facilities requirement	Yes (Height)	Yes (Height)	Yes (Height)	No
Flexibility	High	High	Low	High
Level of development of the technology	Total	Total	High	Medium

Table 2.2 Comparison of available techniques for granulation in research scale. (Aktiengesellschaft, 2015, Parikh, 2009, Vervaet and Remon, 2005)

	Single pot	High shear granulators	Fluid bed granulation	Twin screw granulation
Volume (process capacity)	1-1200 litres	Up to 1800 litres	30 grams-2 tonnes	Defined by the container
Mode of operation	Batch	Batch	Batch	Continuous
API suitability	All the API	Majority of API	PSD of raw materials should be similar	Majority of API
Reproducibility in big scale	Low	High	High	High
Energy required	<0.25 kW/kg	0.25 kW/kg	0.37 kW/kg	0.25 kW/kg
Process control Strategy	End point	End point	End point	Process control model
Process control system safety	Off line systems+ PAT integration	Off line systems + PAT Integration	Off line systems/ PAT integration	PAT integration
Amount of granulation liquid required	Low	Low	Medium low	Low
Footprint	Small	Large	Small	Small
Investment cost	Low	Low	Low	High
Scalability	Bad	Good	Good	Very good

2.4 Twin screw granulation

2.4.1 Overview of twin-screw granulators

Twin screw granulation has its origin in the extrusion process which has been used for over a century. Extrusion mechanism is based on a piston contained in a cylinder where the material is loaded and pushed through an opening hole with a predefined shape (Riaz, 2000). However, the transition from batch to continuous started very early with the appearance of the first continuous machines in the mid-1800s. The piston was substituted by a different type of screws and during the second half of 20th century, twin screw extruders started to be used due to its higher quality and uniform products. Despite their advantages, first interest by the pharmaceutical industry was during the early 1980s increasing its popularity until they were installed into many main pharmaceutical companies by 2010 (Ghebre-Selassie et al., 2018). Although granulation technology is a widely applied technology within the pharmaceutical process, the use of the twin screw extruders to perform granulation is a relatively new method (Djuric and Kleinebudde, 2008, Kleinebudde and Lindner, 1993, Lindberg et al., 1988).

The twin screw granulator (TSGs) is mainly a twin-screw extruder. Two co-rotating screws are contained within the barrel. Those screws are commonly segmented into screw elements which are assembled in shafts. Screw elements

are one of the most important design parameters as they will decide the free volume available for granulation depending on the flight diameter, inside and outside diameter (Figure 2. 9). The distance that a flight traverses axially down the screw for one turn is known as its flight lead whereas the axial distance between two adjacent flights along the axis of the screw is known as the flight pitch (Thompson, 2014). In general, the outer diameter is the one used to refer the different scale of the TSG equipment and the screw elements will be defined depending on its geometry, pitch variation, length as well as the angle with respect to the shaft.

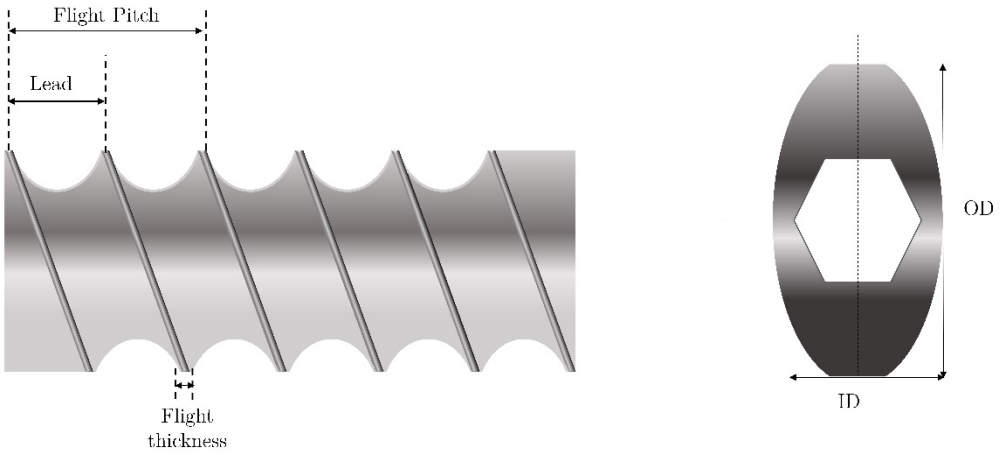

Figure 2.9. Lead, flight pitch, flight thickness, outer diameter (OD) and inner diameter (ID) Adapted from Ghebre-Selassie et al., 2018, Thompson, 2014

Although there is a high number of different screw elements and variations, those can be classified in two main categories: conveying and mixing elements (Pradhan et al., 2017a, Pradhan et al., 2017b, Thompson and Sun, 2010).

- Conveying element

The conveying element (figure 2.10) which is a continuous helical flight is the element which offers more available space for filling and applies lower mechanical energy. Its conveying capacity is defined by the pitch angle which determines the lead of the element. Short leads correspond with less available volume in the screw and are associated with more unevenly distributed product. Also, larger flight pitches decreases the porosity and it is associated with larger granules and more production of fines (Seem et al., 2015, Thompson and Sun, 2010). However, it has been reported that screws composed of only conveyor elements have presented very different morphologies and properties varying another process parameters such as liquid-to-solid ratio, viscosity and feed rate (Dhenge et al., 2013) so the further research is required to understand the full influence of this element.

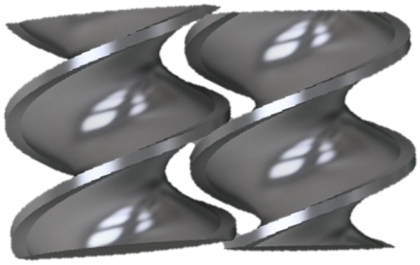

Figure 2.10 Conveying elements

- Mixing elements

There are two main types of screw elements which will increase the mixing: kneading blocks and comb mixing elements. The first category of kneading block has been widely studied and reported in the literature (Dhenge et al., 2012a, Djuric and Kleinebudde, 2008, Li et al., 2014, Vercruysse et al., 2012, Yerramilli and Karwe, 2004) since it is the most commonly used type of non-conveying element. As the figure 2. 11 shows, the kneading block is a group of discs which can be arranged in different angles (offset angles). The choices are typically 30°, 45°, 60° and 90° which can modify the direction of the flow (Li et al., 2014, Seem et al., 2015).

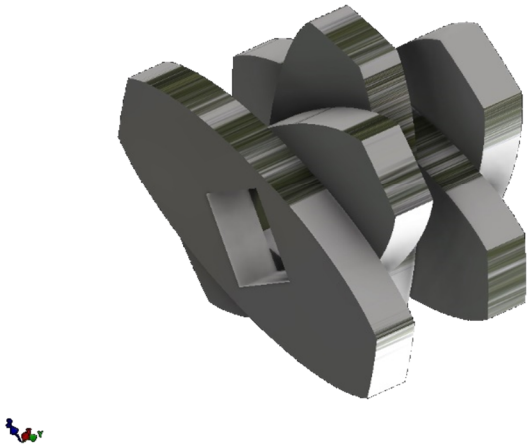

Figure 2.11 Kneading block

Opposite to conveying elements, kneading blocks are typically fully filled with powder producing a high mechanical energy increasing the force applied to the wetted mass and producing less friable and dense products (Djuric and Kleinebudde, 2008). It is considered that they increase the consistency of the granules offering a unique compaction-fragmentation zone. They are assumed to produce densification as well as they help to distribute the interstitial liquid rather than simply densify the product (Li et al., 2014). Many different configurations are possible to build depending on the offset angle and the number of elements used. As smaller angle is more similar is to conveying element behaviour and more dispersive mixer behaviour (Figure 2.12). Consequently, with larger angles, the element has a more distributive action. However, although changes in properties

of the granule such as porosity depending on the angle have been found (Djuric and Kleinebudde, 2008), it will very dependent of the channel fill (Thompson and Sun, 2010) and the number of elements of the block (Vercruysse et al., 2012).

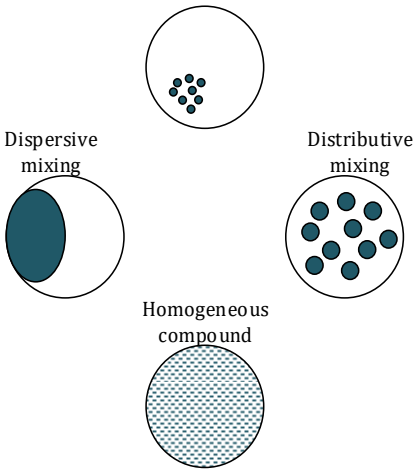

Figure 2.12. Differences between dispersive and distributive mixing on kneading block. (Ghebre-Selassie and Martin, 2003).

The second category, comb mixing elements (Figure 2.13) consists of a group of annular rings with fins situated perpendicularly to the flow direction in order to increase the mixing of the system (Seem et al., 2015). This type of element has been found useful to collide granules with different shear histories (Thompson and Sun, 2010). It has been reported that they produce granules with intermediate density between those produced by conveyors and kneading blocks (Djuric and Kleinebudde, 2008).

Figure 2.13. Comb mixing elements

One important parameter is the angle the fins form with respect to the perpendicular flow since this determines if the elements restrict the flow (under 90^0) or promote it (over 90^0). The element would be called reversing or forwarding respectively. On one hand, the forwarding comb element seems to perform as a kneading block although it maintains a higher fraction of fines and a rounder particle shape. On the other hand, reversing elements produce larger granules due to the creation of a high-pressure zone which completely agglomerates the materials. However, frequently this is achieved by forcing the motor of the granulator and exceeding its torques limits (Thompson and Sun, 2010).

- **Screw configuration**

The configuration of the TSG can be assembled from 10 to 50 elements combining all the different elements producing a huge number of possible combinations on the different shafts (Figure 2.14). As well the relationship between the length and the diameter of the screws can be varied although most pharmaceutical research uses a length to diameter ratio below 40. However, as in the previous examples of the influence of the elements the relationship between the configuration, the quality of the granules and different formulations is not fully understood (Thompson, 2014); therefore, the screw configuration needs to be a practical balance between elements.

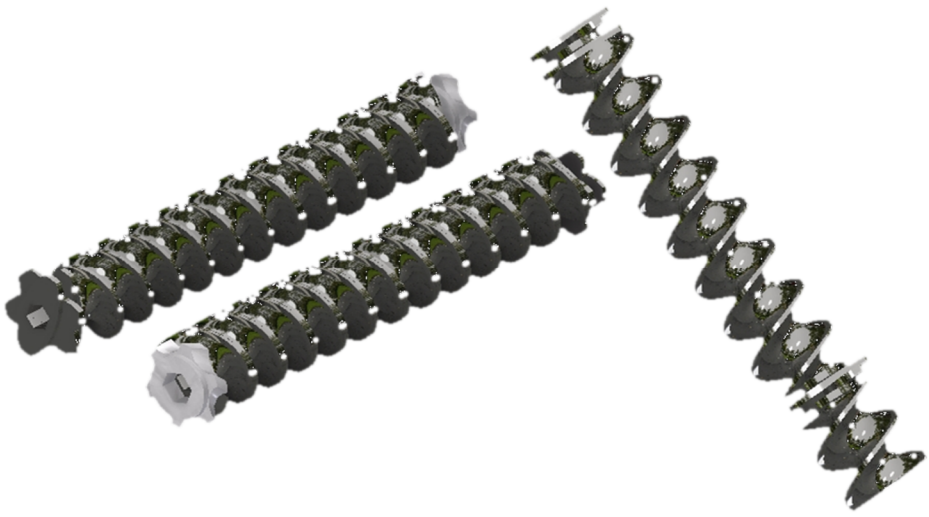

Figure 2.14. Screws assembled example

For instance, conveying elements produce higher friabilities and less dense granules than other elements. However, the friction due the kneading zones significantly increases the temperature which has an important effect on the granule properties (Vercruysse et al., 2012). In addition, kneading zones are more likely to produce blockages (Seem et al., 2015) which can lead to a less safe operation.

2.4.2 Channel fill

The relationship between the filling and the different screws elements has been already covered in the previous section. However, channel fill is normally referred as the total fraction occupied by powder and granules with respect to the full volume of the granulator. It depends on four factors: screw configuration, length to diameter ratio of the granulator, feed rate and screw velocity. The first two parameters are fixed properties during operation opposite to feed rate and screw velocity which are process variables (Seem et al., 2015). Both parameters have been extensively studied in the literature separately or combined where screw speed has been reported to have a minor influence on the granules properties compared with feed rate (Dhenge et al., 2011, Dhenge et al., 2010, Djuric and Kleinebudde, 2008, Keleb et al., 2004, Thompson and Sun, 2010). The screw velocity is inversely proportional to the channel fill obtaining higher channel fills for lower screw speeds. At the same time, increase in the feed rate,

will increase the channel fill. Although extensive research has been done covering both, it has been reported that for the same feed rates and screw speeds but different granulators, a considerable difference in the properties of the granules was obtained (Djuric et al., 2009). The difference of free volume available seemed to play a key factor in the production of the granules and therefore, it will be advantageous to use channel fill in the study of the granules rather than screw speed and feed rate individually.

Those two process variables together have a direct effect in the compaction forces applied to the wetted mass (Thompson and Sun, 2010). When the granulator is at low fill, there is a reduction in the compaction force and more friable and porous granules are produced (Lee et al., 2012). Although different equations for barrel fill have been defined, they all have in common the use of feed rate and screw velocity (Gorringe et al., 2017, Osorio et al., 2017). On one side, Gorringe et al. used the fraction of the capacity of the twin screw granulator which facilitates the direct transfer to production lines from research phases. However, it does not take into account changes of screw configuration which limits the transfer to the same configuration (Gorringe et al., 2017). On the other side, Osorio et al. used the powder feed number to calculate this value where changes in configuration are considered. However, the calculation requires

a higher technical knowledge of the equipment since parameters such the cross-sectional area of the elements or net forward velocity of the powder need to be known (Osorio et al., 2017). Nevertheless, both studies have shown the capability of channel fill level as a main parameter to establish the design space. Channel fill fraction correlates strongly with the granule attributes within same scale obtaining very similar granule size distributions for runs at the same fraction (Gorringe et al., 2017, Lute et al., 2018, Osorio et al., 2017).

High channel fills are associated with more spherical products and low channel fills are more likely to produce elongated granules (Dhenge et al., 2011, Gorringe et al., 2017). The reported changes in granule morphology seem to indicate that changes in the local forces inside the granulator are occurring however, there are few examples of quantitative study of the mechanical stresses in the screw elements. However, it was demonstrated that this correlation is not maintained during the scale up of granulators due to the differences of the available space on the screw geometry (Osorio et al., 2017).

Changes in channel fill can be studied depending on the specific mechanical energy (SME) applied to the unit of mass. Although this parameter is normally disregarded, it can help to directly compare different granulators in terms of

energy and running costs (Dhenge et al., 2013, Seem et al., 2015, Vercruysse et al., 2015).

2.4.3 Liquid to solid ratio

Wetting and nucleation can be considered one of the most important steps within the granulation process having a direct impact in both the properties of the materials and the tabletability of the granules (Shi et al., 2011). Since the liquid bonds are developed in this stage, the efficiency of wet granulation depends on the control of the cohesive and adhesive forces between particles i.e. binder characteristics, liquid to solid ratio and method of addition (Nguyen et al., 2013, Hapgood, 2000, Suresh et al., 2017). Verstraeten et al. determined liquid to solid (L/S) ratio had an overwhelming determinant effect on the properties compared with screw speed or throughput for both hydrophobic and hydrophilic formulations. They found that during wetting a bimodal distribution is produced: higher content oversize agglomerates combined with non-granulated powder (Verstraeten et al., 2017). At higher L/S ratio, the bimodality is reduced obtaining higher granules and reducing the porosity (El Hagrasy and Litster, 2013, Thompson, 2014). This change was more pronounced in the hydrophobic formulation where the hydrophilic particles were preferentially nucleated and the hydrophobic particles depend on the amount of liquid surface available. It was found that

the granules produced with TSG showed several similarities for both formulations depending on the liquid availability and shear forces on the individual particles (Verstraeten et al., 2017). L/S ratio used for hydrophobic formulation was bigger than the one used for hydrophilic which suggests that the L/S required to produce unimodal distributions depends greatly on the formulation (Li et al., 2015, Verstraeten et al., 2017)

2.5 Elements of pharmaceutical development in twin screw granulation

2.5.1 Quality by design

Current pharmaceutical development is based on the design of a quality product and the delivery of the required product performance through the establishment of one suitable manufacturing process. This approach can only be accomplished with a systematic scientific risk-based methodology and greater understanding of all of the elements of the pharmaceutical process. This initiative, encouraged by The Food and Drug Administration (FDA), motivates the use of science and engineering principles for assessing and mitigating risks providing continuous real time quality through all the supply chain of the product. (Food and Administration, 2004)

Most pharmaceutical processes are based on time-defined end points avoiding consideration of physical and chemical differences of raw materials. However, Quality by Design (QbD) requires full understanding and monitoring of the process, and therefore, to accomplish and acquire information is required the use of process analytical technology (PAT). These tools can be classified according to their function as follows (Food and Administration, 2004):

- Multivariate tools for design, data acquisition and analysis

- Process analysers
- Process control tools
- Continuous improvement and knowledge management tools.

These tools will be used at different stages of implementation of the QbD strategy and without them it is not feasible. In Figure 2. 14, a brief diagram of the stages of the process are shown.

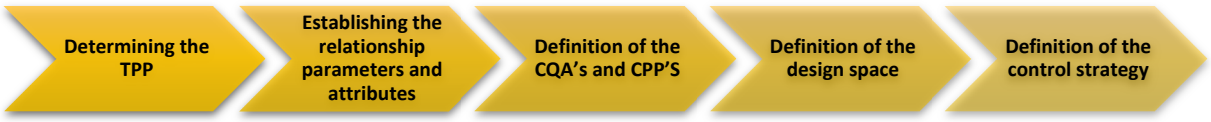

Figure 2.14.QbD strategy tiers adapted from ICH Q8 (R2), (ICH Q8 (R2), 2009)

The first stage is determining the TPP (Target product profile) according to different specifications such as the target population and the intended clinical settings (dosage form, route of administration or delivery systems). The aim of establishing this profile is to determine that the formulation and quality of the desired product will meet these requirements. Prior knowledge about the potential impact of the different parameters on the desired attributes is frequently known in the different operations of the manufacturing process allowing a first identification of the parameters involved.

However, the demands of high-quality manufacture require the use of risk assessment tools to identify which material attributes and process parameter have a direct impact on the desired product. Therefore, a rigorous design of experiment should be applied. Design of Experiment (DoE) consists of statistical techniques based on screening and optimization studies. Using a factorial relationship between the number of parameters and attributes establishes the number of experiments utilised to evaluate the interaction. This method is particularly useful to identify regions where the product is especially sensitive to small changes determining the critical quality attributes (CQAs) and critical process parameters, (CPPs). However, this method is not suitable for its individual use at further stages of the process due to the underlying assumption of linearity and it will be used in combination with other statistical methods (Gibson, 2009).

Once the CQA's and CPP's have been determined, detailed monitoring of the link between them must be developed for multiple reasons. First of all, the range within which each attribute produces the required quality of the desired product should be established, as well as those limits where the conditions of operation are efficient in terms of energy, time and raw material. Due to the complexity and the high level of variables applied in the operations of pharmaceutical process, it is common to use multivariate techniques for analysis of data. The

common strategy for this is the use of one or more PAT tools for acquisition of data and afterwards, analysing the data through an algorithm to determine the magnitude of the effect. The accuracy of the analysis will be determined by the quality of the tool used as well as the precision of analysis of the algorithm. Commonly, an increase of precision of the algorithm is associated with an increase in the complexity of its use and as a result, some assumptions are frequently made.

To sum up, the level of understanding of one process is associated with the level of unclassified parameters at this stage. Therefore, the design space will be defined when the relationships between the final product quality attributes, critical intermediate material attributes and process parameters have been successfully established as well as the ranges of operation and the scale and flexibility of the model. The characterisation of the design space allows the possibility to scale up the models as well as the definition of one control strategy to ensure the quality of the product over time.

Effective innovation can be developed through the use of strategies such as QbD. QbD is based in the core definition of pharmaceutical quality, for instance the absence of deviation from standards in terms of content, distribution and design. In addition, QbD must foresee and assure the potential problems and avoid the

appearance of the same problems through a correct design. In addition, the implementation of QbD improves speed to market and reduces costs at all stages of the process. (Guideline, 2009, Weinberg, 2011).

2.5.2 Design of experiments

The Design of Experiments (DoE) is an important tool to define optimal and robust conditions. It is used with three different objectives related to the different knowledge tiers of the process.

Firstly, DoE is used as a method of screening. Screening is used to identify the influence of the different factors and to determine the ranges of operation. In this step, the number of variables and parameters implied are dramatically large and the use of other systems would consume a lot of time and resources. The second use is as an optimisation tool, which allows the investigator to find the optimal conditions within the range of operation. Finally, the robustness of the system can be tested to provide information about the sensibility of small changes.

According to these three objectives, the complementary algorithm to analyse the data obtained will evolve in accuracy and complexity according to the level required. The main advantage of this method rather than the analysis of one-

factor-each-time is the possibility of analysing many variables in a small number of experiments.

The methodology most commonly used is based on a factorial design. The experiment will lie in the study of the influence of a number 'n' of factors or conditions upon a number 'a' of variables. Therefore, the minimum number of experiments used to evaluate all the possible conditions would be a^n. However, the nature of the factorial number could prove very difficult when using this method for large numbers. This issue can be solved through the assumption of replicability of some of the variables. Furthermore, it is common to add some duplicated points close to the centre of the range to avoid variability in the results (Eriksson et al., 2013).

2.5.3 Population balance models (PBMs) and discrete element method

The definition of the design space and operating parameters could be approached through the development of a mathematical process model. The traditional approach to that is using population balance models (PBMs) which mechanically models the process. Granulation PBMs can be based on the different parameters involved in wet granulation which will give the number of dimensions. One-dimensional PBMs are based on the principle of mass conservation which outlines that for any system closed to all transfers of matter and energy, the mass

of the system must remain constant over time. As a consequence, these PBMs study the change on the granules size distribution as a function of the time within a workspace, showing good correlations within a workspace (Kumar et al., 2016b, Van Hauwermeiren et al., 2018). However, they have a high sensitivity to changes in the process parameters due to the negligence in factoring the direct effect of other properties into the model (Iveson, 2002).

Multi-dimensional PBMs can obtain good agreement between experimental and predicted data introducing liquid-depend kernels but they still show issues at very large and small particle sizes (Barrasso et al., 2015a). Also, although the addition of dimensions increases the model accuracy, they are also computationally expensive making the calculations unfeasible (Barrasso and Ramachandran, 2012). Furthermore, they require a specific calibration of the kernels which can lead to lack of flexibility with process parameters or changes in formulation (Van Hauwermeiren et al., 2017).

Recently, PBMs have been coupled to Discrete element method (DEM) which captures further information on the particles such as collision data and residence times in each compartment (Barrasso et al., 2015b, Barrasso and Ramachandran, 2016). However, those simulations are also very expensive computationally and their successful replacement has been found correlating properties to the collision

frequency and reducing significantly the computational requirements of the simulations (Barrasso et al., 2014, Shirazian et al., 2017).

Another method to reduce the computational cost of the simulations is the introduction of stochastic weighted PBMs. This approach can reduce the computational cost by two orders of magnitude allowing consideration of up to four dimensional PBMs and new steps in the nucleation (McGuire et al., 2018).

2.5.4 Process parameters and quality attributes in twin screw granulation

Although the main process parameters and quality attributes have been already described, there is another number of operational parameters which can affect the process and they will be briefly described in this section.

- Excipients

The understanding of the formulation can help to predict and control the properties of the granules depending on the combination of the excipients (Willecke et al., 2018). However, this parameter is not commonly a design process within twin screw granulation and most of the studies present in literature were based on the hydrophobic character of the formulation or the liquid addition (Djuric et al., 2009, Verstraeten et al., 2017). There was some attempts to study the influence of the initial particle size where it was found that larger sizes produces

larger granules, however, the effect was minimal for TSG (El Hagrasy et al., 2013a).

- Barrel temperature

Very little research has been performed in this area although there is a common assumption that lower temperatures minimize drug damage (Thompson, 2014). However, higher temperatures produce larger size in granules, possibly due to the higher solubility of excipients (Fonteyne et al., 2013).

- Binders properties

Binder has been studied mainly as function of its viscosity and surface tension (Dhenge et al., 2012b, Seem et al., 2015, Thompson, 2014). In general, the relationship between binder viscosity and granule size depends on the hydrophilic degree of the formulation. However, for a common pharmaceutical formulation, Dhenge et al. found that an increase in the viscosity of the binder produces an increase in the strength of the granules and a decrease in the amount of fines due to the production of stronger bonds (Dhenge et al., 2012b).

2.6 Current gap

The potential of twin-screw granulation in pharmaceutical processes has been analysed widely in the literature. However, without a full correlation between

the experimental and the theoretical results, those studies are limited to defined workspaces (Iveson, 2002). This limitation is a key point in the correct implementation of the technology and further knowledge of the equipment needs to be obtained. Fundamental knowledge of the formation of the granules within the TSGs needs to be sought as well as development of methods to ensure the control of the properties of the products (Kumar et al., 2017). Furthermore, equipment limitations, transfer of scales and different formulation regime maps need to be studied.

Therefore, the main aims and objectives of this thesis are:

- Development of tools to increase the knowledge and control of twin screw granulators.
- Increase the understanding of the operational limits of the twin screw granulators and production of safe workspaces.
- Increasing the knowledge of the inner structure of the granules obtained by twin screw granulation and compare with the results obtained by high shear wet granulation.
- Studying the effect of the static drying in granulation by the variation of the drying temperatures.

Chapter 3

Novel metrology for the study of polymodal particle size distributions

3.1 Introduction

The evaluation of the granulation process requires knowledge of the variance of the granules' properties as function of the process parameters, and, the establishment of the variation using general terms such as size, strength, and friability. The study of these terms gives important information allowing process control, as well as establishment of the acceptable limits of the working conditions. However, although terms such as friability or flowability can be expressed as a single

value, particle size distribution is frequently expressed as a curve, which does not allow its direct examination as a quality attribute or a process control variable. A quality attribute should be within an appropriate limit, range, or distribution to ensure the desired product quality (ICH Q8 (R2), 2009). Transforming PSDs into a homogeneity factor (FH) allows the analysis of the influence of operational parameters on the system. In addition, workspaces can be created and the system can be easily optimised after obtaining the regions where the production of granules is homogeneous.

Further potential advantages of homogeneity values calculated from particle size distributions are related to its potential to be used as a characterisation tool for Quality by Design (QbD) which is recommended for adoption by the pharmaceutical industry (Seem et al., 2015). This approach ought to be accomplished with a systematic scientific risk-based methodology.

Therefore, a tool for characterising granule homogeneity would help to provide a greater understanding of the underlying process mechanisms since changes in PSDs have been frequently used to study granulation in itself. For instance, there are examples in literature where it has been used to suggest predominant mechanisms such as breakage or layering (Sayin et al., 2015), to indicate increases on the strength of liquid bridges (Dhenge et al., 2012) or even in the own

design of process parameters (Vercruysse et al., 2015). Also, it will improve the control during granule manufacture as well as being a useful complement to other granule properties such as flowability or strength in the optimisation of tabletting and associated processes (Cardona et al., 2018). Besides, the possibility of defining a desired diameter operating point and controlling the homogeneity around that point allows identification of when the process is within product specifications. This advantage could be used in the comparison of different batches and technologies on both a research and industrial scale.

Due to the possible advantages of quantifying a PSD's homogeneity with a single numerical parameter, the aims of this study were to propose a methodology capable of achieving this. The method developed can transform any PSD into a weight distribution through the hyperbolic tangent method and calculate a homogeneity percentage. In addition, this method was mathematically validated through the study of the response to simulated scenarios of particle size distributions and empirically demonstrated through the application to two different materials (α-Lactose monohydrate and microcrystalline cellulose) and its potential as a characterisation tool was assessed by determining the most critical process parameters for both systems.

3.2 Materials and methods

3.2.1 Materials

α-Lactose monohydrate (PubChem CID: 24896349) with 99% total lactose basis (GC) (Sigma-Aldrich Company Ltd., Dorset, England) and microcrystalline cellulose (PubChem CID: 16211032) with average particle size 50 µm (Fisher Scientific UK Ltd, Loughborough, Leicestershire, United Kingdom) were used as excipients to validate the method. Distilled water (EMD Millipore™ Pure Water Reservoirs, Millipore SAS, Mosheim, France) was added as granulation liquid.

3.2.2 Granulation experiments

In order to produce granules, a Thermofisher Pharma 11mm Twin Screw Granulator (Process 11, 40:1 L/D, Thermo Fisher Scientific, Karlsruhe, Germany) operating within the range of 50-125 rpm in combination with a gravimetric feeder (Brabender Gravimetric feeder DDW-MT, Brabender Technologie Gmbh & Co. Kg Duisburg, Germany) was employed to feed excipients at a rate of 0.05-0.35 kg h^{-1}. Distilled water was fed to the system through a syringe pump (Harvard Syringe Pump, Harvard Apparatus UK, Cambridge, UK) in order to produce liquid/solid ratios from 0.05 to 0.2 for α-Lactose monohydrate, and 1 to 1.8 for microcrystalline cellulose. The upper and lower limits of granule production ratios were chosen since below the lower limit, the product obtained at these

torque velocities was a powder and above the upper limit the product was a wet mass. The design of experiments and following analysis was done through the use of the commercial software Modde 10.1. The chosen model design used to select the experimental setup and to study the relationship between variables was an Onion D-Optimal model with two layers which could be fitted afterwards with PLS-2PLS regression analysis (MKS Data Analytics Solutions, Malmö, Sweden). Figure 3.1 displays the design of experiments for both materials: α-Lactose monohydrate (Figure 3. 1a) and for microcrystalline cellulose (Figure 3. 1b). The screw configuration used was 27 conveying elements for each sheet, chosen in order to minimise the impact that the different screw elements could have on the granules (Seem et al., 2015).

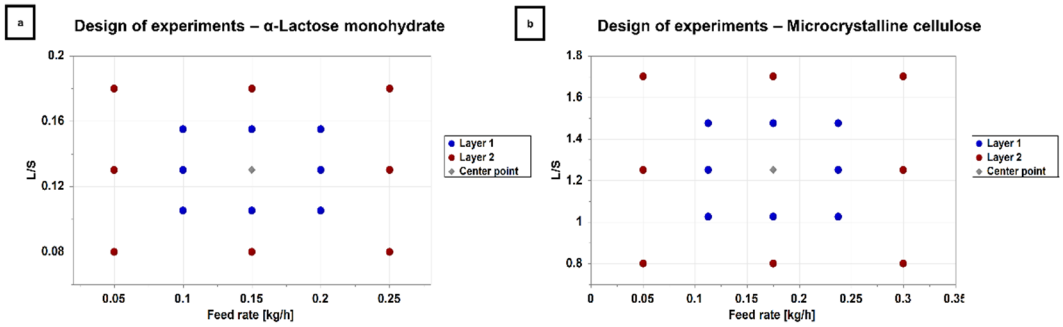

Figure 3.1. Design of experiments for α-Lactose monohydrate (a) and cellulose microcrystalline (b).

3.2.3. Offline granule size analysis

The analysis of the granule size distribution was performed using the QICPIC/RODOS L with vibratory feeder VIBRI/L (Sympatec GmbH System-Partikel-Technik, Clausthal-Zellerfeld, Germany).

All the particle size distributions obtained were produced at 0.5 bar of primary pressure to avoid breakage of the granules during the analysis (MacLeod and Muller, 2012). The disperser conditions were optimised for each set of granules to obtain the optimal optical concentration. All the particle size distributions were plotted in logarithmic volume against the particle size. The volumetric mean diameter (VMD) determined by the system was chosen as mean diameter, and is been calculated based on the arithmetic mean value. All the particle size distributions (PSDs) were plotted in logarithmic scale of the volume mean diameter against the density distribution which were both calculated in accordance with ISO 13222-1:2014 (ISO 13322-1:2014, 2014).

3.2.4 Development of the methodology

All the data and analysis processing were performed using the commercial software package Matlab and Statistics Toolbox R2014a (The MathWorks, Inc., Natick, Massachusetts, United States).

3.2.5 Contour profiles

The results and the effects of the different variables will be presented as contour plots, which are able to show multidimensional interactions between the input variables and process parameters. The contour profiles are a recommended tool to identify the design space of a full workspace (ICH Q8 (R2), 2009). These profiles are built identifying which combinations of the selected parameters produce the same result on the chosen variable and identifying them with the same contour. In this case, for each material analysed four different profiles were produced. Two for each quality attribute (homogeneity factor and volumetric mean diameter) at two different ranges of torque velocity (50-87.5 rpm and 87.5-125 rpm). The chosen process parameters were the mass feed rate of the solid and the liquid/solid ratio (L/S) which is defined as the relationship between the mass feed rate of the solid and the liquid. A schematic of the Design of experiments (DoE) can be found in Figure 3. 1.

3.3. Results

3.3.1 Development of the methodology

In sedimentology an alternative method has been applied to transform the normal distribution for unimodal and bimodal distributions known as the hyperbolic tangent technique (tanh method), which has been used traditionally for dealing with travelling waves and to study evolution equations (Malfliet, 2004). It was successfully applied by Passe (Passe, 1997) in order to transform a grain distribution into a mathematical expression. Due to the fact that the graphical result of the integral of a normal distribution presents an analogous shape to the hyperbolic tangent function; the cumulative expression can be mathematically described by Eq. 3.1.

$$w(d) = \frac{p}{2} - \left(\frac{p}{2}\right) * \tanh(\log(\mu) - \log(d) * s) \qquad \text{Eq.3.1}$$

Where w is the weight, μ is the mean value of the particle size, d is the variable particle size, p is the value of the population of the different peaks in percentage which is equal to 100% for unimodal distributions and s is a sorting factor which is given as $1/(\log d_{75} - \log d_{25})$ (Passe, 1997).

This technique for transforming curves into mathematical expressions can be used as an effective way to smooth distribution curves due to the variation of

the slope depending on the number of peaks. For example, three different particle size distributions have been transformed through this method in Figure 3. 2 representing the weight against the logarithm of the particle size. The first PSD (Figure 3.2a) can be considered as a mono-modal distribution and its equivalent weight distribution is a straight line which slopes up at the greatest rate. The second PSD (Figure 3.2b) corresponds to a bimodal distribution and its weight distribution shows an important decrease of the slope of the curve compared to Figure 3.2a. The third PSD (Figure 3.2c) represents a polymodal distribution with three clear peaks in which the slope of the corresponding weight distribution curve has decreased even more dramatically with respect to Figure 3.2a. Therefore, from Figure 3.2 it can be concluded that the decreasing slope of the curves represents the decrease in homogeneity of distribution as well as the increase in the number of peaks of the distribution.

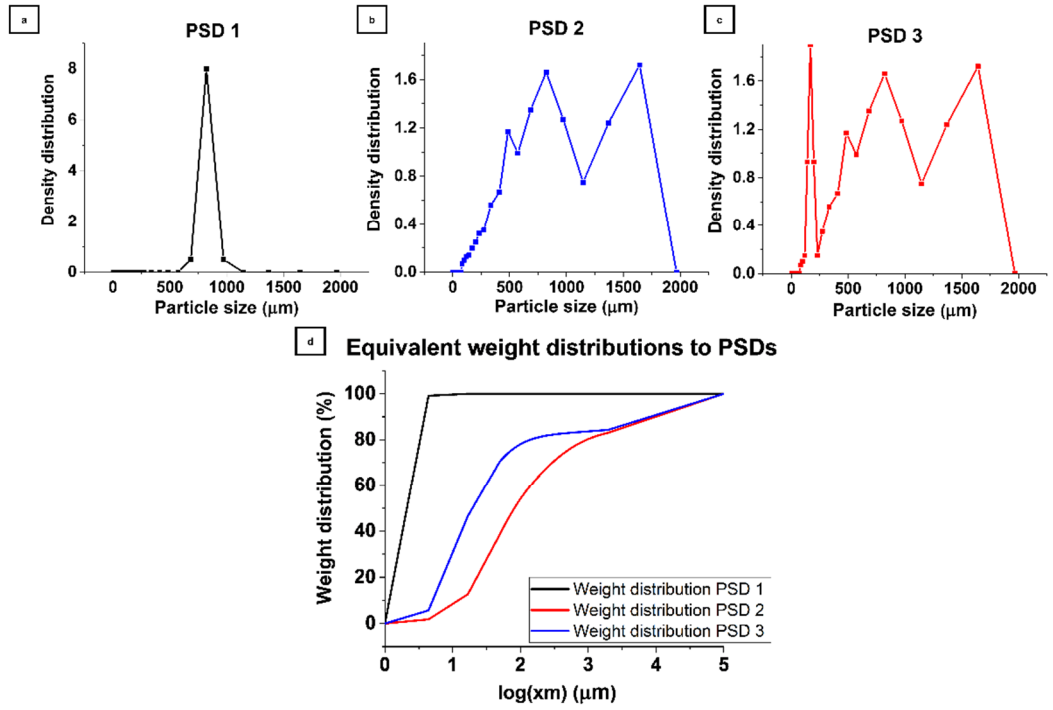

Figure 3.2. Unimodal (a) and polymodal (b-c) particle size distributions transformed to the equivalent weight distributions (d).

The direct relationship between the slope of the weight distribution curve and the shape of the particle size distribution shows an enormous potential as a characterisation tool. The area under the resultant curve can be calculated through integration and it will be proportional to the slope of the curve. The homogeneity can be measured through this method and transformed into a percentage, unimodal PSDs will be associated with larger areas and greater homogeneity percentages.

To quantify homogeneity, PSD curves are smoothed through the hyperbolic tangent method in order to adapt the data to the mathematical expression in Eq. 3.2 based on the equation used by Passe. (Passe, 1997).

$$w(xm) = \sum_{1}^{i=total\ peaks} \left(\frac{p_i}{2} - \frac{p_i}{2} * \tanh(\log(\mu_i) - \log(xm) * s_i\right) \qquad \text{Eq. 3.2}$$

Where the subindex i represents the peak number for appearance order, p_i is the value of the population of the peak in percentage, μ_i is the mean value of the particle size for the peak width, xm is the size of the particles included in the width of the peak, and s_i is a sorting factor defined in Eq 3.3.

This mathematical expression depends on the total number of peaks and a specific expression needs to be developed for each peak. The peaks are local maxima of the particle size distribution. The local maximum is located as the data point which is larger than its two neighbouring points, in those cases that the top of the peak is flat, the point considered is the first to appear (The MathWorks Inc, 2013). After locating the peaks, their population was calculated by means of the integral of the curve formed by the peak.

The sorting factors for each PSD curve are calculated using Eq 3.3 were $d_{25,i}$ and $d_{75,i}$ are the diameter corresponding to the 25% and 75% population weight of each peak. The sorting factor was adapted from the method presented by Passe

(Passe, 1997) through the introduction of the terms k_1 and k_2 which were developed in house for the range 5 μm – 2.2 mm. The term k_1 weights the difference between the peak corresponding to maximum value in the density distribution and the volumetric mean diameter of the particles (Eq. 3.4). Frequently, the limits of the ranges of particles sizes distribution are proportional to the size of particle and those could be different depending on the choice of nest of sieves or the measuring range of the analytical system. To avoid the effect of these possible discrepancies between the different methods, the distribution will be normalised when one considers that it is composed of ten identical intervals. The difference between the maximum peak and the mean diameter will be measured through the number of intervals between them (Eq. 3.5).

$$s_i = k_{1,i} * \frac{p_i}{\log(d_{75,i}) - \log(d_{25,i})} \quad \text{Eq. 3.3}$$

$$k_1 = \exp\left(-\left(\frac{xm_{\max\ peak} - d}{k_2}\right)\right) \quad \text{Eq.3.4}$$

$$k_2 = 10 * \frac{xm_{last} - xm_0}{n_{interval}} \quad \text{Eq. 3.5}$$

Where the subindex i represents the peak number for appearance order, $s_{i,}$, k_1 and k_2 are sorting factors, p_i is the value of the population of the peak in percentage, $d_{25,i}$ and $d_{75,i}$ are d_{25} and d_{75} of each peak, $xm_{max\ peak}$ is the maximum value of the distribution, d is the volumetric mean diameter, xm_0 and xm_{last} are the first

and last values of the distribution, $n_{interval}$ is the initial number of intervals of the distribution.

After the particle size distributions have been smoothed, it is required to achieve the maximum homogeneity possible, e.g. the distribution obtained when all the granules would have the same diameter that coincides with the mean diameter. The maximum homogeneity corresponds to the best-case scenario of a unimodal distribution where the first value which would appear would be unique and it would produce a single peak. After this equivalent perfect particle size distribution has been calculated, it is possible to calculate the weight distribution for that case.

The lower limits corresponding to zero homogeneity would be represented by the curves produced when all the sizes have the same weight inside the distribution. As in the case of the perfect distribution, the PSD needs to be transformed to worst case scenario, allowing the weight distribution to be calculated. Figure 3.3 displays the situation where both maximum and minimum cases have been transformed into their equivalent distribution. The differences in the rise of both curves provides a clear distinction between them as the curve corresponding to 100% homogeneity has a slope 15 times greater than the curve corresponding to 0%.

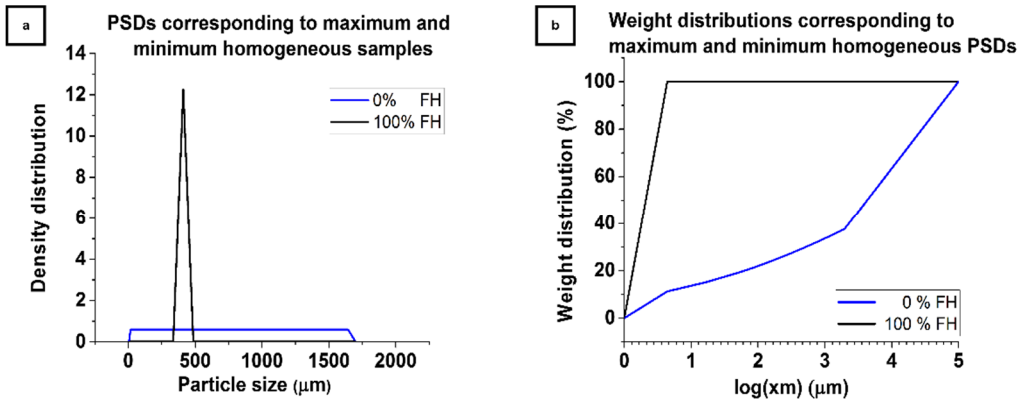

Figure 3.3. Equivalent particle size distributions (a) transformed to weight distributions. (b)

Once the upper and lower limits have been determined, it is possible to calculate the homogeneity for any particle size distribution by calculating the area under the curve corresponding to the PSD and its equivalent best (100% homogeneity) and worst (0% homogeneity) cases. Figure 3.4 displays the three areas in different colours. The area corresponding to 100% homogeneity would be comprised between the solid and dotted black lines with the PSD area shaded in yellow. Since the particle size distribution is given in intervals, it was chosen to obtain the area under curve through the trapezoidal rule (Treiman, 2014).

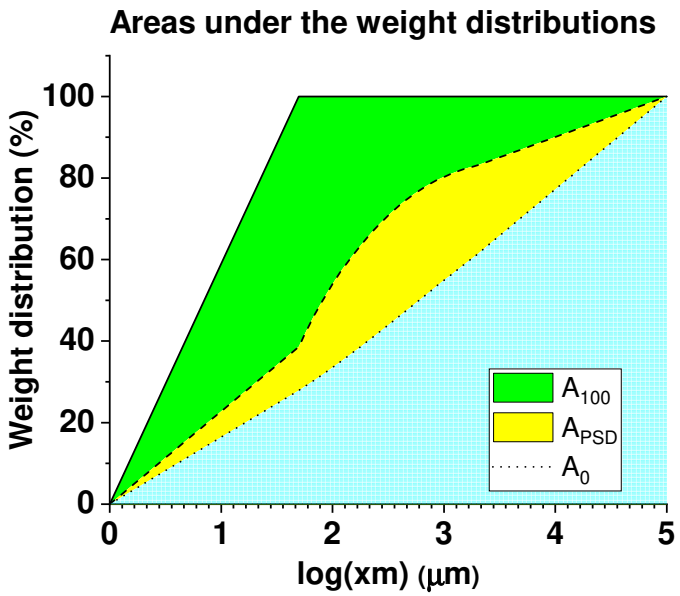

Figure 3.4. Area under the weight distributions

The homogeneity factor can then be calculated as percentage using Eq. 3.6.

$$FH\ (\%) = 100 - \ 100 * \left(\frac{\int w_{PSD}(xm)dx - \int w_0(\mathrm{xm})dx}{\int w_{100}(\mathrm{xm})dx - \int w_{PSD}(\mathrm{xm})dx}\right) \quad \rightarrow$$

$$FH\ (\%) = 100 - \frac{A_{PSD} - A_0}{A_{100} - A_0} * 100 \qquad \text{Eq. 3.6}$$

A summary of the methodology can be found in a flowchart in Figure 3.5.

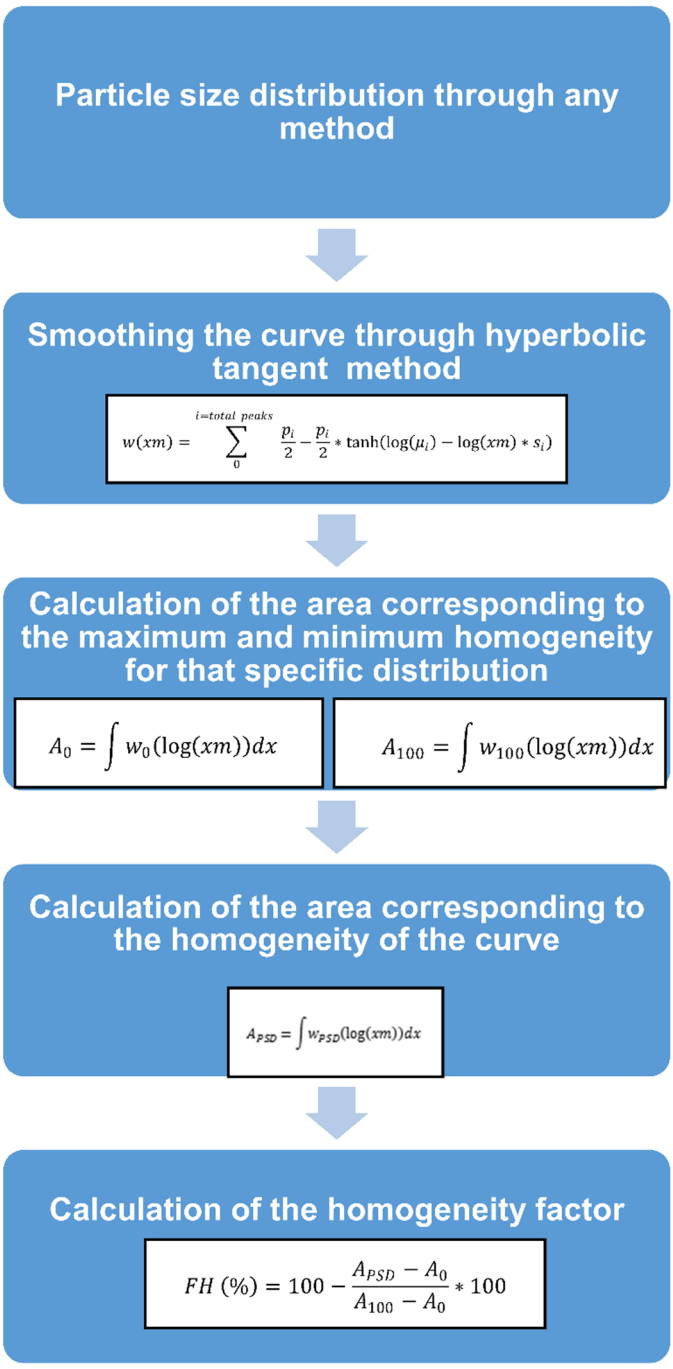

Figure 3.5.Methodology flowchart

3.3.2 Verification of the methodology

According to Eq.3.2, the homogeneity factor is sensitive to changes in factors such as the number of the peaks or the width of the distribution. The methodology was verified through comparing the response of different simulated distributions with volumetric mean diameter equal to 1000 μm.

In the first case (Figure 3.6a), the effect of modification of the distribution shape was studied through the increase of the standard deviation of the distributions from 0.1 to 0.25. The increase of the standard deviation in a unimodal distribution produced a direct change in the width of the distribution, and as Figure 3.6a shows that affects directly in the FH. Additionally, Figure 3.6e shows the trend for greater increases in the standard deviation.

In the second case, the effect of introducing a peak (Figure 3.6b) and three peaks (Figure 3.6c) can be studied in two different widths. The effect of introducing a new peak produced a fall in the homogeneity as the initial homogeneity is considerably lower than that corresponding to a single peak for both widths. Figure 3.6f shows the effect of the increase of number of peaks from a unimodal distribution with a standard deviation of 0.25 to five peaks in the same width. As it can see, the addition of peaks produces dramatic falls in the homogeneity.

In the last case (Figure d and g), the distance between peaks was studied. The FH is sensitive to the introduction and distance between peaks as the two peaks are far apart showed a lesser degree of homogeneity than when they were closer (Figure 3.6d).

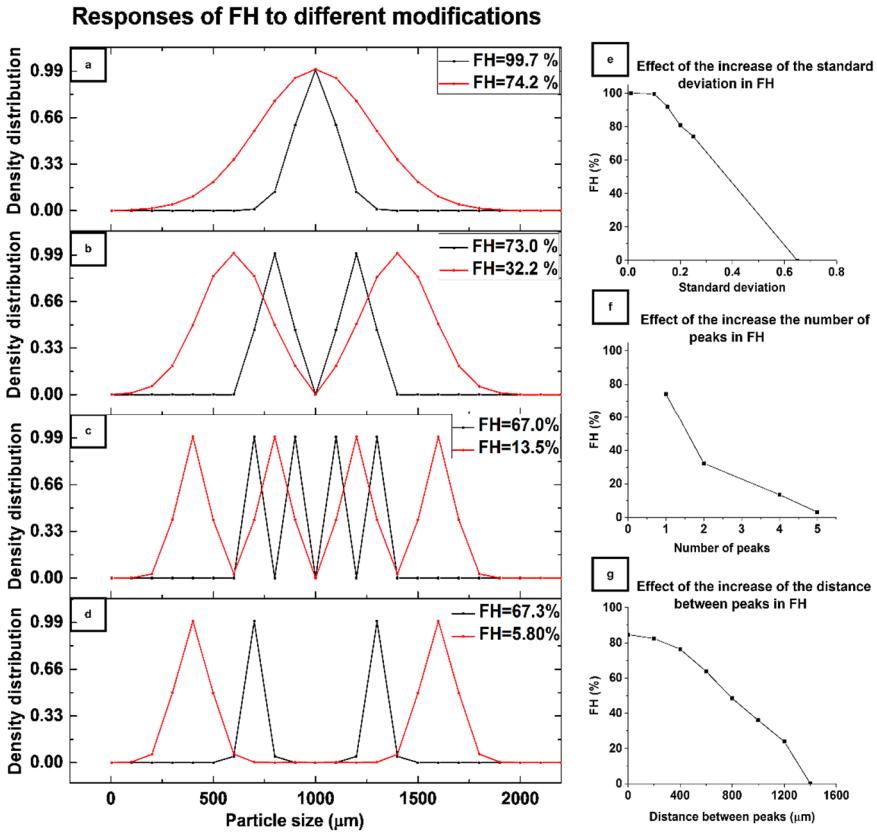

Figure 3.6. Study of the effect of the deviations produced by a change in the amplitude of the peak (a, e).

Other factors which will affect the FH are the distance between the volumetric mean diameter and the main peak. Those cases in which the diameter is situated

around the main peak will have greater homogeneity than those in which the diameter is more distant.

To illustrate this the analysis was applied to three different real samples (see Figure 3.7) where the homogeneity varied from 0 to 75%. In the first case (Figure 3.7a) homogeneity is negligible (0%), since the sample has three main classes of particles with two of them with similar intensity in the density curve. However, the volumetric mean diameter (VMD) is skewed by a greater percentage of fines which reduces dramatically the homogeneity. In the second case (Figure 3.7b), there are again three classes of particles but even if the width is bigger than in the other cases, the mean diameter is placed closer to the middle of the three peaks. Therefore, the sample is more homogeneous than previous case as the VMD is closer to the biggest peak (38.3%). In the third case (Figure 3.7c), the PSD shape is more similar to a lognormal distribution suggesting the product is more homogeneous (74.8%). In this example, most of the particles have the same diameter. This can be observed from the PSD as well as from the photographs (Figures 3.7a-c).

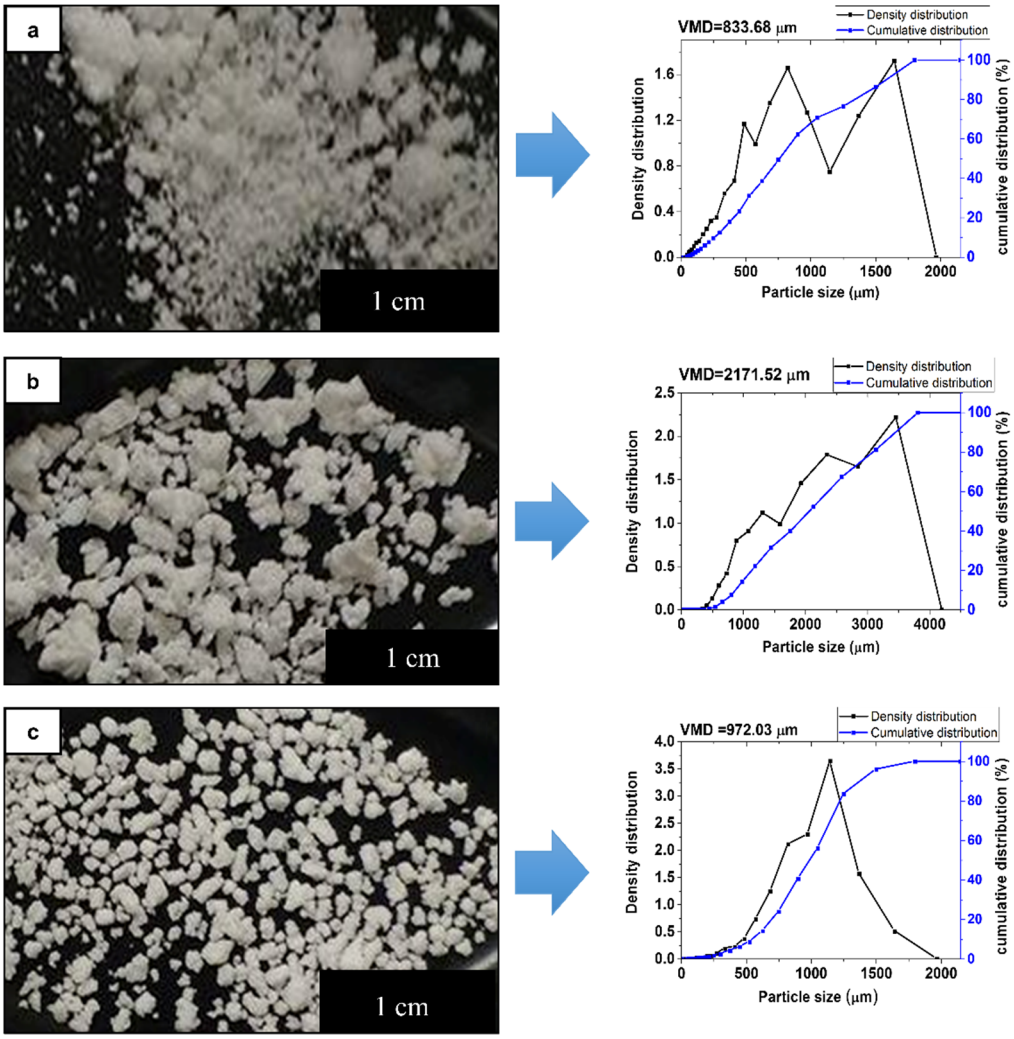

Figure 3.7. Granules with homogeneity 0% (a), 38.3% (b) and 74.8% (c).

3.3.2 Application of the methodology

The methodology was applied to granules produced in the TSG with two different excipients commonly used in pharmaceutical processing, α-Lactose monohydrate and microcrystalline cellulose, in a wide range of conditions. The results allow understanding of the influence different parameters have on the product homogeneity.

The results obtained were presented through contour profiles (Figure 3.8 and 3.9). These types of graphs are really effective for summarising entire workspaces. On one hand, once the region of the desired diameter has been located, the operational conditions which produce the most homogeneous granules for that exact diameter can be easily determined. On the other hand, the contour profiles allow examination of the effects that operational parameters have over the chosen variables. For instance, on a workspace created by changing the value of two parameters, it is possible to identify if the response of the variable has been controlled by only one or both operational parameters. That effect would be noticed since the variable would change linearly and proportionally to the axis of the most relevant parameter. In those cases, that the system would vary depending of both parameters, the response of the variable could adopt different shapes such as slanting or curved lines.

As it can be observed in Figure 3.8, granules of α-Lactose monohydrate were produced using different conditions of liquid/solid (L/S), feed rate and torque velocity. The results show that at low torque velocities (Figures 3.8 a and b), the diameter shows higher dependence on the feed rate than the L/S ratio. The larger granules are produced when the feed rate is reaching the maximum with

a high ratio of homogeneity and it can be observed that homogeneity of the process is more influenced by the feed rate than by the L/S ratio.

At high torque velocities (Figures 3.8 c and d) homogeneity decreases with respect to the low torque velocities. The maximum homogeneity for this case does not reach 70% and the greater diameter which homogeneity over 50 % is not bigger than 1600 μm. On the contrary to low torque velocities, homogeneity and diameter displayed a nearly equal dependence for both parameters: L/S and feed rate. The production of homogeneous granules is achieved when the feed rate and the L/S ratio are at middle point conditions of the range of operation. At the same time, the diameter increases proportionally to both. For instance, Figure 3.8 d would give a range of operational conditions which produce a target granule diameter. The most adequate parameters to produce a homogeneous product would be found in the Figure 3.8c, corresponding to a proportion to L/S ratio to feed rate close to 1.3 to 1.

Besides, comparing low torque velocities (Figures 3.8 a and b) with high torque velocities (Figures c and d), it can be concluded that for α-Lactose monohydrate the degree of filling of the screw is a very important factor. At low torques velocities, high degrees of filling are achieved and the system is more dependant of the amount of powder introduced. At higher velocities, the degree of filling

is considerably lower and the system requires a balance between both parameters to obtain a desirable product.

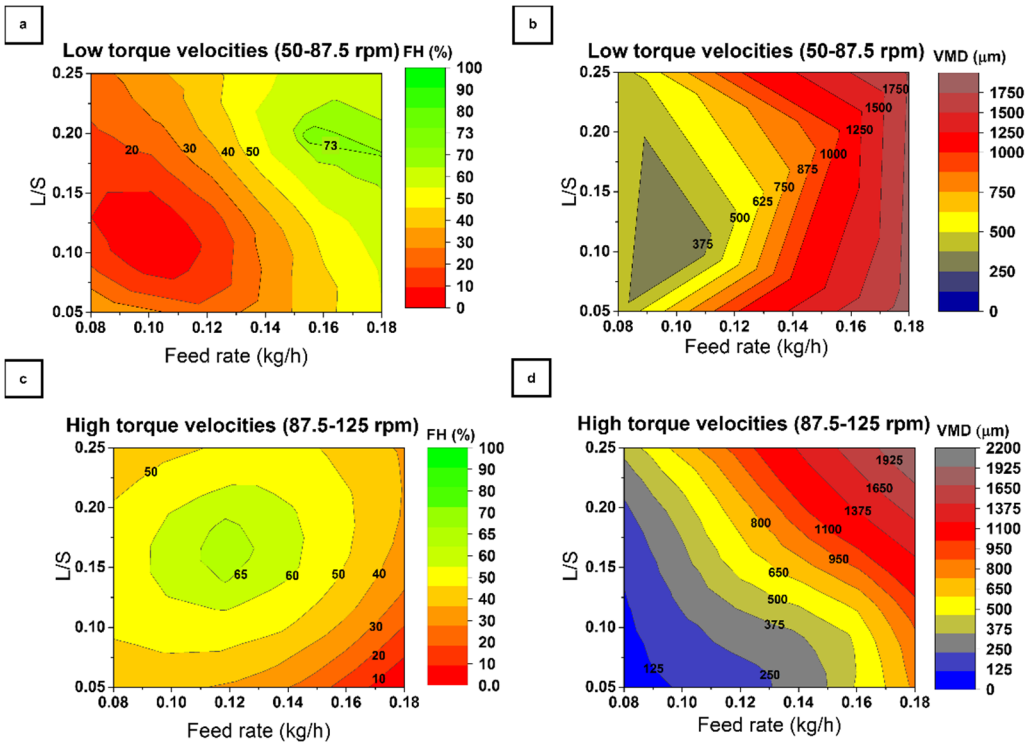

Figure 3.8. Homogeneity and diameter contour profiles for α-Lactose monohydrate low torque velocities (a,b) and high torque velocities (c,d)

Granules of microcrystalline cellulose were produced in an identical manner and the results are presented in Figure 3.9. Unlike the previous example, the diameter profiles (Figures 3.9 b and d) show nearly equal dependence to both parameters L/S ratio and feed rate in both cases of torque velocity. However, there is a great difference between the diameters of the particles resulting in granules up to seven times larger than when the system is operated at low torque velocities.

On the contrary, homogeneity (Figures 3.9 a and c) shows greater dependence to the L/S ratio than to feed rate. Furthermore, at L/S ratios above 1.52, the product reaches homogeneities of over 50% in both cases. Comparing the differences between contours profiles at low and high torque velocities indicates that the degree of filling is one of the main factors to take into account in the cellulose microcrystalline example as the low torque velocities show more disturbances than the high torque velocities.

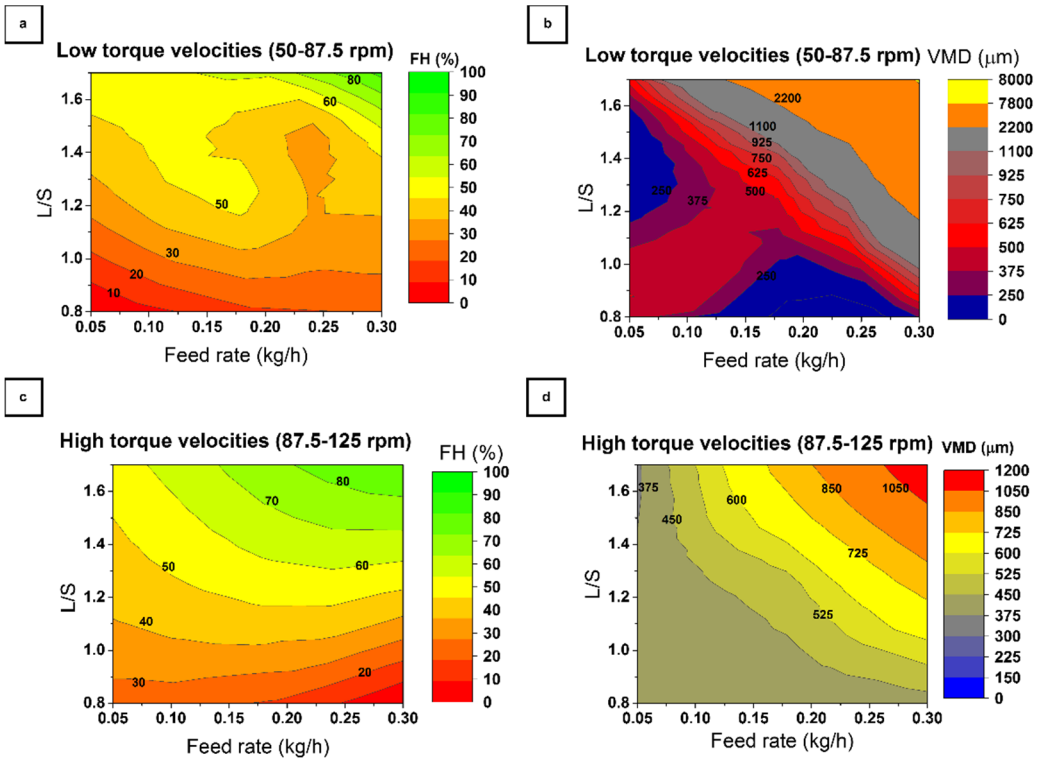

Figure 3.9. Homogeneity and diameter contour profiles for microcrystalline celulose low torque velocities (a,b) and high torque velocities (c,d)

In addition to the study individual effects, a comparison between Figures 3.8 and 3.9 permits appreciation of the strong behavioural differences between both materials. The growth of both microcrystalline cellulose and α-Lactose monohydrate granules depends dramatically on the L/S ratio, feed rate and torque velocities. Microcrystalline cellulose displays a dramatically greater dependence to the amount of liquid present in the system than α-Lactose monohydrate. This effect agrees with the molecular differences of both materials and the capability of microcrystalline cellulose to physically hold higher amounts of water than α-Lactose monohydrate (Fielden et al., 1988). In addition, these results agree with the outcomes reported by Dhenge *et al.*, where larger granules were also found at the higher L/S ratios (Barrasso et al., 2013, Dhenge et al., 2010). Furthermore, it was described that an increase in powder feed rates reduced the number of peaks in the PSDs (Dhenge et al., 2011), which corresponds with the increase of homogeneity reported in the case of low torque velocities for both materials. Although the most homogeneous product for the studied range were obtained, not all the experimental results can be entirely compared with those presented in the literature due to the crucial role of the screw elements configuration.

However, this and published studies all present similar responses to the modifications of the operational parameters as well as similar range of diameters of granules which indicates the validity of this proposed analysis method.

Furthermore, this analysis identified the degree of filling as a limiting operational parameter for both materials which will require to be measured quantitatively in further studies of the equipment.

3.4. Conclusions

A new methodology for measuring homogeneity of particle size distribution was introduced and validated through its use in two different cases of granulation. The method is able to calculate the homogeneity of PSDs with different shapes allowing easy numerical comparison. The method responded to different modifications such as the addition of peaks, increments on the variation of the distribution or discrepancies between the main diameter and main particle size class. The improvement of this method with respect to the traditional measures such as span was demonstrated through the comparison of PSD curves with different shape but similar span. In addition, the potential of the quantification of homogeneity was demonstrated through the application to simple liquid granulation with two different excipients. In both cases, it was demonstrated that knowing the diameter individually does not give enough information for the ideal conditions to operate or which operational parameters have more influence on the process. Therefore, using homogeneity as a quantified quality attribute leads to a better understanding of powder technology and its possible implementation as characterisation tool in the design and control of wet granulation systems. Future work will involve the study of this tool as process control variable through a sensitivity analysis in an inline process analytical technique.

Chapter 4

Development of an algorithm to analyse inner granule structures

4.1 Introduction

One of the less studied topics in twin screw granulation is the internal structure of granules. Most of the previous studies have focused on the cause-effect relationships between factors and formulation properties leading to probabilistic and validated modelling methods (Barrasso et al., 2013, Kumar et al., 2016a, Kumar et al., 2015). Whilst these studies have provided useful information about production process of granules, they are limited in providing data about the effect

of the parameters on the interior granule structure. Verstraeten et al. stated the bimodal size distributions are mainly due to the limited availability of granulation liquid and there is a significant difference in the mechanisms between batch and continuous (Verstraeten et al., 2017). Therefore, obtaining more information about the morphological differences within nuclei, will lead to an increase and deepened understanding of the underlining mechanisms occurring in granulation.

One of the techniques which allows the visualization the inner core of a granule is X-ray Computed Tomography. Although the commercial software reconstructions allows the measurement of simple core properties, it does not allow recognition or visualisation of individual nuclei (Oka et al., 2015). In order to measure all the morphological properties, the nuclei need to be isolated and extracted from the granule and be treated as its own entity.

For isolating the nuclei inside the granules, an algorithm has been developed allowing mathematical extraction of selected parts of the cross-sectional images. Before removal, the algorithm recognises all the clusters inside the granule measuring their volume and density. Once this analysis has concluded, it is possible

to separate the desired structures of interest from the original images. Furthermore, they can be rendered with a volume viewer application to be visualised in space and study of the morphological properties.

In this chapter, the development and validation of the algorithm has been discussed as well as its application to different granules produced in both high shear wet granulator (HSWG) and twin-screw granulator (TSG).

4.2 Materials and methods

4.2.1 Granules production

Granules of α-lactose monohydrate with 99% total lactose basis (Sigma-Aldrich Company Ltd., Dorset, England) were produced in both continuous and in batch at the same liquid-to-solid ratio of 0.16. The granules in batch were produced using a high shear wet granulator (Glatt GmbH, Binzen, Germany) introducing 150 grams and using an agitation speed of 600 rpm and a chopper speed of 300 rpm adding the liquid by dropping. The granules in continuous were produced using the same setup than the described in section 3.2.2 operating at 75 rpm in combination with a gravimetric feeder operating at 0.15 kg/h ad L/S=0.175 which according to the workspaces in figure 3.9 will produces an almost unimodal distribution. Distilled water (EMD Millipore™ Pure Water Reservoirs, Millipore SAS, Mosheim, France) was fed to the system through a syringe pump (Harvard Syringe Pump, Harvard Apparatus UK, Cambridge, UK). The screws were composed by all conveyor elements. This configuration was chosen to maintain a constant available space for the granulation. The granules were collected and dried at room temperature in a single layer over a stainless-steel tray. The samples were sieved afterwards and the fractions analysed in X-ray computerised tomography were 0.85-1 mm for continuous (TSG) and 2-6 mm for batch

(HSWG) which corresponded with the greatest peaks fraction in the particle size distribution (Figure 4.1)

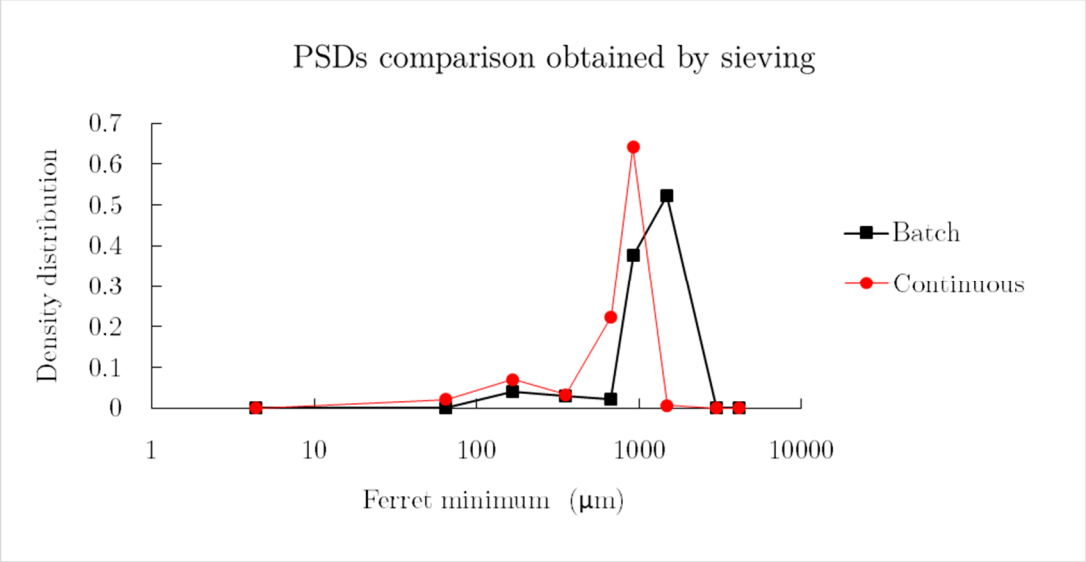

Figure 4.1 PSDs comparison obtained by sieving

4.2.2 X-ray computerised tomography

X-rays is a type of electromagnetic radiation which is capable to imaging a body by passing through it. Since the absorption or scattering of the X-Rays beam is dependent on the material, it is possible to obtain a projected image where each pixel is the attenuation coefficient defined from Lambert-Beer's Law. Although conventional X-ray radiography analyses the object from one angle, computerised X-Ray tomography is able to generate cross-sectional images by rotating the sources and the detectors around the body. The projections are obtained in different angles and reconstructed by a back-projection algorithm creating three-

dimensional images without destructing the sample (Jacobs et al., 1995, Florence and Siepmann, 2009, Wong et al., 2014).

In this case, computerised tomography (CT) was performed to α-lactose monohydrate granules in a multiscale X-ray nanoCT with cone-beam arrangement (SKYSCAN 2211D, Bruker LTD, Coventry, United Kingdom). Therefore, it will provide a reconstruction of internal microstructure of the granules as well as images of individual slices of the granule. The samples were scanned with an image pixel size of 1.4–4 µm, frame averaging of 8 and a rotation step size of 0.3 °. The X-ray acceleration voltage was set to 40 keV producing 647 projections.

4.2.3. Development of the technique

X-ray CT images were processed using the commercial software package Matlab and Statistics Toolbox R2017a with Image processing package. (The MathWorks, Inc., Natick, Massachusetts, United States).

4.2.3.1 Image segmentation

Image segmentation can be described as subdividing an image into its essential parts in order to extract their regions of interest (Zhang, 2006). The automation of this process is one of the most critical parts of image analysis as it will affect all the subsequent processes. In this case, the dataset is a stack of individual

images of the plane xy (figure 4.1a) which are separated by 1.4 μm in the plane z. Each individual image is cropped to isolate the studied granule (figure 4.1b).

The cropped images in greyscale are transformed to a binary matrix where the values are replaced by ones (i.e. white) and zeros (i.e. black) using Otsu method (Liu and Yu, 2009). This technique classifies every pixel in two types depending if they are over (foreground) or below (background) a determined threshold pixel intensity. The threshold will be the one which minimizes the intra-class variance and maximises the inter-class variance. This technique does not require any prior knowledge to analyse the image which will standardize and simplify the process (Otsu, 1979). However, the threshold will not be calculated directly in the image as this one undergoes firstly under a contrast enhancement function known as contrast-limited adaptive histogram equalization (CLAHE). This method divides the image in eight not-overlapping regions (tiles) and produces individual histograms of pixel intensity with 256 bins. After this division, each histogram will be transformed according to the surrounding areas embedded in the tile. However, this method includes a clip limit which limits the transformation of the histograms to avoid over enhancement of the picture noise in homogeneous coloured areas. This parameter is calculated as a function of the total number of the greyscales and the number of pixels (Pizer et al., 1987,

Robinson et al., 2009). These steps correspond with the changes from figure 4.2b to 4.2d. Afterwards, the contrast of the image has been enhanced (In figure 4.2c) and finally transformed to binary (figure 4.2d) which was found visually representative of the original figure.

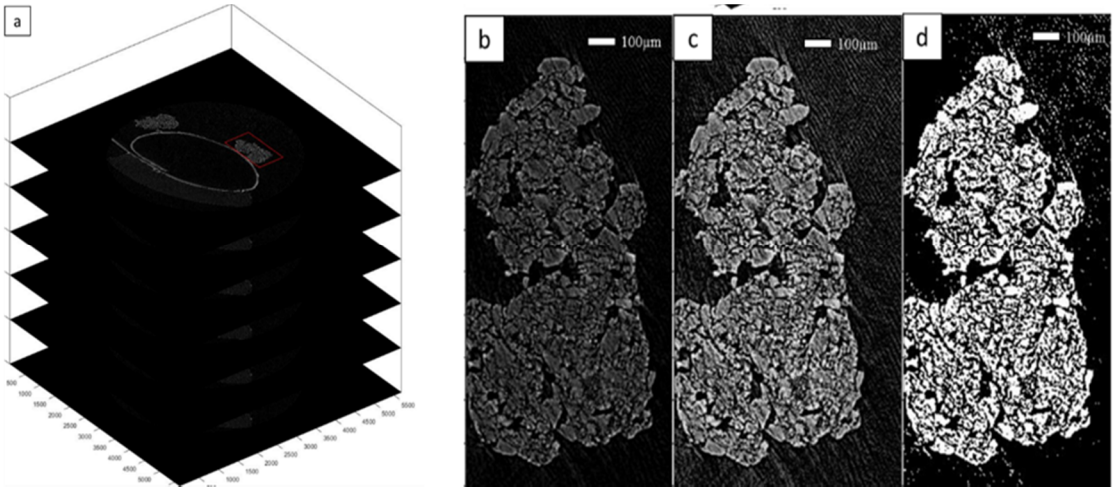

Figure 4.2. Extraction of the image from the a) images stack b) image extracted c) contrast enhancement and d) transformed to binary.

Despite the previous contrast treatment, certain amount of unwanted blank pixels are created during the transformation to binary giving as a result figure 4.3a. Since the filling algorithm does not make a distinction between blank pixels produced by insufficient contrast in the area or background blank pixels it is necessary to perform extra operations in order to fill only the first blank pixels. Since all the images are matrix of zeros and ones, the following operations were performed using them as mathematical entities and they were identified by the

letter M with a subindex from 1 to 6. In table 4.1, the correspondence between matrix and figure are specified.

Table 4.1. Operations performed to the figures with matrix identifier associated

Matrix identifier	Figure	Operation performed
M1	Figure 4.3a	Original
M2	Figure 4.3b	M1 after all blank pixels are filled
M3	Figure 4.3c	M2 -M1
M4	Figure 4.3d	Blank areas under 1000 pixels eliminated from M3
M5	Figure 4.3e	M4-M3+M1
M6	Figure 4.3f	All the blank areas under 50 pixels from M5 eliminated

Therefore, all the blank pixels were filled (M2), and extracted from by subtracting M2 -M1 (figure 4.3b to 4.3a) giving as a result M3 (figure 4.3c). Afterwards, all the blank pixels under 1000 pixels (similar value to the average of areas in the figure) were eliminated from M3 (figure 4.3c) resulting in M4 (figure 4.3d). Then, the small blank pixels which corresponded with those produced by insufficient contrast were calculated subtracting M4 (figure 4.3d) from M3 (figure

4.3c) and added to M1 (figure 4.3a) producing M5 (figure 4.3e). M5 (figure 4.3e) will be morphologically treated to delimit the borders of the particle depending of the chosen bridge condition. This operation will allow to remove all the detected areas under 50 pixels which in this step will correspond with unwanted noise. The resulting figure will be the final binary image further used for segmentation M_6 (figure 4.3f).

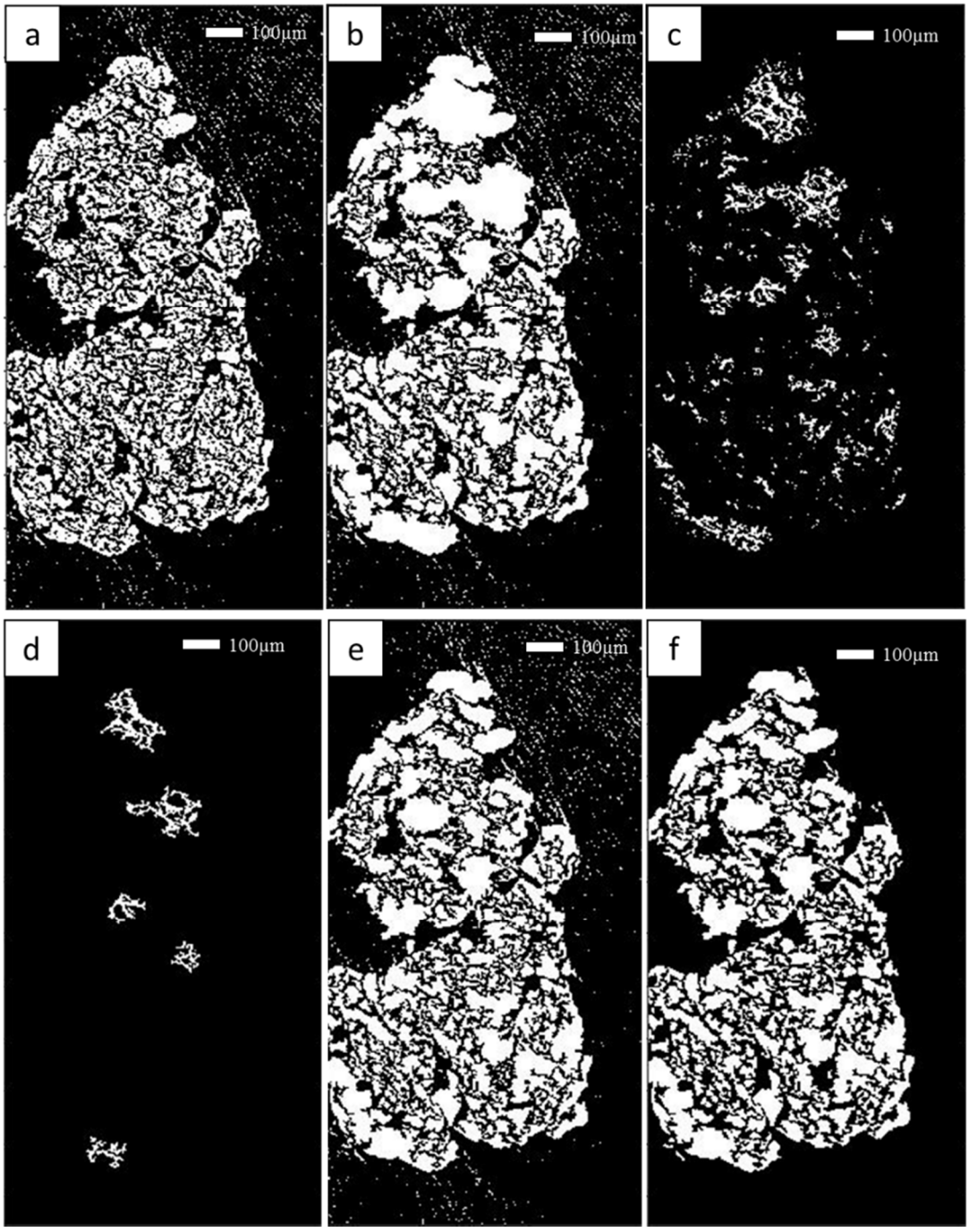

Figure 4.3 Evolution of the binary of the image to complete the segmentation. a) image in binary b) all holes filled c) all holes isolated d) holes over 1000 pixels of area isolated e) image in binary with filled holes under 1000 pixels of area f)final

The delimitation of the particle borders is one of the critical decisions for segmentation which will affect how the particles are being separated. For that, it is necessary to define the size of the bridge between regions. As pixels in a binary image are represented by ones and the background by zeros, the bridge can be defined as a matrix of zeros and ones, hence varying the size and number of ones in the matrix will change the size of the bridge. Each number will correspond with a pixel and the size of each pixel which is in this case 1.4 µm.

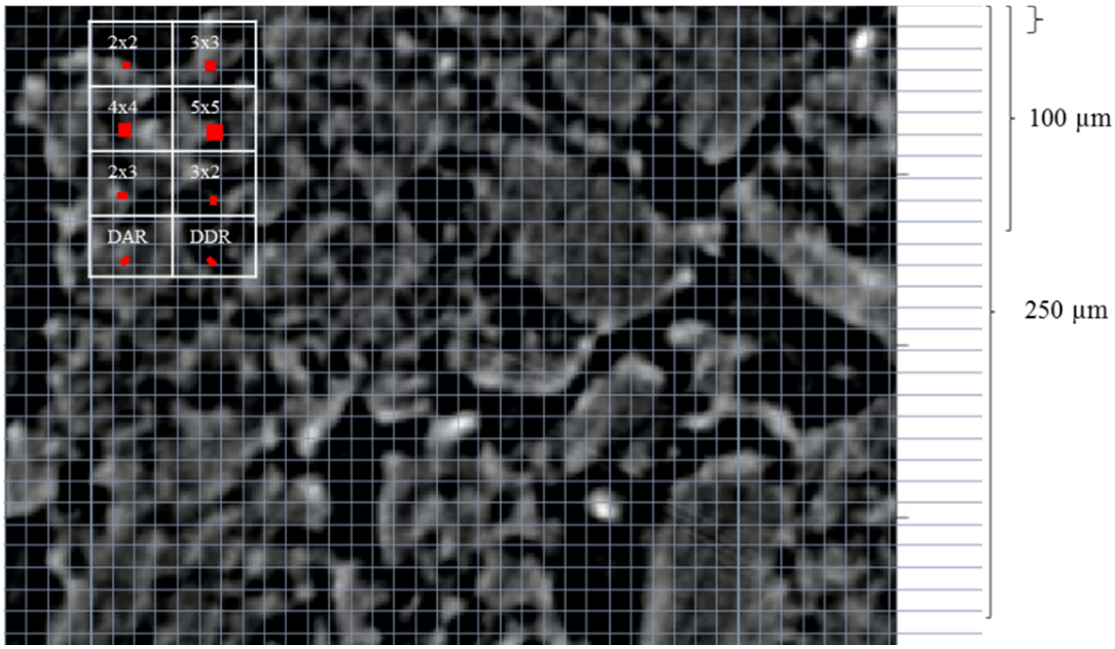

Figure 4.4.Matrix of ones in scale over an image.

In table 4.2, the matrixes corresponding to figure 4.4 are shown.

Table 4.2. Different possible bridges in matrix of ones and zeros

2x2 ones matrix Maximum length=4.2 µm// Area=7.84 µm² $\begin{pmatrix}1 & 1\\1 & 1\end{pmatrix}$	3x3 ones Maximum length=7µm// Area=17.64 µm² $\begin{pmatrix}1 & 1 & 1\\1 & 1 & 1\\1 & 1 & 1\end{pmatrix}$
4x4 ones Maximum length=9.8 µm// Area=31.36 µm² $\begin{pmatrix}1 & 1 & 1 & 1\\1 & 1 & 1 & 1\\1 & 1 & 1 & 1\\1 & 1 & 1 & 1\end{pmatrix}$	5x5 ones Maximum length=12.6 µm// Area=49µm² $\begin{pmatrix}1 & 1 & 1 & 1 & 1\\1 & 1 & 1 & 1 & 1\\1 & 1 & 1 & 1 & 1\\1 & 1 & 1 & 1 & 1\\1 & 1 & 1 & 1 & 1\end{pmatrix}$
2x3 ones Maximum length=5.6 µm// Area=11.76 µm² $\begin{pmatrix}1 & 1 & 1\\1 & 1 & 1\end{pmatrix}$	3x2 ones Maximum length=5.6 µm// Area=11.76 µm² $\begin{pmatrix}1 & 1\\1 & 1\\1 & 1\end{pmatrix}$
Diagonal ascendant right 4x3 Maximum length=8.4 µm// Area=11.76 µm² $\begin{pmatrix}0 & 0 & 1\\0 & 1 & 1\\1 & 1 & 0\\1 & 0 & 0\end{pmatrix}$	Diagonal descendant right 4x3 Maximum length=8.4 µm// Area=11.76 µm² $\begin{pmatrix}1 & 0 & 0\\1 & 1 & 0\\0 & 1 & 1\\0 & 0 & 1\end{pmatrix}$

The matrix chosen as a bridge has to be a balance between definition and resemblance to the original shape (figure 4.5). When small size matrixes are used, the probability of having at least one bridge is very high and therefore, the number of regions decrease (figure 4.5b). Larger size matrixes will produce the

opposite result, increasing the number of regions and reducing definition of the shape (figure 4.5d and e). In this case an intermediate value of 6-ones matrix which was tried in the different directions (figure 4.5.4f, g, h and i). It was concluded that the direction of the matrix did not have a stronger visual impact in the final results and therefore, a matrix of ones 2x3 was used as a bridge. The most common method for evaluating effectiveness of a segmentation method is a subjective visual evaluation of the results since there is no yet an objective indicator for image segmentation (Zhang et al., 2008(Buenestado and Acho, 2018)). In this case, this bridge presented a compromise between considering as much links as possible within the granule component and reducing possible interferences of noise in the picture and remains the original shape of the granules

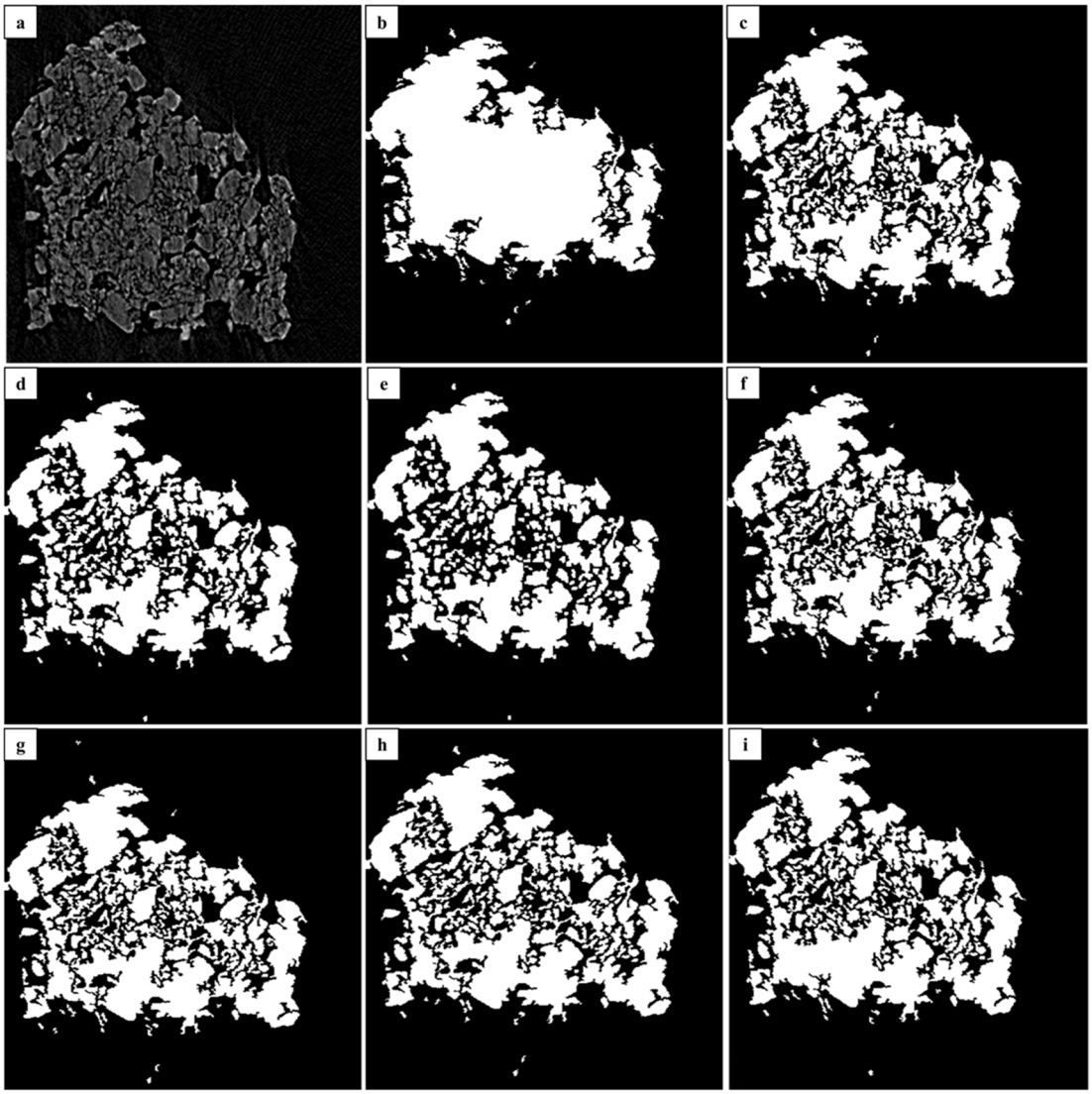

Figure 4.5. a) original and matrix of ones size of b) 2x2 c) 3x3 d) 4x4 e) 5x5 f) 2x3 g) 3x2 h) Diagonal ascendant right i) Diagonal descendant right.

After the previous steps, all the different regions in the image will be solid without any background points within the delimited boundaries, however, to avoid further issues in the segmentation, an extra condition was added to the algorithm in order to ensure this condition is always true. The segmentation used in this case is the watershed transformation which consists in four different steps

(Beucher, 1992). In the first step, the distance function creates a gradient for the inverted binary image (i.e. zeros will become ones and vice versa) calculating the distance from every pixel (zero) to the nearest nonzero-valued pixel. The calculation of this gradient can be performed in different ways depending how the connection of the elements is defined (Paglieroni, 1992). In order to be able to respect the delimited boundaries of the particles during the segmentation, it was chosen the chessboard distance function which will locate the nearest non-zero-value in horizontal and vertical but not in diagonal. In figure 4.6a the result of this calculation can be seen where the darkest points are those further for any white pixel. The second step is to calculate the geodesic zones of influence of each set of points within of a delimited region, i.e. the shortest path between the points of each region to any of the darkest points embedded in that region. Afterwards, all the regional local minima will be found and the image will be manipulated to ensure that the segmentation is only done to the foreground particles and not to the background, i.e. limiting the area of influence (figure 4.6b). Once this manipulation has been made (figure 4.6c), it is possible to apply the function watershed which will isolate each region assigning each point within its boundaries to its corresponding regional minimum. The final images can be

seen in figure 4.6d and 4.6e which are equivalent. Image 4.6e has been transformed to colour format in order to help to visualise easily the separation between regions by the pixels will be in the same position and number than 4.6 d. This process will be applied to all the images of the stack obtaining a new set of segmented images in which each individual image will have delimited labelled regions.

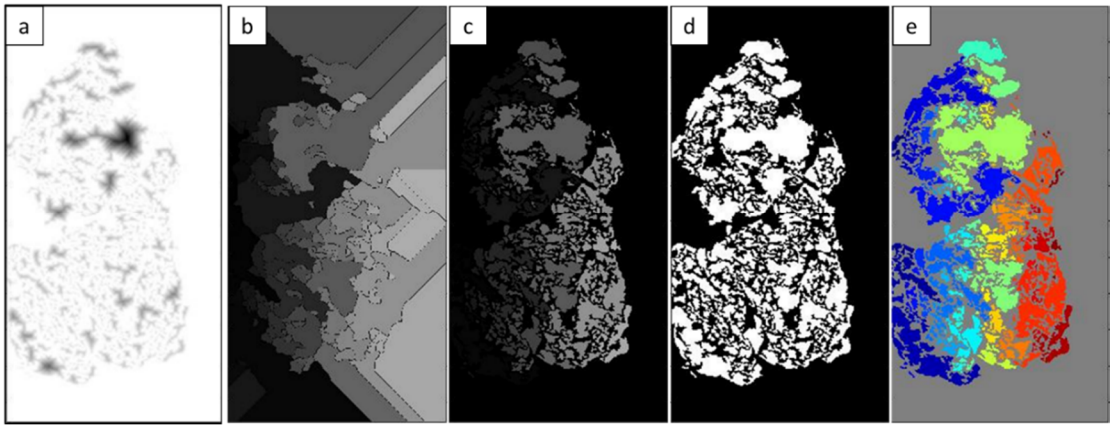

Figure 4.6. Watershed transformation a) Distance transformation performed b) Geodesic distance transformation before limiting the area of influence c) Geodesic distance transformation after limiting the area of influence d) final segmented image and e) coloured final segmented image.

4.2.3.2 Tracking algorithm: Location and identification of the clusters within the granule

Once the images have been segmented, the location and identification of the volumetric clusters is performed by tracking regions in the plane xy of a slice

and analysing how they are connected to the adjacent image in the z axis (figure 4.7).

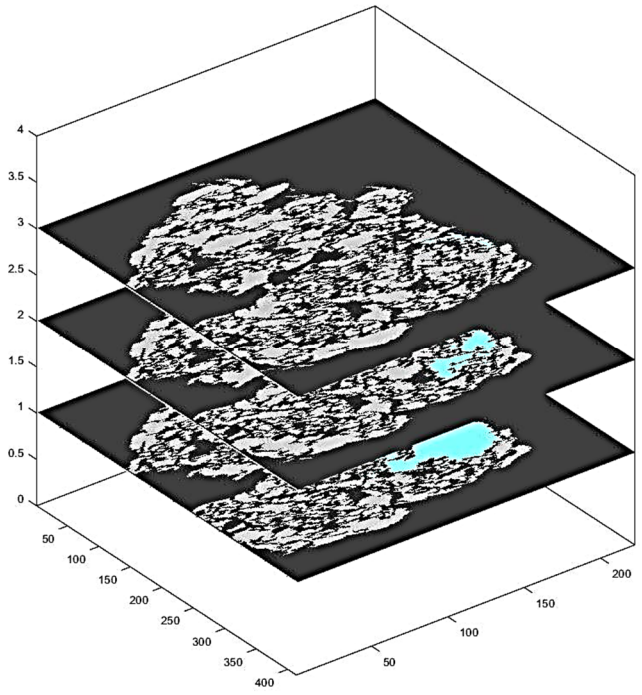

Figure 4.7. Tracking of a region of interest along z axis.

Therefore, it is required to define the possible situations that the region of interest undergoes from one image to the following one. Since the regions are relabelled for each image, it is necessary to record both the label and the individual properties before the next image is analysed. However, to perform the tracking analysis, the regions need to have a unique label along full z axis, i.e. if the continuity between two consecutive images is demonstrated, the region in the following picture adopts the original label, the properties are updated and a record of the original region is saved. This is made through a table which will

save shape properties such as maximum and minimum length, area, eccentricity, and orientation as well the centroid of the region and the number of the images analysed. All the shape properties are calculated using *regionprops* from Matlab Image Analysis Toolbox (MathWorks, 2018), where the centroid is defined as the centre of mass of the region and it will be unique to each region.

In the transition of images, the same region can undergo by seven different situations: remain, increase or decrease in size, split into one or more regions, merge with another region, appear or disappear.

The simplest cases are when the regions slightly increase, decrease area or remain the same which is called category one. In those cases, the centroid of the region in the following image remains close or the same to the original centroid and the new label is erased and the information of that particle is added to the original one. This is similar to the behaviour that the slices of a perfect sphere would have. Moving along z axis would cause the diameter become larger or smaller remaining the same centre (figure 4.8).

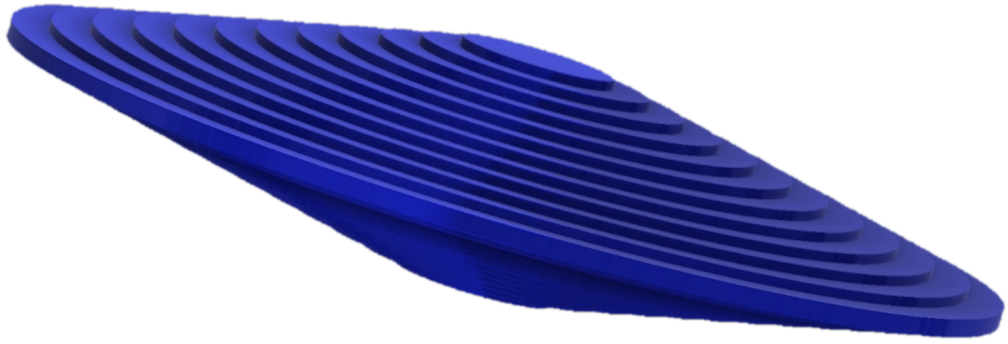

Figure 4. 8. Concentric circumferences of different radios along z axis

If instead perfect concentric circumferences, the volume was an oblate spheroid with irregular surface, the centre would move slightly around along the axis z.

However, it always will comply with the condition that the distance between the centres of two following planes would be smaller than the ratio of the circumference. This distance can be calculated using Pythagoras theorem and when this condition is met (figure 4.9a), the region is considered the same, and the new centroid label will adopt the original label. In those cases, that the new centroid does not meet the condition (figure 4.9b), the new centroid will further analyse by another condition.

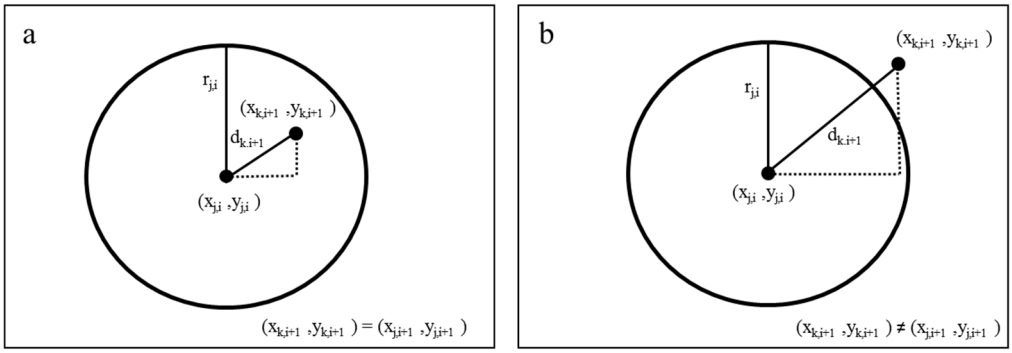

Figure 4.9.New centroid point distance to the old centroid a) meeting condition b) no meeting condition

Therefore, category one can be described as:

$$\forall \{x_{j,i}, y_{j,i}\} \in Z_i \, \exists \, r_{j,i} = \left(\frac{A_{j,i}}{\pi}\right)^{0.5}$$

$$\forall \{x_{j,i}, y_{j,i}\} \in Z_i \, , \forall \{x_{k,i+1}, y_{k,i+1}\} \in Z_{i+1} \, \exists \, d_{k,i+1} = \sqrt{\left(x_{j,i} - x_{k,i+1}\right)^2 + \left(y_{j,i} - y_{k,i+1}\right)^2}$$

$$if \; d_{k,i+1} \leq r_{j,i} \; \rightarrow \; \{x_{k,i+1}, y_{k,i+1}\} = \{x_{j,i+1}, y_{j,i+1}\}$$

Equation 4.1

Being: $x_{j,i}$,$y_{j,i}$ *: coordinates x and y of the centroid*

$x_{k,i+1}$,$y_{k,i+1}$ *: coordinates x and y of the centroid*

j: index corresponding to centroid labels set from Z_i *(j=1: total number of centroids in set)*

k: index corresponding to centroid labels set from Z_{i+1} *(k=n+1: total number of centroids in set)*

Z_i*: set of points of image i*

Z_{i+1}: *set of points of image i+1*

$r_{j,i}$: *equivalent radio of the circle for centroid of coordinates* $x_{j,i}$,$y_{j,i}$

$A_{j,i}$: *equivalent area of the circle for centroid of coordinates* $x_{j,i}$,$y_{j,i}$

$d_{k,i+1}$ *: distance between centroid of coordinates* $x_{j,i}$,$y_{j,i}$ *of image* Z_i *and centroid of coordinates* $x_{k,i+1}$,$y_{k,i+1}$ *of image* Z_{i+1}

However, the regions of a granule presented very irregular shape and the radio required to search for the centroid can be overestimated if a circular shape is assumed. However, the software provides the longest and smallest distances within a region and a restriction could be introduced to overcome this issue. In those cases that the aspect ratio (minor distance/major distance) was greater than 0.8, the area to calculate the radio was considered 60% of the real one of the regions and the shape was consider a circle. In those cases that the aspect ratio was less than that, the region was consider to elongated to a direct calculation and it was hard-coded to 15 pixels (21 μm) for pixel size between 0.8-1.5 μm. When the area has increased or remains the same from the previous image it falls under the first case and when the area decreases, it falls under the second case of the category one.

The second category is when two regions split in two or more regions (figure 4.10). In this case, the centres of the new regions are not aligned to the original

one although they still belonging to the same region and the nucleus will be incomplete without these ramifications. This can be seen as the branching of a plant in which a limb split in two or more. Essentially, they remain part of the same branch but they will show different regions for all the following images.

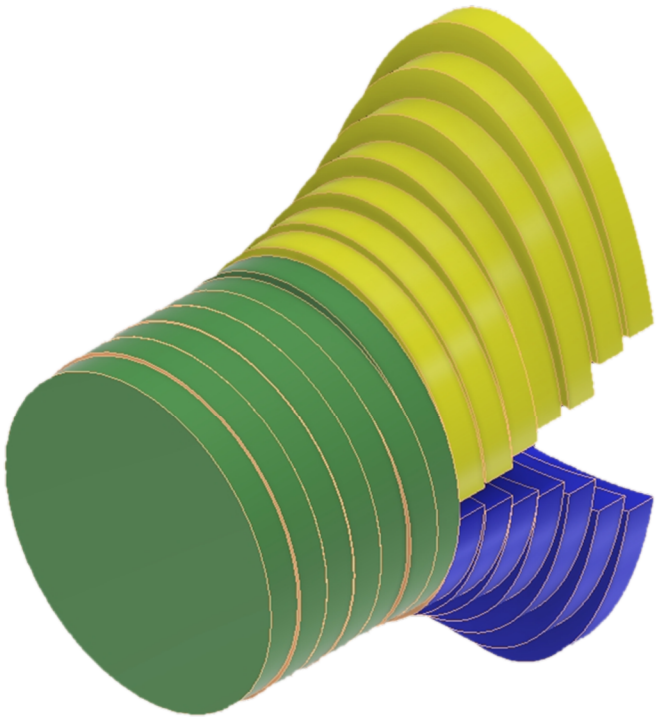

Figure 4.10. Split condition

In order to track this case, firstly it is required to create an equivalent ellipse to the original region with the same orientation and eccentricity to the original region. In figure 4.11, an ellipse has been defined according to equation 4.2.

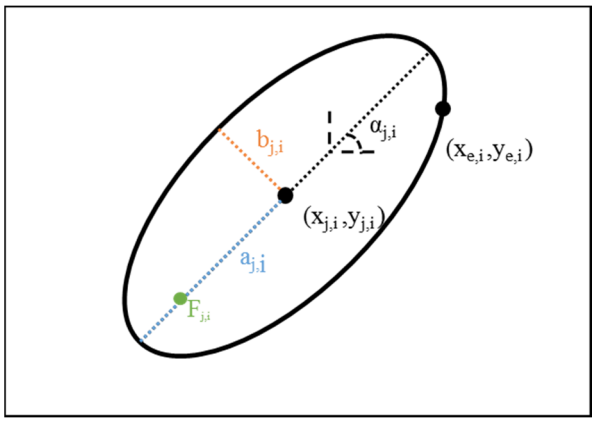

Figure 4.11. Ellipse

Where $\{x_{j,i}, y_{j,i}\}$ is the centroid coordinates, $\{x_{e,i}, y_{e,i}\}$ is any point of the ellipse, $\alpha_{j,i}$ is the angle of rotation, $b_{j,i}$is the minimum length axis of the ellipse and $a_{j,i}$ is the maximum length axis of the ellipse. However, due to the irregular shapes of the region, using the maximum length directly produced a large error in the calculation. As a result, the term $a_{j,i}$ will be calculated as a function of the eccentricity $e_{j,i}$and $b_{j,i}$ using the analytical equations of the ellipse. Therefore, $c_{j,i}$ is solved of equation 4.2 and substituted in equation 4.3.

$$e_{j,i} = \frac{c_{j,i}}{a_{j,i}} \rightarrow c_{j,i} = \mathrm{a}_{j,i} * e_{j,i}$$

Equation 4.2

$$c_{j,i}{}^2 = a_{j,i}{}^2 - b_{j,i}{}^2 \rightarrow \left(a_{j,i} * e_{j,i}\right)^2 = a_{j,i}^2 - b_{j,i}{}^2$$

Equation 4.3

Solving $a_{i,j}$ from equation 4.3, we obtain equation 4.4

$$a_{j,i} = \sqrt{\frac{b_{j,i}^2}{1 - e_{j,i}^2}}$$

Equation 4.4

Once that the ellipse has being defined in Cartesian coordinates, each centroid from the new set can be replaced in equation 4.5 and by definition, they will be inside the ellipse if p is smaller or equal than one. If the new regions comply this condition and verify that the area of the added sum of the new regions is smaller than the original one, the new regions will be considered as part of the original and the process will be repeated for the following image.

$$\forall \{x_{j,i}, y_{j,i}\} \in Z_i \,, \forall \{x_{k,i+1}, y_{k,i+1}\} \in Z_{i+1}$$

$$\exists \frac{\left((x_{k,i+1} - x_{j,i}) * \cos(\alpha_{j,i}) + (y_{k,i+1} - y_{j,i}) * \sin(\alpha_{j,i})\right)^2}{{a_{j,i}}^2} +$$

$$+ \frac{\left((x_{k,i+1} - x_{j,i}) * \sin(\alpha_{j,i}) + (y_{k,i+1} - y_{j,i}) * \cos(\alpha_{j,i})\right)^2}{{b_{j,i}}^2} = p$$

Equation 4.5

The fourth case is when two or more regions merge into one. That will mean that one or more of the regions need to be added to another. In this case, the process will be the opposite of the one described for splitting, i.e. as if the branch-

ing was observed in the opposite direction. The new region will act as the original and the previous ones will act as the branches. The equivalent equation of the ellipse will be created and the coordinates of previous centroids substituted. If the previous region comply with this condition and the added area of them is smaller than the new region, they will be added to the new one with the new label and the previous ones will be erased.

In the transition of images, a fully new region can appear in the new image. A region is labelled as totally new when it does not comply with any of the previous cases. In the opposite scenario, if a region does not fall under any of the previous cases is considered that it disappeared. In this case and for avoiding to add regions separated in space but with similar centroids, the region will stop to be analysed, the data will be saved but it will not appear in the list of previous regions in the following image. The full algorithm flowchart is included in appendix b.

In order to validate the code, an additional script was written to confirm that any single cluster has unique values and none of the areas has been associated to more than one cluster. Following this step, the sum of all the areas analysed during the tracking was compared with the result produced by the full set of

images without any tracking. Since both results were consistent, it was concluded that the tracking algorithm associated every area to a specific cluster.

4.2.3.3 Volume analysis and representation

After the regions have been connected individually along axis z, the volumes of interest can be extracted from the full granule. The volumes will be transformed to a 4-D format which includes colour as fourth variable and is necessary to be visualised in the Matlab volume viewer. Every parameter is calculated in voxels and they will then need to be transformed to length units. A voxel is a cube which has equal lengths defined by the pixel size of the image. In this case, that equivalence used was 1.4 μm/pixel, i.e. a voxel is a cube with a length of 1.4 μm for each side, surface area of 1.96 μm^2 and volume of 2.744 μm^3.

The main parameters calculated to characterize the nuclei are the volume, the surface area (Lehmann and Legland, 2012), the relative density and the equivalent diameter what is defined as the equivalent diameter of a circle of equal projection area (EQPC). The relative density can be analysed in two ways depending if they are analysed in 2-D or in 3-D. Both ways are based in the calculation of the smallest polygon containing the region which is included in Matlab function *regionprops* for 2-D and *regionprops3* for 3-D (MathWorks, 2018). However, since regionprops3 cannot be used for extremely large (over

1500 images) set of images due to its very computationally expensive nature, therefore only the data from the 2-D algorithm will be analysed. However, due to the irregular shape of these types of images, the minimum polygon will produce some errors and therefore, the main deciding parameter would be the volume of the region or the equivalent diameter. Once the largest and denser clusters have been found, those were individually represented.

4.3. Results and discussion

4.3.1 Representation of granules and comparison with Bruker software results

Granules of α-lactose monohydrate produced by high shear and twin-screw granulation were analysed in X-ray CT. In figure 4.12, a comparison between Bruker software and the developed algorithm was performed through the full reconstruction of two granules (images corresponding to granule obtained by HSWG: figures 4.12a, 4.12c and 4.12e and granule obtained by TSG: figures 4.12b, 4.12d and 4.12f). Despite the differences of orientation, both reconstructions show high visual similarity between them although they cannot be directly compared. The Bruker reconstructions does not allow the extraction of selected parts. However, since the blue colour represents the empty space inside the granules, it seems to be significant differences in nuclei structure between both type of samples where the batch sample have significant less contrast between both colours than the continuous one.

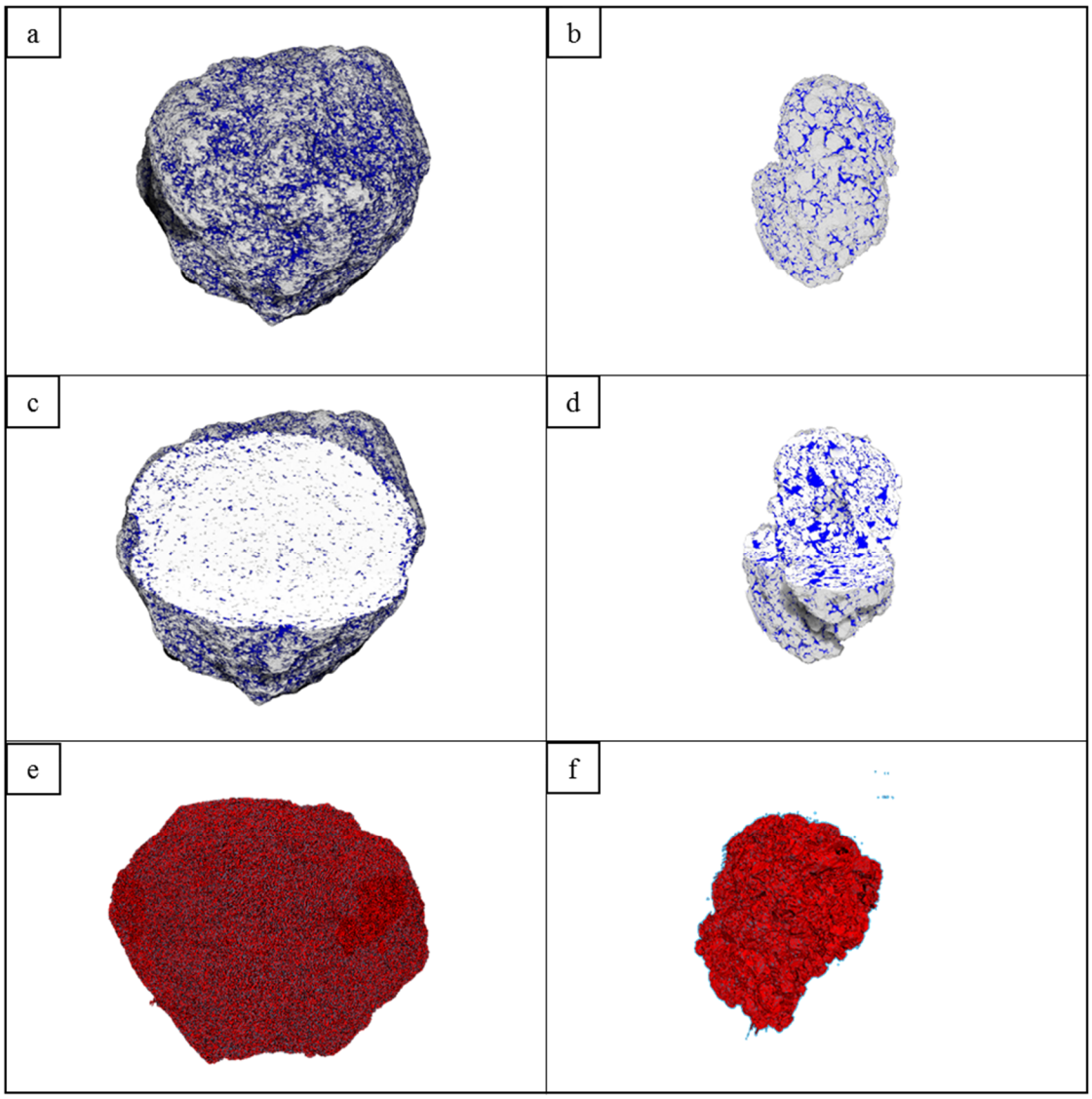

Figure 4.12. Granules reconstruction a,b) Bruker full reconstructed, c,d) Bruker inner part e,f) Algorithm full reconstruction.

4.3.2 Analysis of nuclei within the granules

In this section, the algorithm was applied to extract nuclei from granules obtained both from HSWG and TSG. From the Bruker software was already possible to appreciate differences between internal structures of the granules (figure 4.12). These differences became clearer after segmentation and tracking is applied.

The total number of clusters found for the TSG case has been plotted in figure 4.13 representing relative density against the equivalent diameter of the cluster volume. As seen, a grouping of points with similar density and volume suggests more than one nucleus is present. In order to understand the big cloud of points under 40 μm, raw α-lactose monohydrate was analysed and it can be seen in figure 4.14 the same cloud of points appears suggesting they are un-granulated powder fines. As it was mentioned in the methodology, the relative density is the relationship between the different volumes and the smallest polygon containing the area provided by the software, however, due to the irregular shape of the particles, it gives a considerable error and it will only use as indication.

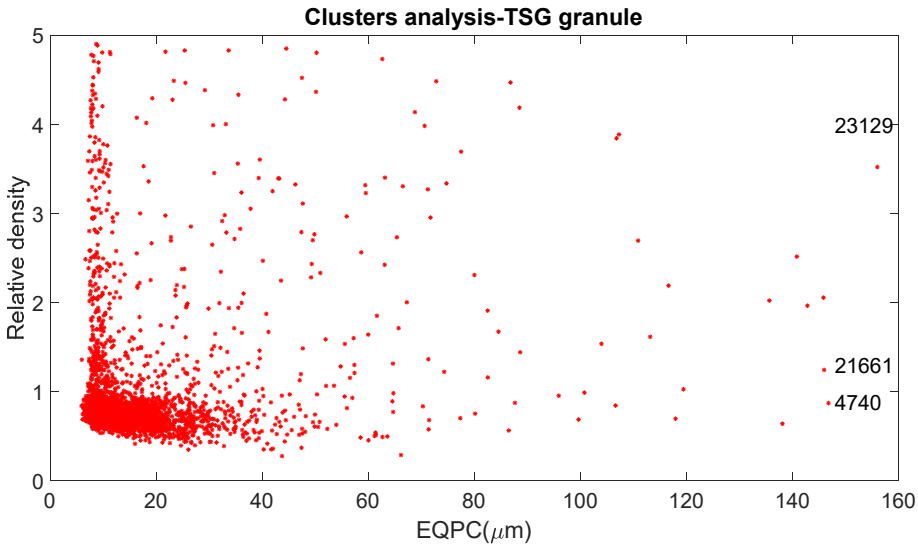

Figure 4.13.Clusters –TSG granule

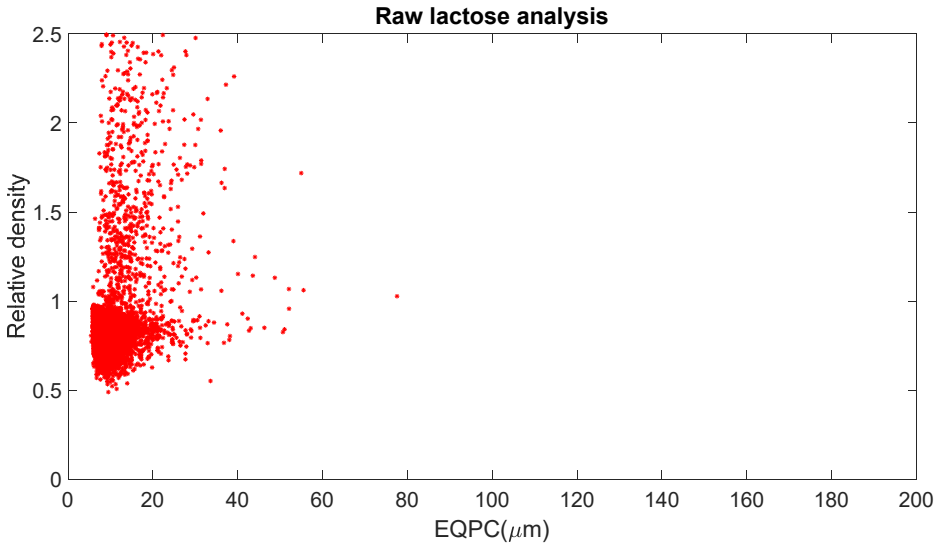

Figure 4.14. Raw lactose analysis

In the case of HGSW, one nucleus is obtained with larger volume and density than the rest of the clusters analysed (Figure 4.15)

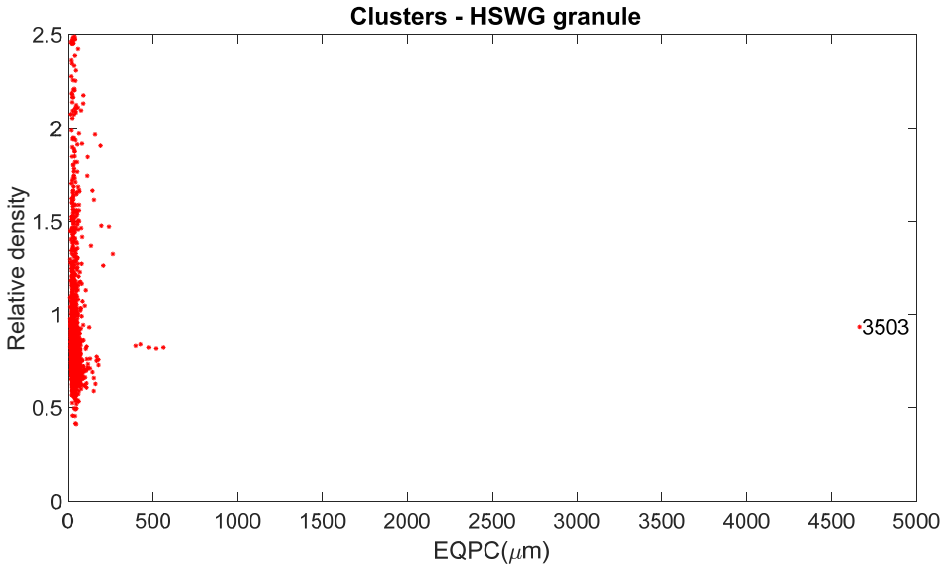

Figure 4.15. Clusters - HSWG granule

Although the definition of big clusters is subject to the parameters chosen during segmentation, the algorithm seems to be able to recognise big clusters or connected sections of the granules despite the differences between batch and continuous. In the case of batch, the big cluster has a good agreement with the nuclei morphology for lactose and water granule described by Hapgood et al. where the nucleus was estimated 5 mm with almost spherical shape (Hapgood, 2000). However, there is not possible to compare the continuous results since there were not available data in the literature.

4.3.3 Extraction and visualization of nuclei produced by batch and continuous

After the analysis has been completed, the nuclei have been extracted and they can be analysed individually. In order to study the shape and improving the visualisation, the images 4.16 and 4.17 are not in scale, however, all the properties of the represented nuclei are included in table 4.3.

The nucleus of the HSWG is a very dense oblate spheroid located in the centre whose volume constitutes 98% of the total volume of the granule with a radio of 4.66 mm (figure 4.16).

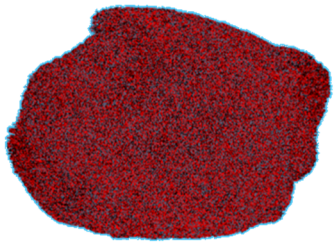

Figure 4.16. Batch nuclei granule (Number 3503).

In the case of the TSG granule, three of the main nuclei have been extracted (Figure 4.17 a, b and c) where they showed an irregular hemispherical shape with some plane edges.

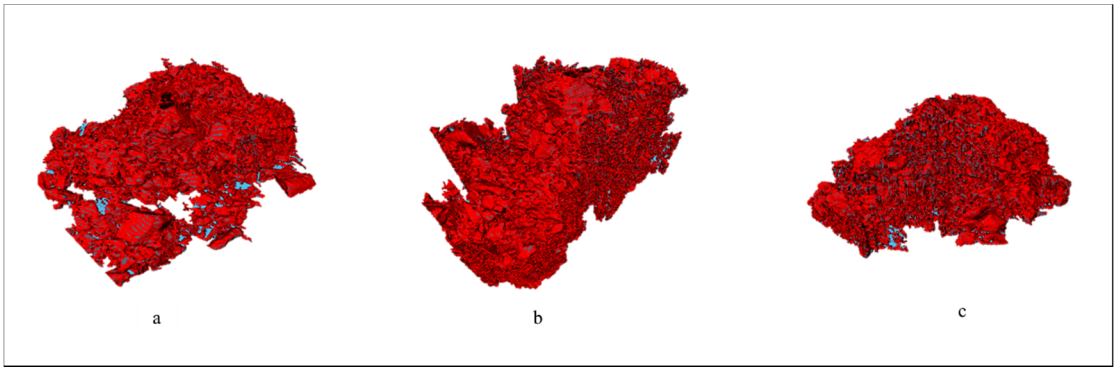

Figure 4.17. Largest nuclei reconstruction for a continuous granule. a) Number 23119 b) number 21661 c) number 4740

Table 4.3. Properties of the nucleus

Number	EQPC (µm)	Volume (µm³)	Volume/Volume total (%)	Surface area
23129	156.75	6.31×10^6	3.79	8.14×10^6
4740	147.42	5.25×10^6	3.16	8.14×10^6
25116	146.67	4.89×10^6	3.10	1.80×10^7

A junction of two nucleus is shown in figure 4.18 where they have two points of connection. On figure 4.17b five nuclei were reconstructed together showing that they are not specifically located in the centre of the granule and they are in a more external position.

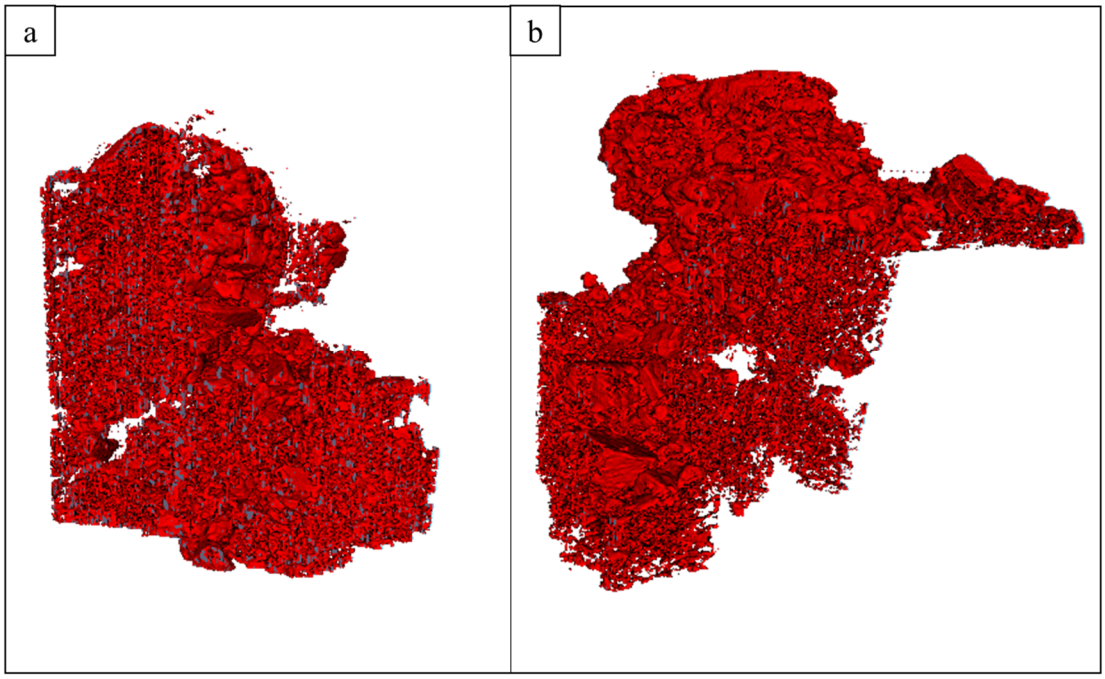

Figure 4.18. Nuclei reconstruction for a continuous granule: 2 nuclei a) 5 nuclei b)

4.3.4 Analysis of continuous granule nuclei

The HSWG nucleus have been largely studied in literature (Agrawal and Naveen, 2011, Hapgood, 2000) and as it was expected for α-lactose monohydrate, it has a spherical shape.

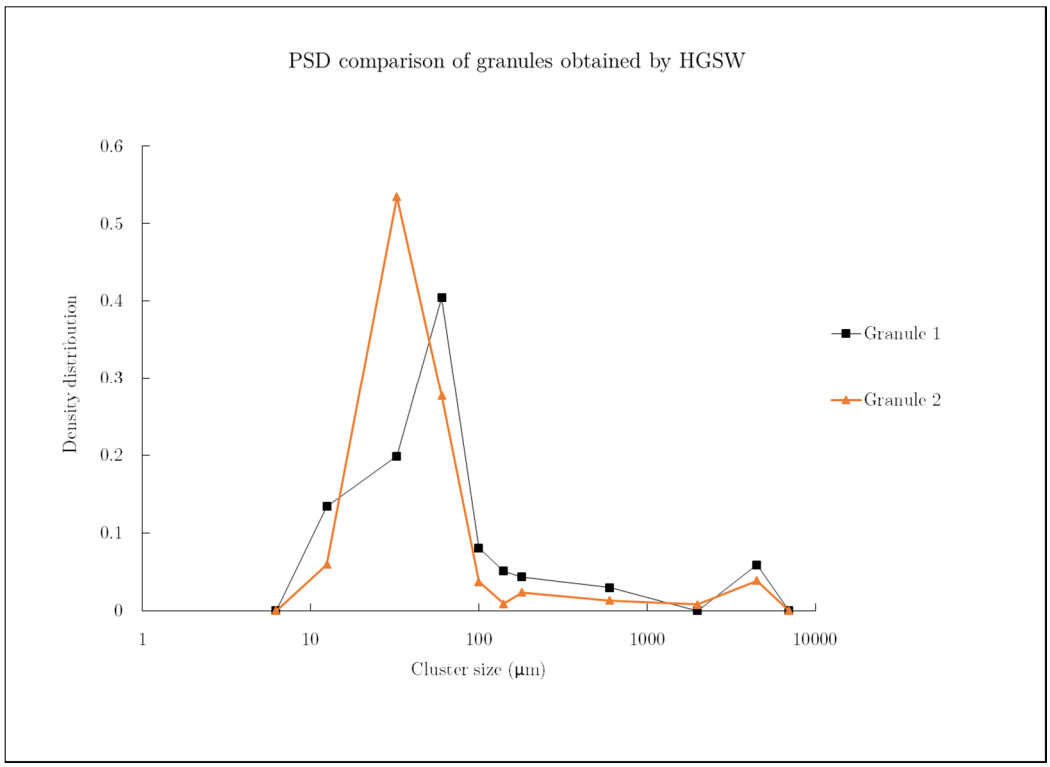

Figure 4.19. Particle size distribution comparison between HSWG granules

On the other side, granules obtained by TSG have a different inner structure with a greatest number of smaller clusters and some relatively large clusters. In Figure 4.20, a set of continuous granules was analysed and the results were overlaid. The particle size distribution was calculated (Figure 4.21) showing that there is not a predominant class of clusters and there the TSG granule would be formed by a mixture of sizes.

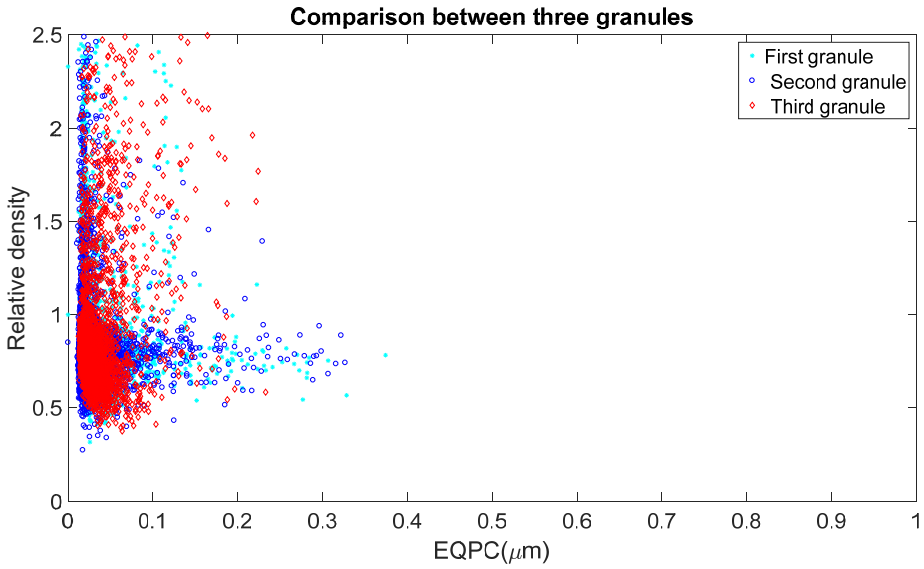

Figure 4.20. Relative size of three TSG analysed granules

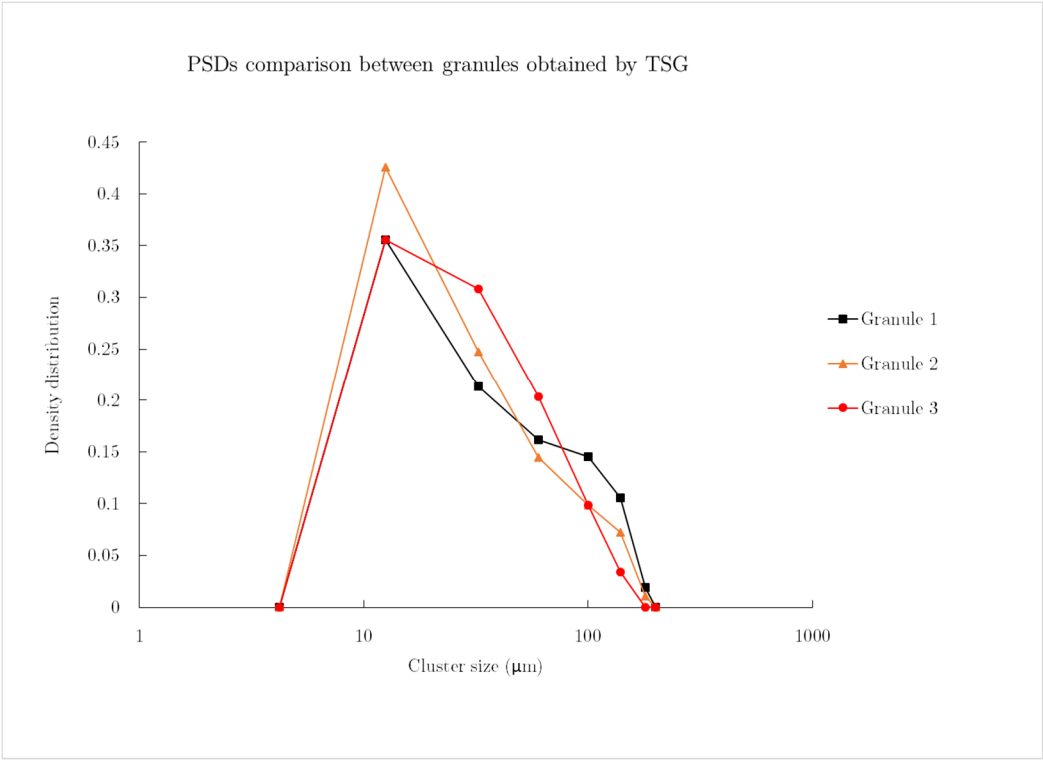

Figure 4.21.PSD for three granules

These differences between both granulators can be explained from the differences between TSG and HSWG. In HSWG, large drops fell discontinuously in the layer of powder in constant centrifugal movement penetrating the surface and producing one unique nucleus. This nucleus was layered with powder and it continued growing until there is not more available binder. In this type of granulator, all the mechanisms occur simultaneously in certain locations. In TSG, the mechanisms are more likely to be produced along the length of the granulator. In this case, the dry powder will be moving constantly depending of the ongoing internal stress produced by the torque velocity. Although the addition of liquid is done in drops, those drops does fall over moving powder rather than a layer. Therefore, nuclei in this case are relatively smaller with low density agreeing with the difference between batch and continuous mechanisms explained in the literature (Verstraeten et al., 2017). In this case, the granules were obtained at conditions of high homogeneity of particle size distribution and low channel fill which maximise the interaction between liquid and solid i.e. the powder wetting.

4.3.4 Modification of the code to the selective extraction of nucleus

One modified version of the previous algorithm was adapted to increase the computational speed. This version will be used in those cases that the particle

size distribution is not required and the algorithm is only used to reconstruct the nucleus. In this case, as soon as a particle is classified as fine (<40 μm) is erased. Ignore all the fines reduces significantly the amount of particles to be treated. In figure 4.22, one granule was analysed for both methods obtaining a good agreement with the largest granules and reducing the memory necessary for doing the analysis significantly.

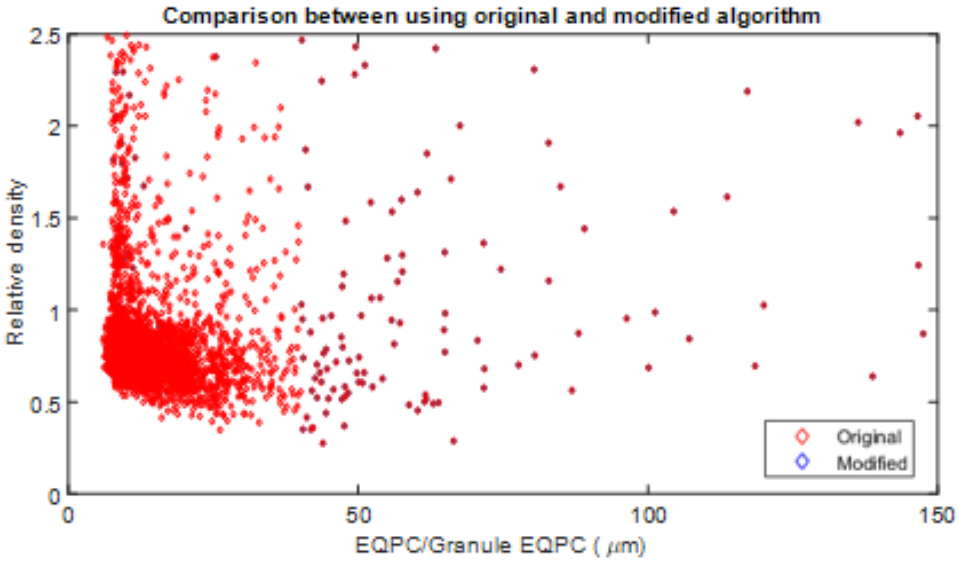

Figure 4.22. Comparison between original and modified algorithm.

4.4. Conclusions

The inner structure of granules requires to be analysed in order to understand the effect on the nuclei morphology depending of the applied granulation conditions. However, there was not a successful technique to study only partial areas of a set of X-ray computed tomography images and specifically with irregular shapes. The development of an algorithm able to segment granules depending on the decided bond length will lead improved exploration and understanding of different types of structures in a further level.

The described algorithm in this chapter is able to recognise and extract individual clusters from image stacks and perform further calculations to classify them. All the different operations such as contrast enhancement, segmentation and reconstruction were visually optimised since there is not any statistical analysis available to compare with other possible methods. They were successfully combined to allow the tracking of regions. The recognition and tracing of regions with irregular shapes has been possible applying mathematical geometric concepts which address all the possible situations that the areas of interest could undergo. Furthermore, the reconstruction of individual nuclei allowed visualisation and comparison the specific morphologies of granules obtained. The potential of the methodology was demonstrated from the study of granules obtained

by different methods (TSG and HSWG) showing high differences in terms of number, morphology, relative size and density between systems. The application of this method will lead to consider the internal morphology of the granule as an extra parameter to consider during the study of granulation and it will be considered in further research.

Chapter 5

Effect of static drying temperature on internal granular modifications

5.1 Introduction

The drying of materials is frequently the subsequent operation after granulation (Kleinebudde et al., 2017). Although the operation in itself can be an essential part of the manufacturing process and can be employed to understand and control the liquid and solid relationship in the granule. Liquid to solid ratio has been recognised as one of the most influential parameters during TSG for the

growth of the granule (Verstraeten et al., 2017), having a direct influence on strength and size of the granule (Nieuwmeyer et al., 2007a, Nieuwmeyer et al., 2007b). There are few examples of L/S study as function of its properties such as viscosity, surface tension or liquid/solid ratio (Dhenge et al., 2012b, Dhenge et al., 2013) and the dynamic character of the liquid bridge (Nieuwmeyer et al., 2007b). Since strong solid bridges develop from liquid bridges during the drying step, in this study different rates of drying were investigated by varying the temperature between -20°C and 80°C for α-lactose monohydrate and water granules. Within this range, five temperatures were chosen to ensure sufficient differences in the properties of the liquid. The ratio of liquid to solid was confirmed by a moisture analyser and the full drying of the granules was confirmed measuring the differences in weight before and after the degassing of the samples. The degassing is made under vacuum conditions which produce the release of loosely bound water at low temperatures that reduces the damaging of the samples (Quantachrome Instruments, 2009). The granules were analysed by differential scanning calorimetry to discard changes in the crystalline structure. The internal changes were studied by the comparison of the surface area as well as the assessment of the morphology of different nuclei of granules dried at different temperatures.

5.2 Materials and methods

5.2.1 Materials

α--Lactose monohydrate (PubChem CID: 24896349) with 99% total lactose basis (GC) (Sigma-Aldrich Company Ltd., Dorset, United Kingdom) was used as granulation powder and distilled water (EMD Millipore™ Pure Water Reservoirs, Millipore SAS, Mosheim, France) was added as granulation liquid.

5.2.2 Production of granules

In order to produce granules, same setup than the described in section 3.2.2. The TSG was operating at 75 rpm in combination with the gravimetric feeder operating at 0.15 kg/h. The addition of liquid was made at three L/S ratios 0.1, 0.13 and 0.16. Four independent separate experiments of each L/S ratio were performed. In order to ensure continuous behaviour was reached and maintained during each experiment, particle size stability tests were performed during each run by collecting five samples for analysis.

5.2.2 Static drying

The granule samples were air dried at five different temperatures (-18 °C, 2 °C, 20 °C, 50 °C and 80 °C) to obtain different rates of drying. The temperatures were selected depending of the equipment available to ensure sufficient difference between the drying rates. The samples were not disturbed during the required

time to ensure that the modifications in the internal structure were only due to the evaporation of water. The summary of experiments is shown in Table 5.1 where n corresponds to the number of repetitions of the four independent separate experiments of each L/S ratios. Drying temperatures were identified with letters in order of reducing possible mislabelling during experimentation and they have not physical meaning.

The coldest temperature (-18 ± 2 °C (TB)) was obtained using a freezer (Labcold RLVF14201, Labcold Ltd, Hampshire, United Kingdom) where the samples were stored for over two weeks due to the slow drying process. The second coldest temperature (2 ± 1°C (TFC)) was obtained using a fridge (LEC essenChill BRS50W, Glen Dimplex Home, Prescot, United Kingdom) where the samples were stored over a week which was found empirically sufficient to ensure full drying. One drying was performed at room temperature (20 ± 2 °C (TA)) was measured each 12 hours with a thermometer and kept overnight. The hottest temperatures (50 ± 1 °C (TOW)) and 80 ± 2 °C (TOR)) and fastest drying rates were performed in an oven (Memmert UNB100, Memmert GmbH + Co. KG, Schwabach, Germany) and removed after two hours.

Table 5.1. Summary of experiments

	Temperature (°C)				
	-18.5	2	20	50	80
L/S=0.10	TBn2	TFCn2	TAn2	TOWn2	TORn2
L/S=0.13	TBn3	TFCn3	TAn3	TOWn3	TORn3
L/S=0.16	TBn4	TFCn4	TAn4	TOWn4	TORn4

5.2.3 Analysis of granules

Multiple analysis was performed to the granules. However, the total number of samples used to perform each analysis varied depending on the type of analysis. For instance, particle size distribution was analysed five times (m=5) for each round (n=4) and therefore, twenty samples were used to find the average diameter for each liquid-to-solid ratio. They can be calculated from figure 5.1 by multiplying the number of repetitions (n) by the number of samples used to perform the analysis (m).

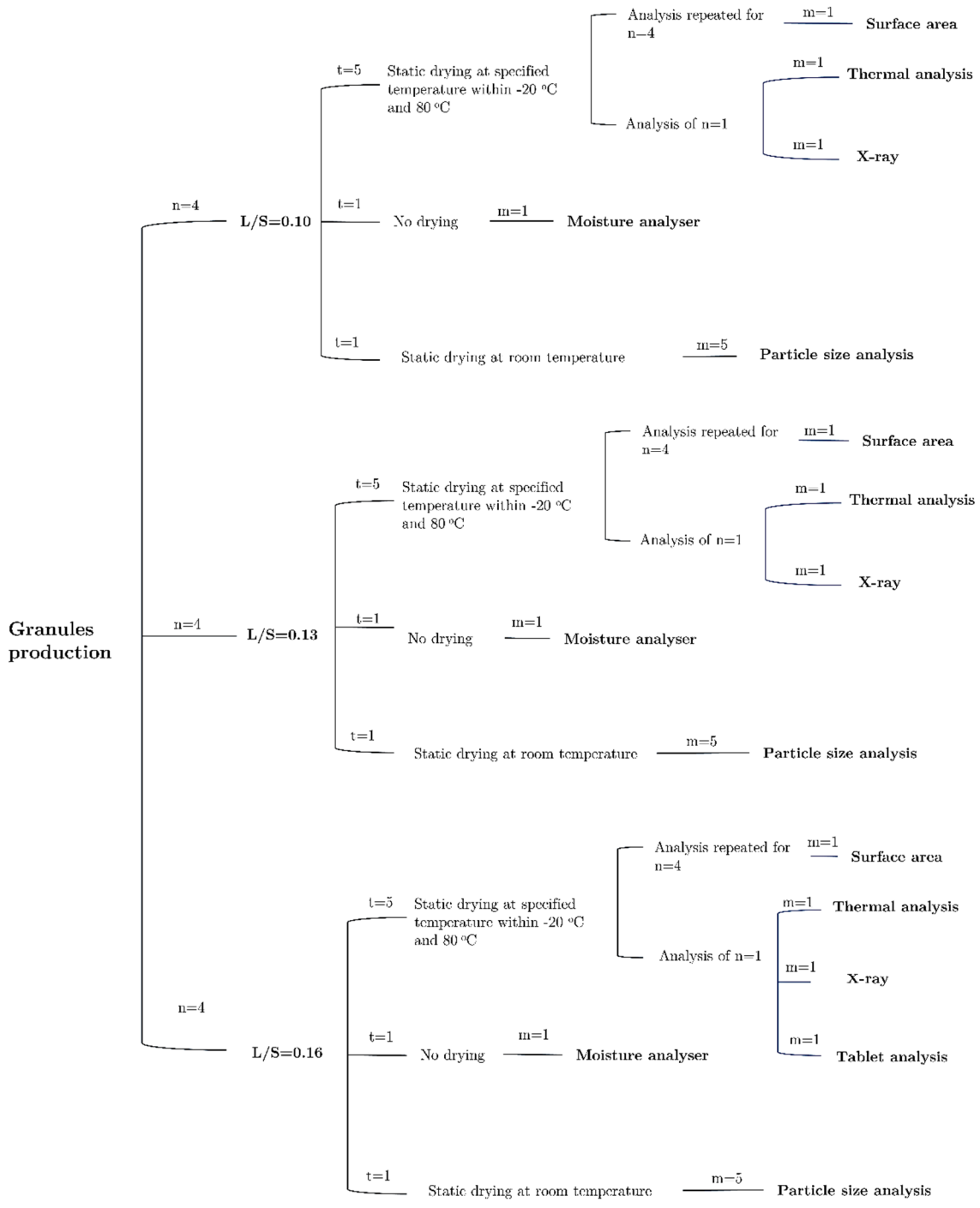

Figure 5.1. Organigram of the sample analysis. n=number of repetitions, t=number of temperatures analysed, m=number of samples used for one single analysis.

5.2.3.1. Offline granules size analysis

The analysis of the particle size distribution was performed following the same procedure described in section 3.2.3. In order to compare if the PSDs are equivalent, ANOVA with Homogeneity of Variance Brown–Forsythe test was performed at 0.05 level in Origin 2018 (OriginLab, Northampton, Massachusetts, United States). This test is recommended for samples with data size over 20, regardless the shape of the population (Wang et al., 2017). The comparison was performed between samples obtained from the same experiment and for samples obtained at the same L/S ratio.

5.2.3.2 Thermal analysis

Differential Scanning Calorimetry (DSC) and thermogravimetric analysis (TGA) were carried out simultaneously using a Netzsch STA449 F1 Jupiter (NETZSCH-Gerätebau GmbH, Wolverhampton, West Midlands, UK). The samples were prepared by weighing the pans before and after loading the granules with an average sample weight of 5.5 mg. Analysis was carried out for all the samples after full drying over a range of 20 ˚C to 250 ˚C and at a 5 °C/min heating rate. From this analysis it is possible to extract if the samples of α-lactose monohydrate experienced any modification in its crystalline structure and discarding any polymorphism change in the samples e.g. from α to β or amorphous forms. The

amorphous form of lactose is identified as exothermic peak at 167°C, which will recrystallize into α-Lactose monohydrate and β-Lactose monohydrate as endothermic peaks at 210 and 216 °C respectively. However, 100% α-Lactose monohydrate in powder will present two endothermic peaks, one within 130-160°C associated with the loss crystalline water and one at 213 °C associated with the α-Lactose monohydrate (Gombas et al., 2002). As the peaks are very dependent on the crystallinity of the compound, α-Lactose monohydrate in powder prior to granulate was analysed as a reference.

5.2.3.3 Surface area

The characterisation of the surface of the granules was performed by gas sorption (Autosorb IQ Model 6, Quantachrome Instruments, Florida,United States). All the samples were pre-treated by prior outgassing at 40 °C for 150 minutes in which the residual humidity after drying will be removed. Also, the full drying of the sample was confirmed in this step by the measurement of the weight before and after the treatment. The cell types used were 9 mm with rod which were transferred to the physisorption camera. The void volume was measured at the beginning of each run with Helium. The adsorbate gas chosen was Nitrogen at 77.35 K and 41 points were selected for producing both adsorption and desorption isotherms. The data was analysed by the Non-Local Density Functional

Theory method (NLDFT) with calculation model of N_2 at 77 K on carbon (slit pore). In order to compare if each set of experiments was significantly equivalent, One Sample Wilcoxon Signed Rank Test was performed at 0.05 level in Origin 2018 (OriginLab, Northampton, Massachusetts, United States).

5.2.3.4. Water content

In order to study the evolution of the water content of the granules, the moisture was analysed both before and after drying. A moisture analyser (MA37-1, Sartorius Lab Instruments GmbH & Co. KG, Goettingen, Germany) was used immediately after granulation. The samples were placed in a metal tray preheated at 50ºC and they were left at constant heat until the variations of weight were negligible (minor to 0.01% variation of the weight). After the drying occurred, the water content was analysed by degassing. The equilibrium humidity which will be evaporated during the degassing of the material can be quantified measuring the weight before and after the analysis. The results will be compared with the original L/S ratio used.

5.2.3.5 X-ray computerised tomography

Granules were analysed using a multiscale X-ray nano computer tomography (NanoCT; SKYSCAN 2211D, Bruker LTD, Coventry, United Kingdom). This non-destructive technique generates three-dimensional density profiles inside

opaque objects. Therefore, it will provide a reconstruction of internal micro-structure of the granules as well as images of the all the individual slices of the granule. Nuclei analysis was performed in order to compare the relationship between surface area and internal granular structure depending on the drying and the L/S ratio. In order to perform this analysis, the technique described in chapter 4 will be used for 3 samples embedded in a subset of 1000 images where the main nuclei will be extracted and compared.

5.2.4 Tablets analysis

The impact of the drying effect on tabletting was studied by comparing five samples of each drying temperature for one experiment of L/S=0.16. The tablets were individually produced in a single punch machine (XP1, KORSCH AG, Berlin, Germany) with a die diameter of 9 mm and a circular flat face. The hardness and height of the tablets was measured using a manual tablet-tester (HC 6.2, Kraemer Elektronik Gmbh, Darmstadt, Germany). The final weight was measured with a mass balance (Sartorius Quintix 125D-1S, Sartorious, Goettingen, Germany). The strength of the tablets (σ) was determined by equation 5.1 (Fell and Newton, 1970).

$$\sigma = \frac{2 * F_{applied}}{\pi * D * T_{tablet}}$$

Eq. 5.1

Where σ the tensile stress of the tablet, $F_{applied}$ is the applied load, D is the tablet diameter which is determined by the die, T is the tablet thickness.

5.3. Results

5.3.1 Effect of the L/S ratio on the granules size

In order to study the effect of the L/S ratio, five samples were taken for each repetition and dried at room temperature, the average size for each L/S ratio was calculated as the average of the diameter for all the experiments. An increase in volumetric mean diameter of the granules is observed when the L/S increases which agrees with the results found in the literature. El Hagrasy et al. found an increase of d_{50} from 500 μm to 1500 μm for an increment of 0.1 in the L/S ratio for a blend with 73.5% lactose (El Hagrasy et al., 2013b). At L/S=0.10, the granules of α-lactose monohydrate have an average size of 458.43 ± 16.46 μm. The granules at L/S= 0.13 were 725.08 ± 92.25 μm and at L/S=0.16, they were 956.73 ± 95.63 μm. The results of the ANOVA test are included in the appendix c.

5.3.2 Effect of the L/S ratio on the nuclei size

X-ray images were analysed using the algorithm described in chapter 4 for a set of 1000 images which contained at least 3-4 granules for each L/S ratio at one single temperature. It was found that actually the PSDs of the clusters (figure 5.2) have a peak under 40 μm for all the L/S ratios. In chapter 4, it was found that the raw lactose powder has an average size under 40 μm and therefore, this

peak corresponds with original lactose particles. In figure 5.2, it can be observed that after 100 μm, the peak increases significantly when the L/S ratio increases e.g. there is an increment in higher nuclei and a decrease in amount of raw lactose which seems to not be granulated.

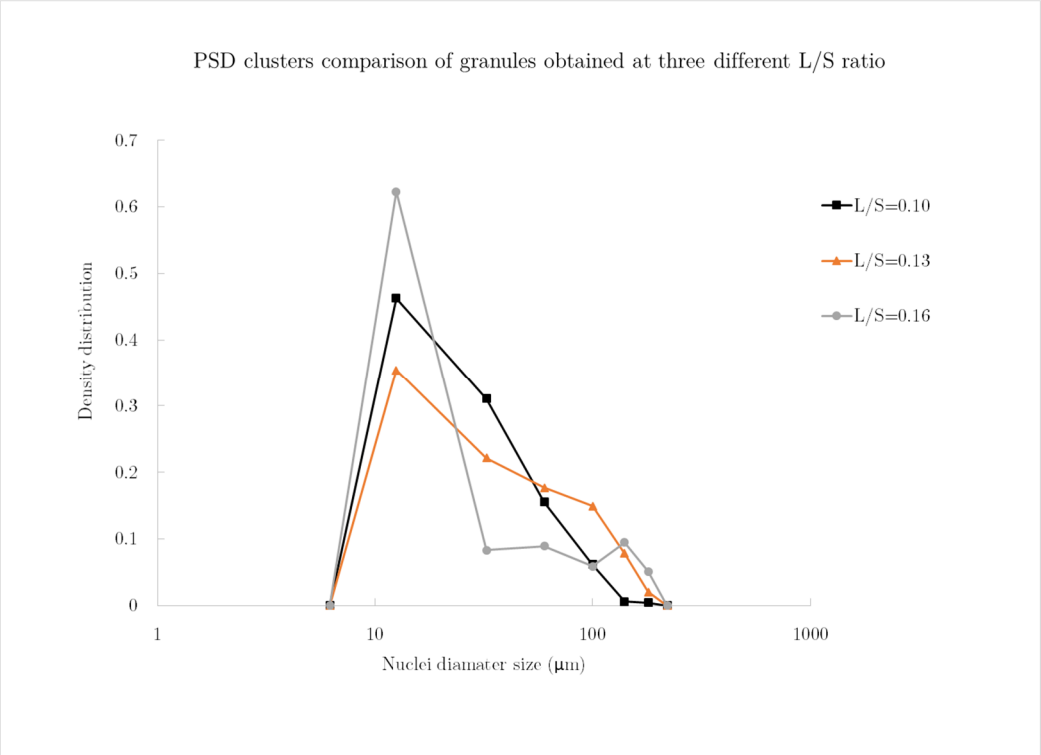

Figure 5.2. Comparison of the PSDs of the clusters at different L/S ratio

5.3.3 Thermal analysis

Since lactose aqueous bridges of α-lactose monohydrate consist of a mixture of α-lactose monohydrate and anhydrous β-lactose (Farber et al., 2003), the change of any possible crystalline structure from the raw material was studied by DSC. α-Lactose monohydrate in powder prior to granulation (Figure 5.3)

was analysed obtaining two main endothermic events. The first one is at endothermic peak at 146.6 ± 0.1 °C which is within 130-160°C associated with the loss crystalline water. The second one corresponds with α-Lactose monohydrate which was expected to be an endothermic peak at 214 °C (Gombas et al., 2002) and for this raw material corresponds with 214.95 ± 0.45 °C. There is an extra exothermic around 175 °C which is likely to correspond with the impurities of the raw material stated on the product specification sheet of the material. A sample of each L/S dried at different temperatures was analysed (Figure 5.4, Figure 5.5 and Figure 5.6). Due to the similarity between both powder and granules, it was concluded that the granules are formed by α-lactose monohydrate.

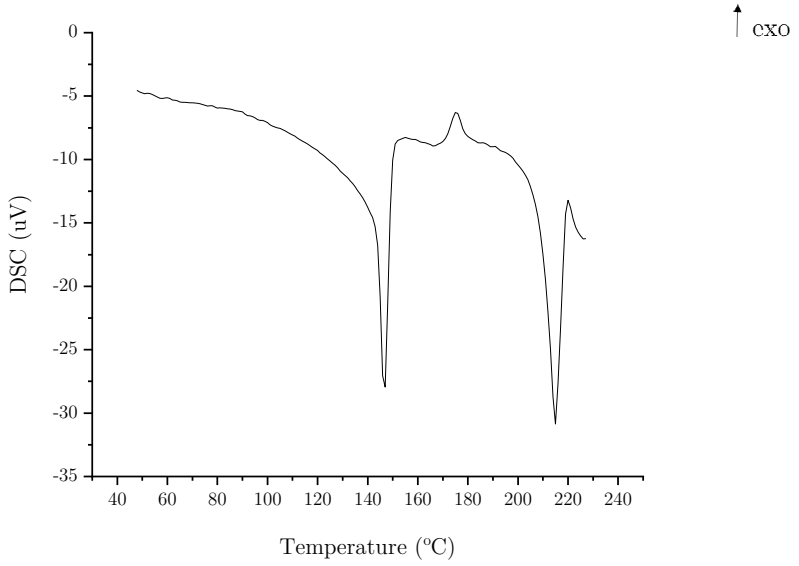

Figure 5.3. DSC of the raw α-Lactose monohydrate powder

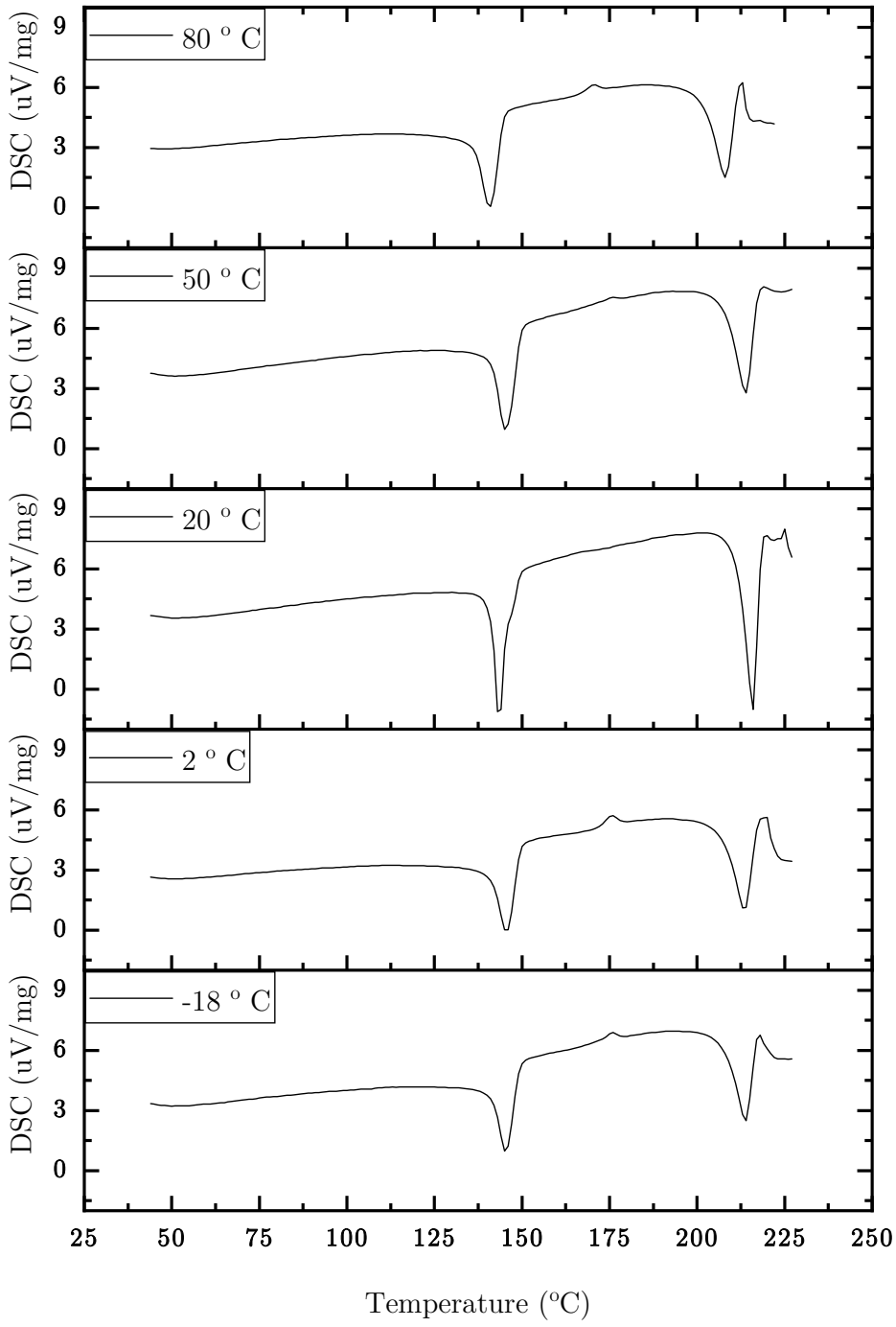

Figure 5.4.DSC for L/S=0.10 at five different drying temperatures

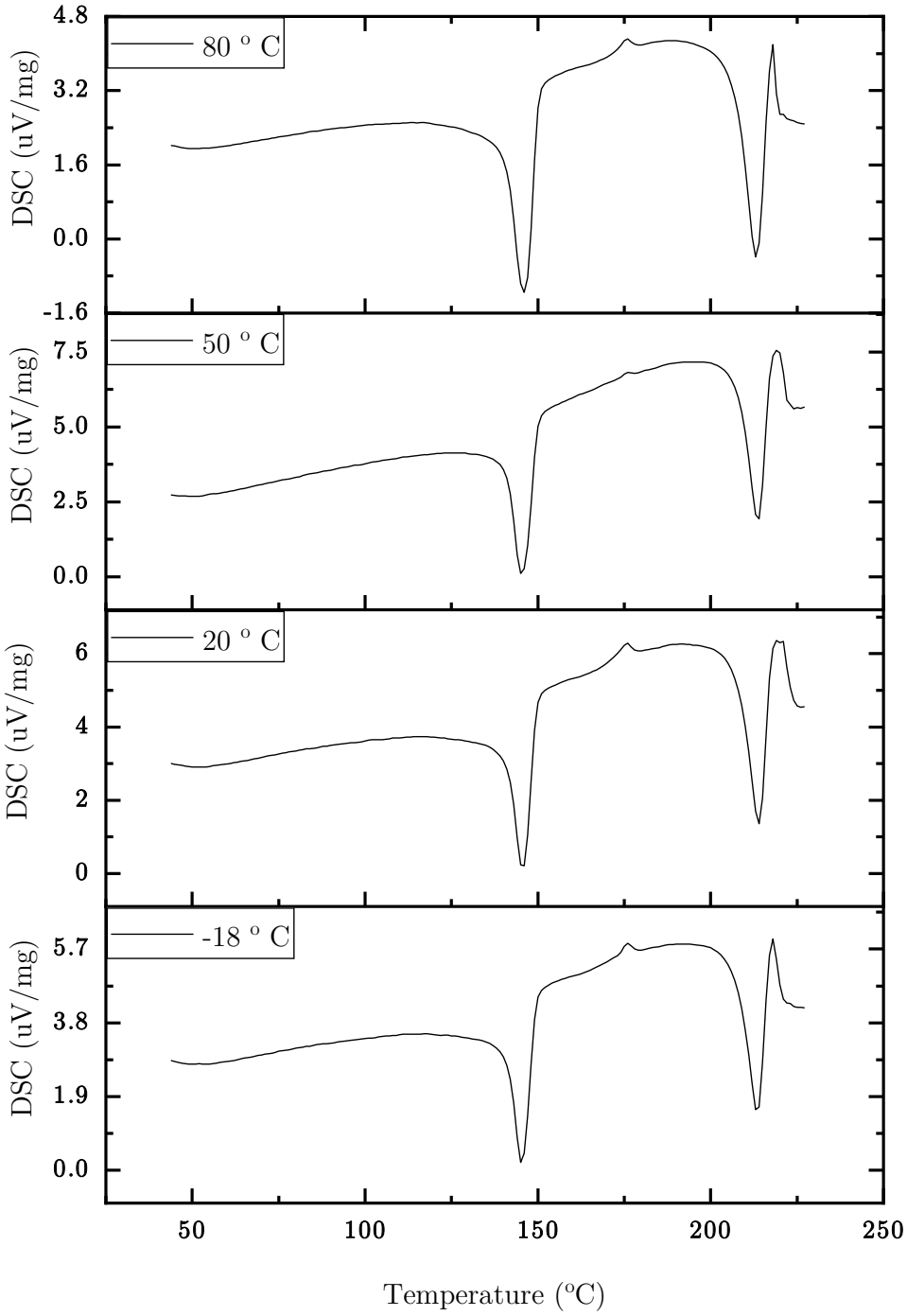

Figure 5.5.DSC for L/S=0.13 at four different drying temperatures

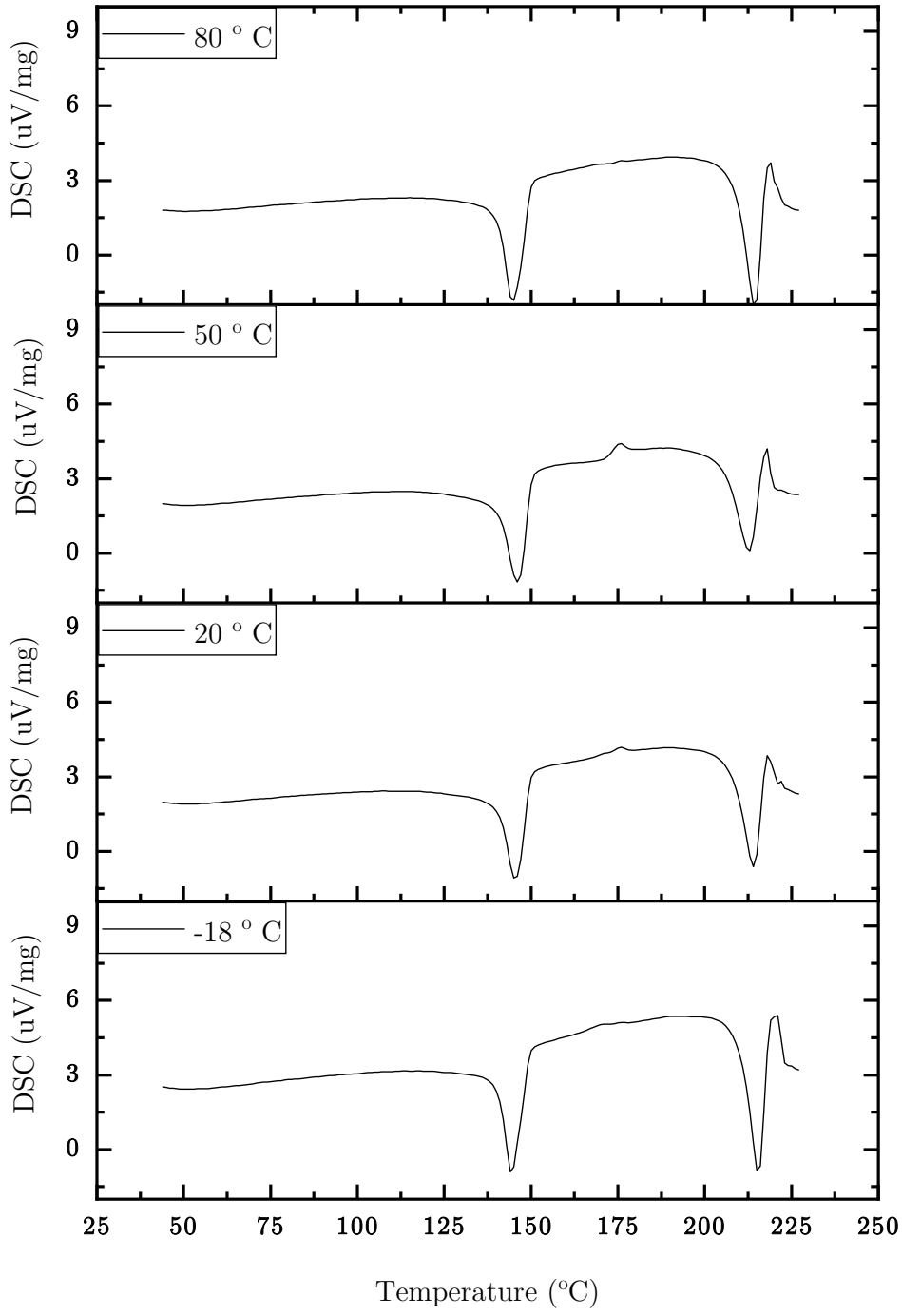

Figure 5.6.DSC for L/S=0.16 at four different drying temperatures

5.3.4 Water content

The water content of the samples was studied to ensure that the samples L/S targeted was achieved. In figure 5.8, the water content obtained with the moisture analyser is very similar to the L/S targeted. In order to ensure that the drying had been completed, the weight was measured before and after the degassing associated with surface area measurement. In this operation, the granules will release any water which is not chemically attached and therefore, if the granules were not fully dried, the water will be released in this stage. However, the difference in weight was always minor, 0.5% in weight, which indicates that the drying was complete at all different temperatures.

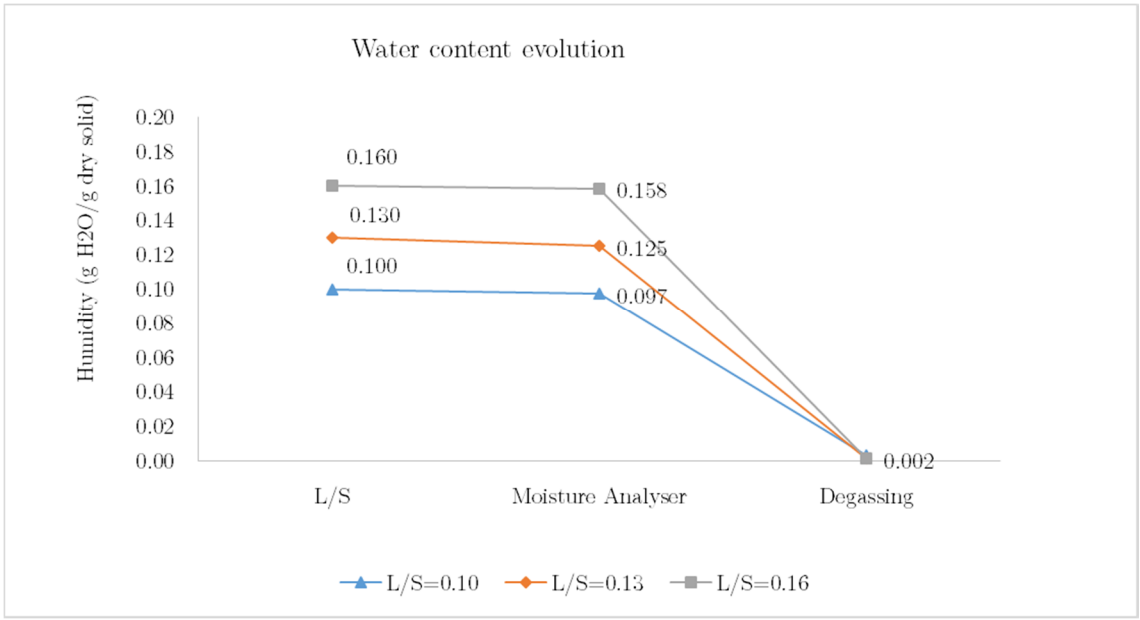

Figure 5.7. Water content analysis

5.3.5 Effect on the surface analysis depending on the drying temperature

The surface analysis study requires the preliminary analysis of the isotherm sorption curves which are provided in figure 5.9. All the isotherms at different ratios of L/S and temperatures correspond to a type III according to IUPAC classification (Sing, 1985), which is confirmed by the χ-representation of the isotherms. These types of isotherms don't exhibit a point B which is often taken as an indicator of the end of the monolayer coverage and start of multilayer coverage. These curves are associated with materials which are microporous and have a low energy of adsorption. However, the χ-representations of the isotherms shows a multiplane adsorption that is not due to the presence of multiple species or contamination since the STA-TG results show that the only component in the samples are α-lactose monohydrate and water and it could therefore be due to the presence of microporosity (Condon, 2006, Sing, 1985). These types of graphs can be analysed by the Non-Local Density Functional Theory method (NLDFT) with calculation model of N_2 at 77 K on carbon (slit pore). Physisorption isotherms for all the temperatures analysed are included in the appendix d.

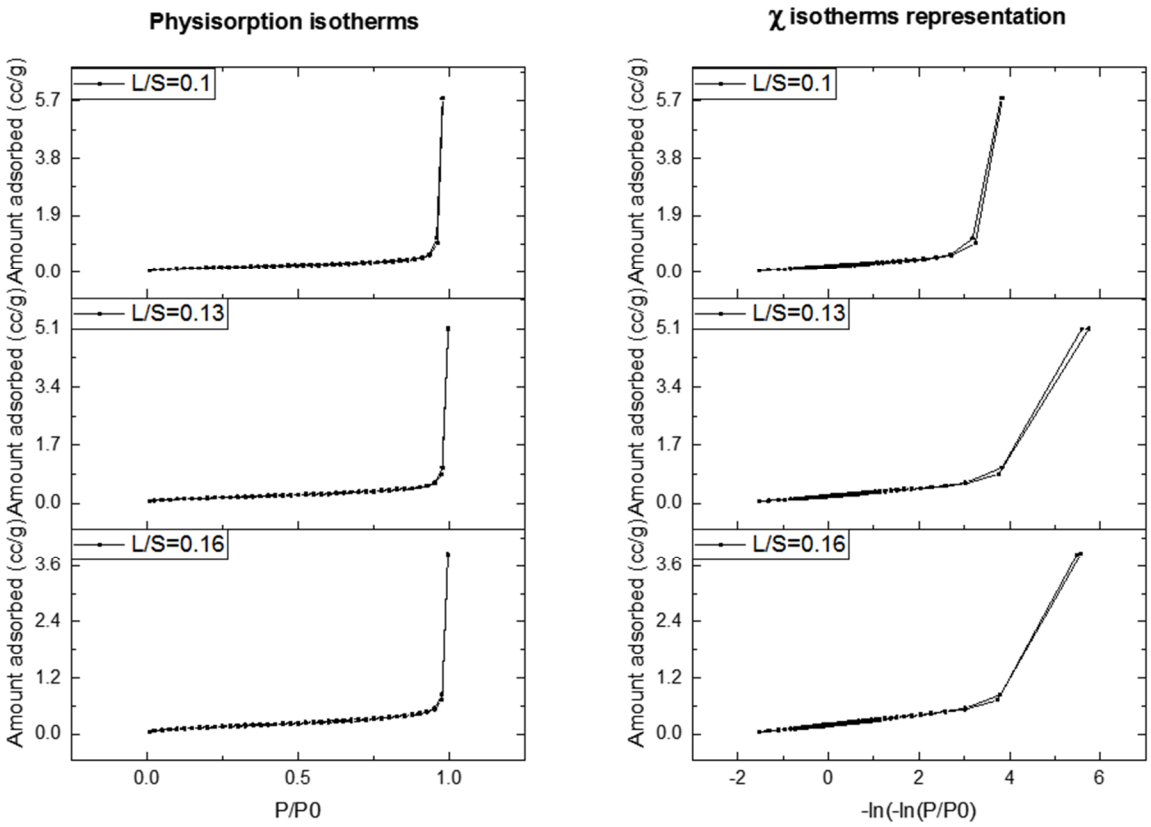

Figure 5.8.Physorption and χ-representation isotherms of the granules of α-lactose monohydrate at different L/S ratios dried at 20 °C

The surface area is presented in figures 5.9, 5.10 and 5.11 for the three L/S ratios. Independently of the L/S ratio, the cumulative surface area shows differences depending on the drying temperature and the average trend is the same at all the L/S ratios. Error bars for -18°C at L/S=0.10 and L/S=0.13 are relatively larger compared with the rest. However, this variance is due to two samples which although dried at the same time are remarkable different to the rest of the samples. One Sample Wilcoxon Signed Rank Test was performed for each

set of experiments which confirmed that each set of experiments was significantly equivalent and it can be found in appendix e.

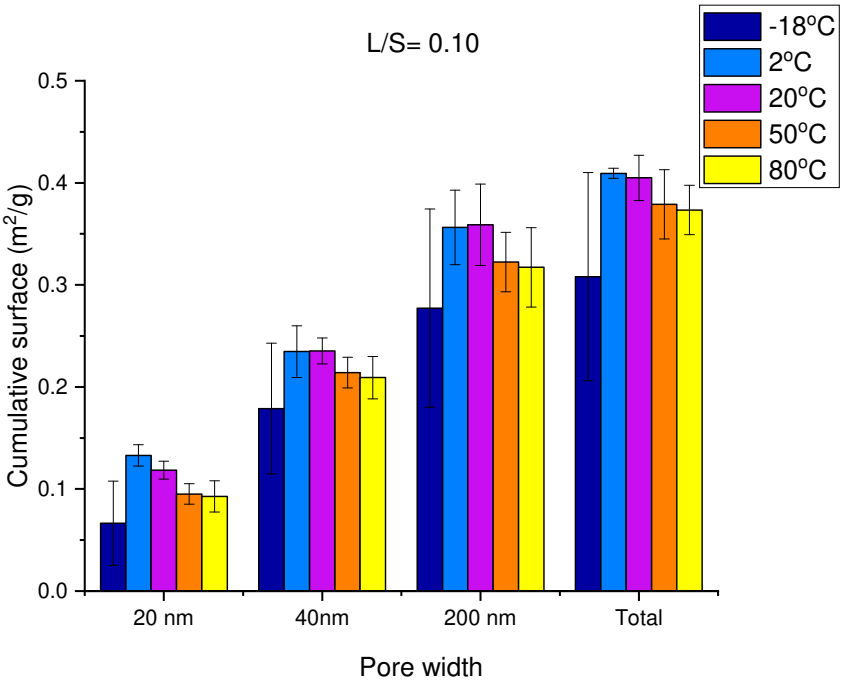

Figure 5.9. Surface area of granules of α-lactose monohydrate at L/S=0.10 ratio dried at different temperatures (n=4, error bars= standard deviation)

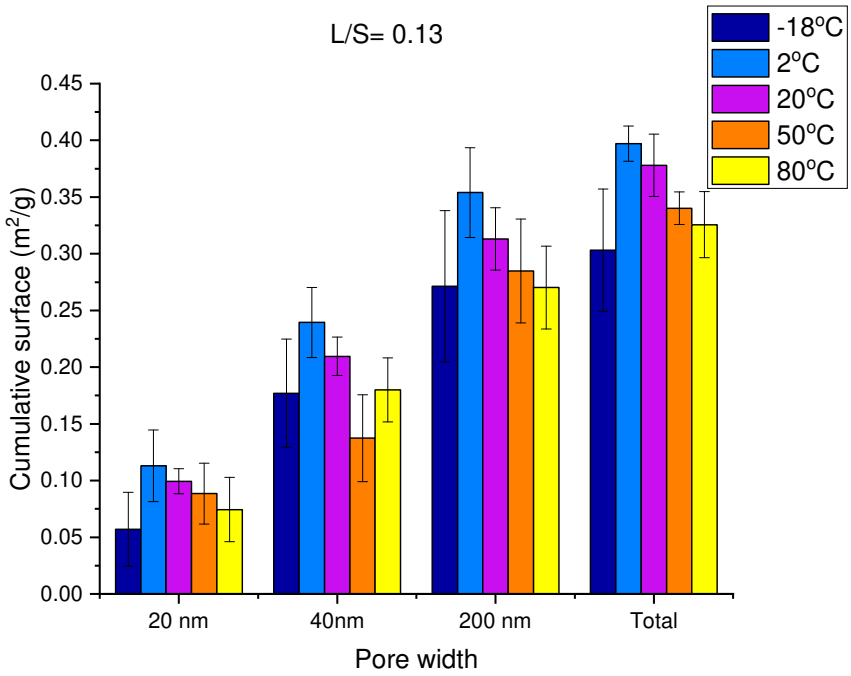

Figure 5. 10 .Surface area of granules of α-lactose monohydrate at L/S=0.13 ratio dried at different temperatures (n=4, error bars= standard deviation)

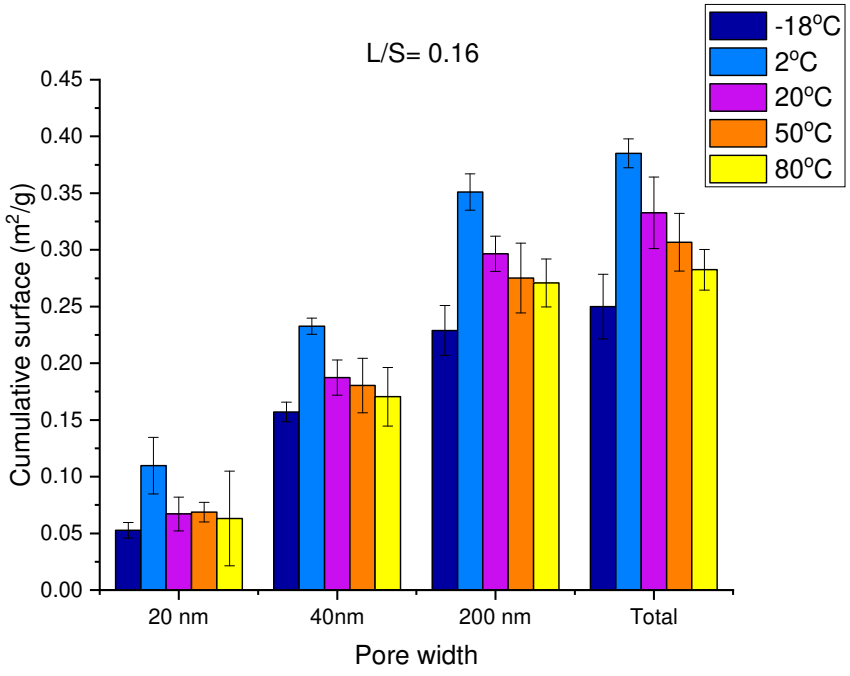

Figure 5.11. Surface area of granules of α-lactose monohydrate at L/S=0.16 ratio dried at different temperatures (n=4, error bars= standard deviation)

This type of change corresponds to the typical behaviour when the drying mechanism is governed by capillarity (Richardson and Coulson, 2002). At temperatures over 0 °C, the forces controlling the movement of water are capillary which can modify the porosity and the morphology of the granule since the water is removed depending on the suction potential produced by the liquid. However, under 0 °C, there is not capillary movement since water is frozen and the moisture from the granule will be removed by vapour diffusion i.e. the granule does not experience great porosity modifications (Richardson and Coulson, 2002). The surface areas were compared for the three L/S ratios at the different temperatures over 0 °C since they have same drying mechanism (Figure 5.12, 5.13, 5.14 and 5.15). For all the temperatures the surface area decreases when the L/S increases, which was already reported in the literature for α-lactose monohydrate where the porosity of the granules decreased by half with an increment of L/S ratio of 0.3 for blend with 73.5% lactose composition (El Hagrasy et al., 2013a). However, it was observed that the difference between the three L/S ratios is remarkable depending on the drying temperature. The lowest L/S ratio has been less influenced by the drying temperature than the higher ratio. For the L/S=0.16, a change in temperature produces a decrease of the surface area of over 25% when for the L/S=0.10 the change was under 9%.

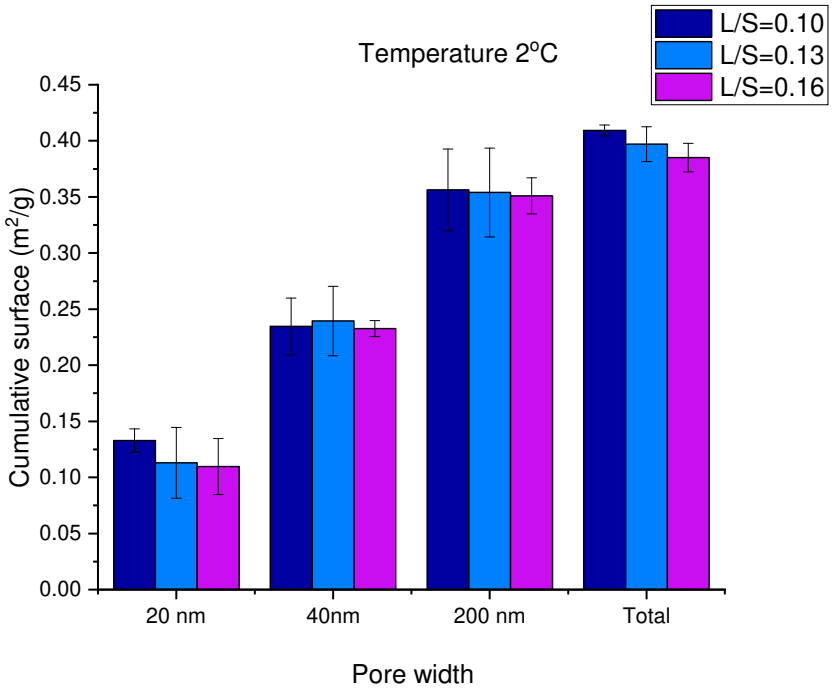

Figure 5.12. Surface area of granules of α-lactose monohydrate dried at 2°C (n=4, error bars= standard deviation)

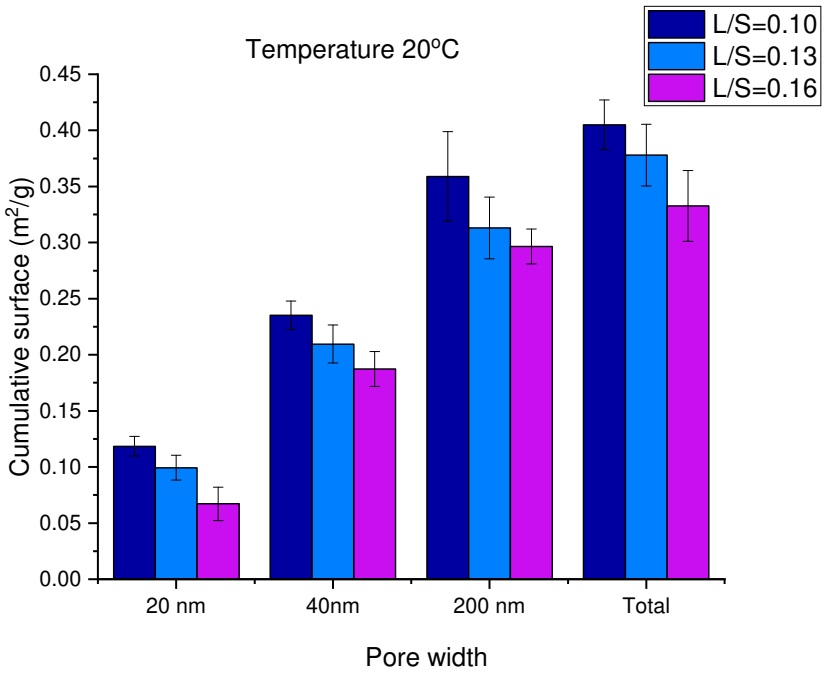

Figure 5.13.Surface area of granules of α-lactose monohydrate dried at 20°C (n=4, error bars= standard deviation)

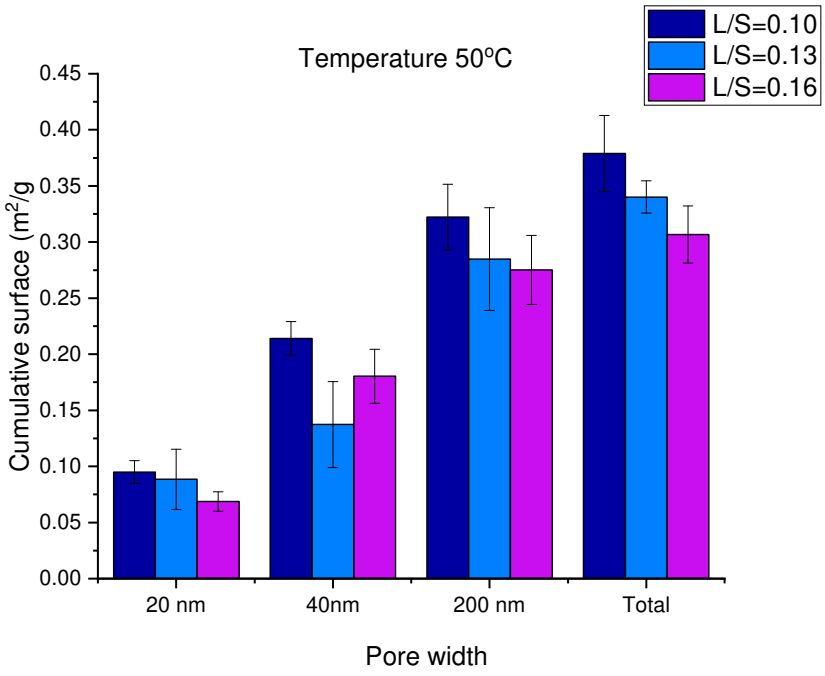

Figure 5.14. Surface area of granules of α-lactose monohydrate dried at 50°C (n=4, error bars= standard deviation)

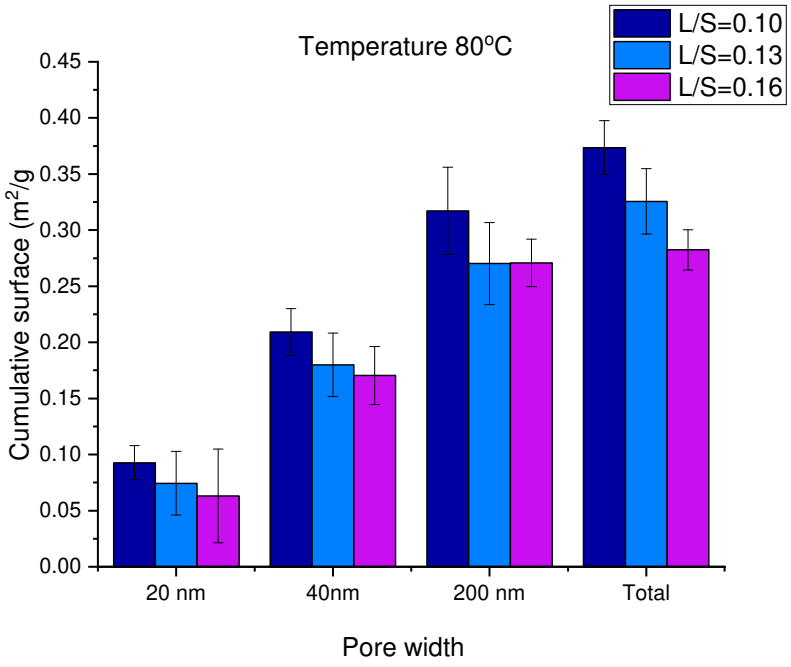

Figure 5.15. Surface area of granules of α-lactose monohydrate dried at 80°C (n=4, error bars= standard deviation)

The negative pressure of a pore containing water which will drive the liquid to rise is known as capillary force and is given by equation 5.2 (Richardson and Coulson, 2002).

$$h_t = \frac{2\,\sigma}{r'\rho\,g} \qquad \text{Eq 5.2}$$

Where σ is the surface tension, ρ is the density of the liquid and r' is the radius of the particle which was assumed constant in this case. Since, the only variables which change depending on the temperature are density and surface tension, in figure 5.13, the surface area was plotted versus the ratio between surface tension and the density of the water for temperatures over 0^{o}C. Since under 0^{o}C, drying is not produced by this mechanism, -20^{o}C results will not be included. There is a good linearity between both parameters in figure 5.16 and the slope increases when the L/S increases i.e. the size of the granules increases. Also, at higher temperatures, the differences between L/S is less pronounced than at lower temperatures where the drying is very slow which seems to indicate than at higher temperatures this phenomenon is less prevalent than for lower temperatures which has not been reported in the literature.

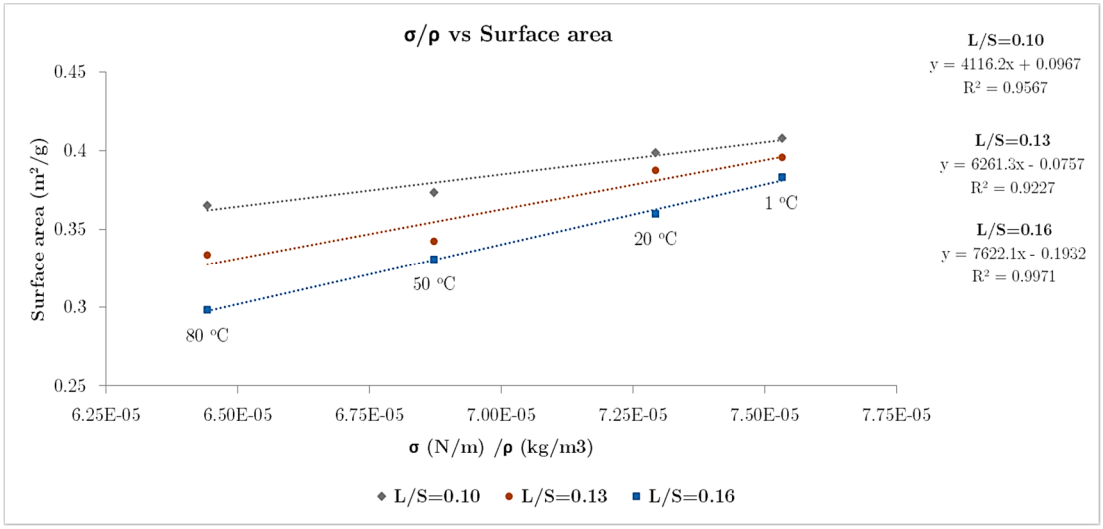

Figure 5.16. Surface area depending of the surface tension and liquid density ratio of water.

Although figure 5.16 helps to understand the changes of porosity at different temperatures, it is not possible to calculate the suction potential from this equation which assumes a systematic packing of uniform spherical particles. As it was seen in chapter 4, the nucleus composing the granules of α-lactose monohydrate in TSG are not arranged in uniform packing and the components of the full structure are far from being perfect spheres.

5.3.6 Effect on the tabletting depending on the drying temperature

The tensile strength of the tablets was calculated using equation 5.1. Tensile strength does not show any direct relationship with the surface area for the L/S studied (Figure 5.17a) nor the temperature were the results were not significantly different (Figure 5.17b). However, it was noticed that between 20°C and 80 °C

there is an increase of the tablet strength depending on the increase of temperature which would require further investigation.

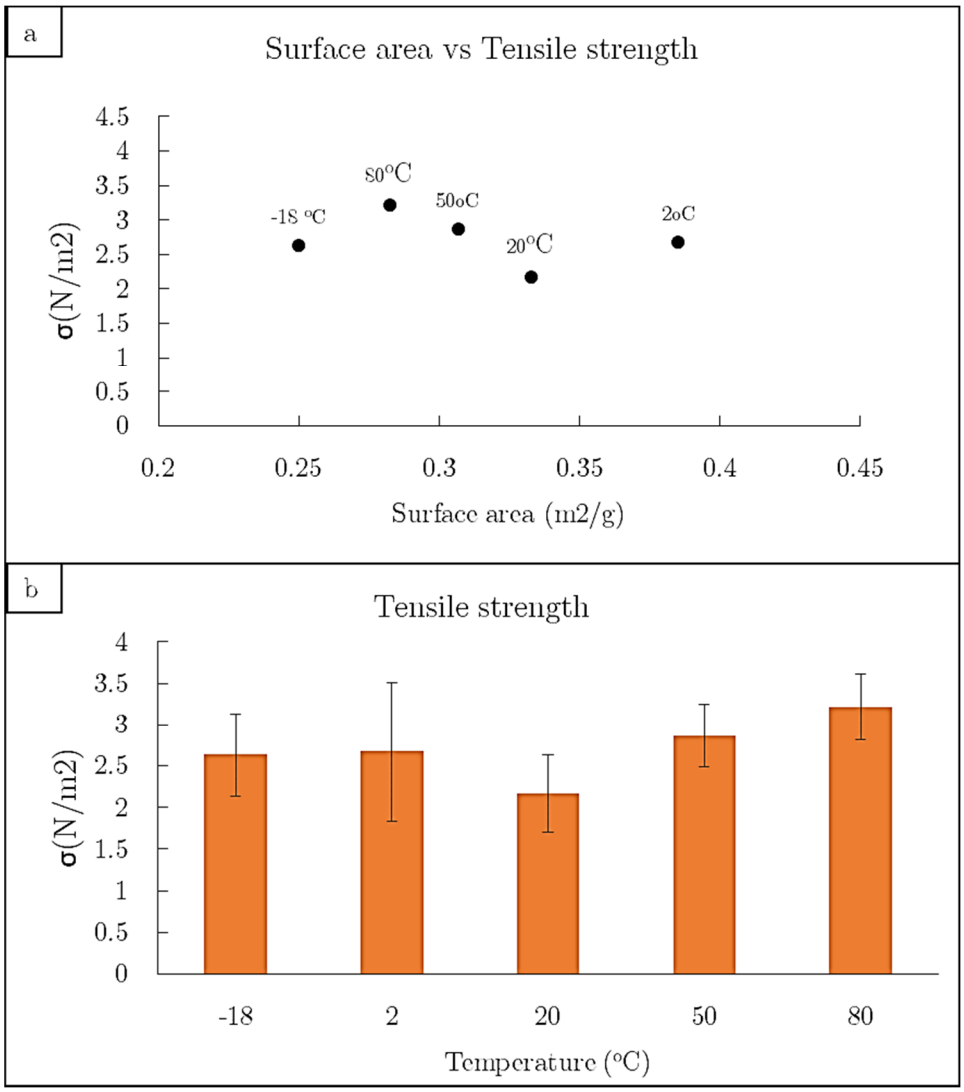

Figure 5.17. Tensile strength versus a) Surface area and b) temperature for L/S=0.16

5.4. Conclusions

The static drying of granules at different temperatures produced at three L/S ratios was used to improve the understanding of liquid bonding. After discarding any polymorphic events during the drying, it was concluded that drying temperature had an important role in the final surface area of the granules. Since surface area has a critical importance during tableting (Berggren and Alderborn, 2001), it is very important to ensure that the characteristics obtained in granulation are not modified due to the drying process. The effect of no controlling this parameter could potentially produce misleading results in research and lack of uniformity in industry.

In addition, it was observed that the increase of the L/S ratio has a determinant effect in the growth of the granule, doubling the size of the granules and reducing the porosity when there is an increase in the liquid-to-solid ratio. This results agrees with those found in the literature (El Hagrasy et al., 2013b). However, it was found that in the case of the surface area, the decrease of the surface area depends also on the temperature of drying which has not been reported in the literature before. Furthermore, the drying temperature reduces drastically the differences between liquid-to-solid ratio since at 2°C the difference between 0.10 and 0.16 was 0.025 m^2/g and at 80 °C was 0.091 m^2/g.

When the effect of the L/S on the nuclei was studied it was found that there were not remarkable differences in the maximum size achieved which was never over 200 μm. Nevertheless, an increase in the height of the peak of the particle size between 100-200 μm was found. This seems to indicate that the granules grow by coalescence of the nuclei and the final size of the granule depends on the amount of nuclei which have bonded together. This results agrees with Verstraeten et al. who stated that at higher L/S ratio, the bimodality is reduced obtaining larger granules (Verstraeten et al., 2017). Nevertheless, the effect of varying the temperature of drying on the tablets was not conclusive and further study will be required.

Chapter 6

Determination of the internal forces depending of the channel fill level

6.1 Introduction

Despite of the potential of channel fill as a design tool, there is not an extensive knowledge base indicating how the increase of channel fill affects the process within the TSG. Some studies have already suggested there is inner variations due to the change in shape of the granules. High channel fills are associated with more spherical products and low channel fills are more likely to produce

elongated granules (Dhenge et al., 2011, Gorringe et al., 2017). The reported changes in granule morphology seems to indicate that changes in the local forces inside the granulator are occurring, however, there are few examples of quantitative study of the mechanical stresses in the screw elements. Traditionally, the stresses experienced by the granules in the TSG have been calculated at a global level as direct function of the torque applied by the granulator(Dhenge et al., 2012b) or as function of the screw speed (Lute et al., 2018).

The local stress applied to the granules can be measured directly by the use of microencapsulated sensor particles (CAMES), calibrated to rupture at specific critical stress levels releasing a dye which can be measured spectrophotometrically. Therefore, it is possible to have an accurate measurement of the total stresses which a sample has been exposed during its production. These stress sensitive beads have already been used before in continuous extrusion obtaining insight into the stress history of a twin screw extruder (Bigio et al., 2011, Pappas et al., 2012). These microencapsulated sensors are sized equivalent to the powder input so they provide information at the correct scale of scrutiny.

In this chapter, the applicability of the channel fill fraction to the 11 mm TSG as well as the transferability of the microencapsulated sensors measurement from

extrusion to granulation has been studied. In addition, it will establish the relationship between the stress experienced by the granules at different channel fills and torque requirements.

6.2 Materials and methods

6.2.1 Materials

6.2.1.1 Granulation

The powder formulation contained 73.5% w/w lactose monohydrate (PubChem CID: 104938, Pharmatose 200,DFE Pharma, IMCD UK Ltd, Sutton, Surrey, United Kingdom), 20% w/w microcrystalline cellulose (PubChem CID: 14055602, Avicel PH101, Sigma-Aldrich Company Ltd., Dorset, England), 5% w/w hypromellose (PubChem CID: 57503849,Pharmacoat 603, Shin-Etsu Chemical Co. Ltd, Wiesbaden, Germany) and 1.5% w/w croscarmellose sodium (PubChem CID: 6328154, Ac-Di-Sol, Danisco, Copenhagen, Denmark). The formulation was blended in batches of 5 kg in a 15L blender bin for 10 minutes at 17 rpm in an Agiblend AB015 (Pharmatech, Coleshill, United Kingdom). Granulating liquid was distilled water (EMD Millipore™ Pure Water Reservoirs, Millipore SAS, Mosheim, France) which was maintained at a liquid-to-solid ratio of 17.5% in weight. The volumetric mean diameter of the formulation was 71.54 μm with a homogeneity of the PSD of 69.9% .

6.2.1.2. Mechanical stress measurement

In order to measure the local mechanical stress, microencapsulated chemical sensors (Lot 9-13-553CAMES™, Mach I, Inc.,Pennsylvania, USA) were used. These microcapsules (diameter < 44 µm) contain an organic UV detectable blue dye in xylene encapsulated in a polymeric sphere with rupture determined by the applied shear stresses (Condo and Kosowski, 1991). In this case, the rupture and shear stress are related linearly in a range of 231.75 to 1224.25 kPa (0-100% breakage). The blue dye is an anthraquinone (Automate™ Blue 8AHF, Keystone Inc, Chicago, USA) which is fully soluble in IPA (2-Propanol, ≥99.8%, HiPerSolv CHROMANORM® for HPLC, VWR International Limited, Lutterworth, United Kingdom) with λmax of 645.77 nm. The sensors were added to 125 g batches of the formulation in a proportion of 0.53% w/w and mixed in 5 l blender at 3 rpm for 40 min.

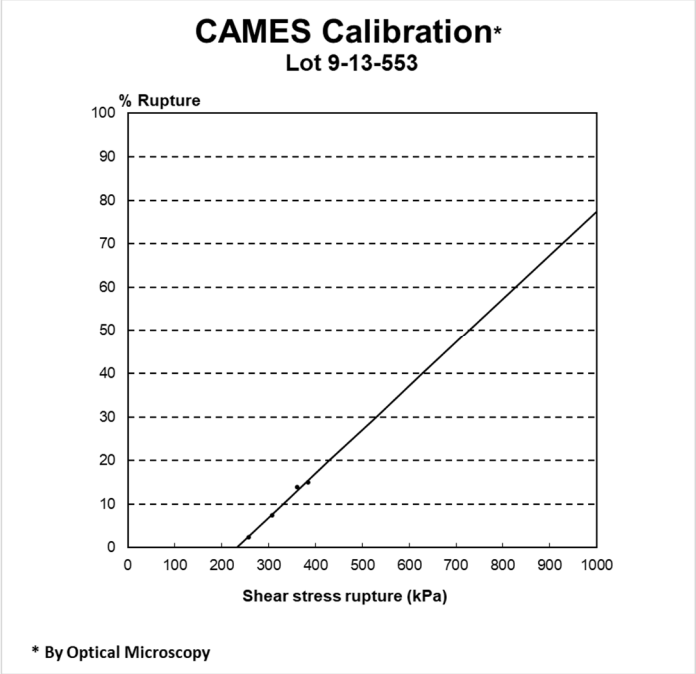

Figure 6.1 CAMES calibration (provided by the manufacturer)

6.2.2 Granulation experiments

The experiments were carried out using both a Thermofisher Pharma 11 mm Twin Screw Granulator (Process 11, 40:1 L/D, Thermo Fisher Scientific, Karlsruhe, Germany) and a 16 mm Prism Euro Lab Twin Screw Granulator (Process 25:1 L/D, Thermo Fisher Scientific, Karlsruhe, Germany). Both TSGs was fed via a gravimetric feeder (Brabender Gravimetric feeder DDW-MT, Brabender Technologie Gmbh & Co. Kg Duisburg, Germany) and the liquid added by a syringe pump to remain a constant Liquid-to-solid ratio of 0.175 (Harvard Syringe Pump, Harvard Apparatus UK, Cambridge, United Kingdom). The screw

configuration consisted of 2 sets of 7 × 0.25D bilobe kneading element (60° forward), 1 set of 3 × 0.25D bilobe kneading element (90°) and the rest conveyors. Samples for analysis were taken when steady state was reached after 2.5 min. Afterwards, the samples were dried for 2 h in an oven at 60 °C (Memmert UNB100, Memmert GmbH + Co. KG, Schwabach, Germany).

The channel fills for the 11mm TSG was studied using the following summary of experiments which can be found in Figure 6.2 where the points of measurements are represented. The channel fill (Φ) is calculated using equation 6.1 (Gorringe et al., 2017).

$$\Phi = \frac{\dot{m}}{n_v \rho_B \left(V_F \frac{S_L}{L}\right) N}$$

Eq 6.1

Where $\dot{m}$ is powder flowrate (kg/h), n_v is volumetric efficiency of the screw to convey powder which is assumed 100%, ρ_B is the bulk density (kg/m^3), V_F is the conveyor free volume considered 25.04 cm^3 for the 11mm TSG, S_L/L is the inverse of length to diameter ratio of the TSG, i.e. inverse of 40:1 for the 11-mm TSG and N is the screws velocity (rpm/60). Channel fill fraction was calculated based in bulk density since the liquid will be absorbed into the voids of bulk powder. Although, the profile of the parameter is difficult to determine experimentally

due to changes within the granulator, mean bulk density can be assumed constant for a given liquid to solid ratio, screw configuration and formulation

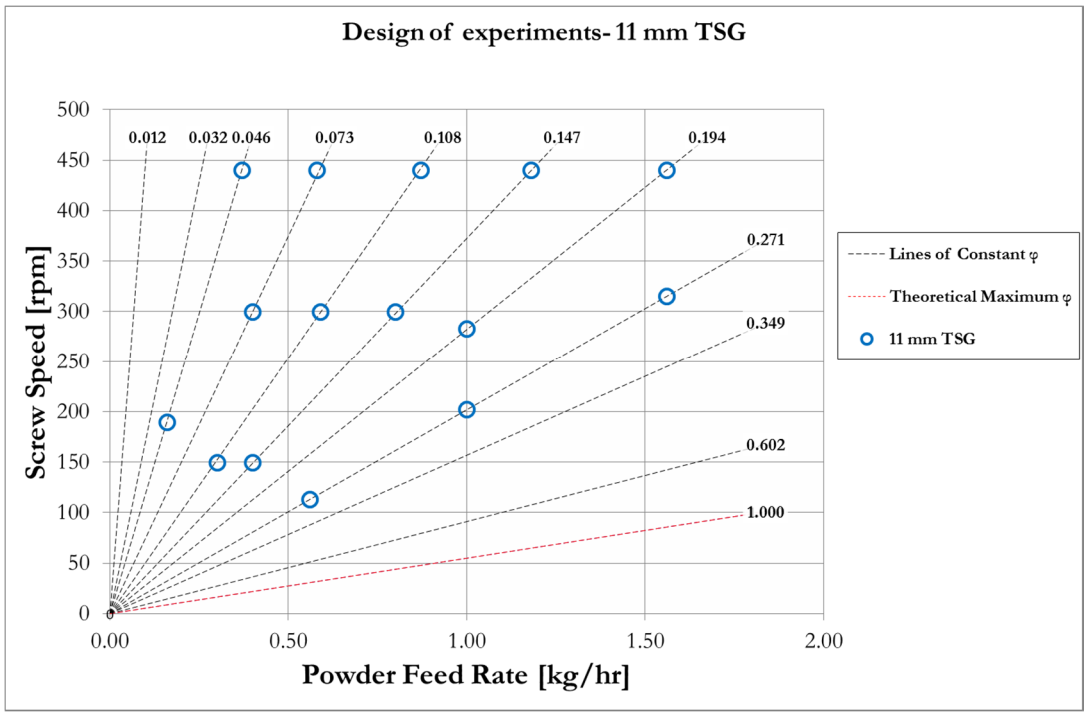

Figure 6.2 Summary of experiments for 11mm-TSG

6.2.3. Offline granule size analysis

The analysis of the granule size distribution was performed distribution was performed following the same procedure described in section 3.2.3. In order to compare if the PSDs are equivalent, two methods were used depending of the number of experiments carried out for channel fill. For those cases under three experiments, F-test was used comparing the curves by the variance. When three or more experiments were carried out, Anova with O'Brien homogeneity of variance assumption which is recommended for those samples whose size is smaller

than 10 regardless the shape of the population (Wang et al., 2017). Both methods test if series of measurements carried out under different conditions are significantly different (Brandt and Brandt, 2014, Eriksson et al., 2013). All the analysis was performed using the software Matlab and Statistics Toolbox R2017a (The MathWorks, Inc., Natick, Massachusetts, United States) using each PSD as an individual level with a 0.05 level of tolerance. The PSDs were compared also depending of the screw speed which will have a direct effect in the shear rate exerted on the powder mass (Lute et al., 2018). Three screw speeds were compared at three level of differences between channel fills (low: 0.108-0.147), medium (0.073-0.194) and high (0.046 -0.271).

6.2.4 Calibration of the microencapsulated stress sensors

6.2.4.1 UV calibration

To measure the microencapsulated stress sensor rupture a UV calibration relationship between absorbance and concentration, covering the possible range of rupture, was determined with ten systems, prepared gravimetrically (BP211D Analytical model, Sartorious, Surrey, United Kingdom), between 0-60 ppm by weight. A concentrated dye provided by the manufacturer (Automate™ Blue 8AHF, Keystone Inc, Chicago, USA) was weighted and dissolved in IPA obtaining three initial stock solutions of 115, 116 and 216 ppm. The dye was fully

soluble in IPA and it was found to be fully mixed after 10 manual rotations. The subsequent solutions with concentrations between 0-60 ppmw were prepared by dissolving a specific volume of stock (V_{stock}) in IPA to reach a final total volume of 5 ml. The volume of stock required was calculated according to equation 6.2. The final concentrations were recalculated depending on the exact weight added in order to increase the accuracy of the calibration.

$$V_{stock} = \frac{V_c\, C_c}{C_{stock}}$$

Eq. 6.2

Where V_{stock} is the volume required of the stock solution, C_{stock} is the concentration of the stock solution, V_c is the final volume of the solution (5 ml) and the C_c was the final concentration of the solution which varied between 0-60 ppm.

The absorbance was analysed in a UV Spectrometer (Carl Zeiss MCS600, Oberkochen, Germany) with off-line cell holder attachment (Fibre-coupled cuvette holder of 10 mm cuvettes with UV Fiber Optics, Hellma GmbH & Co, Müllheim, Germany). The calibration was repeated three times with an acceptance criterion of coefficient of regression (R^2) over 0.999 (Figure 6.3).

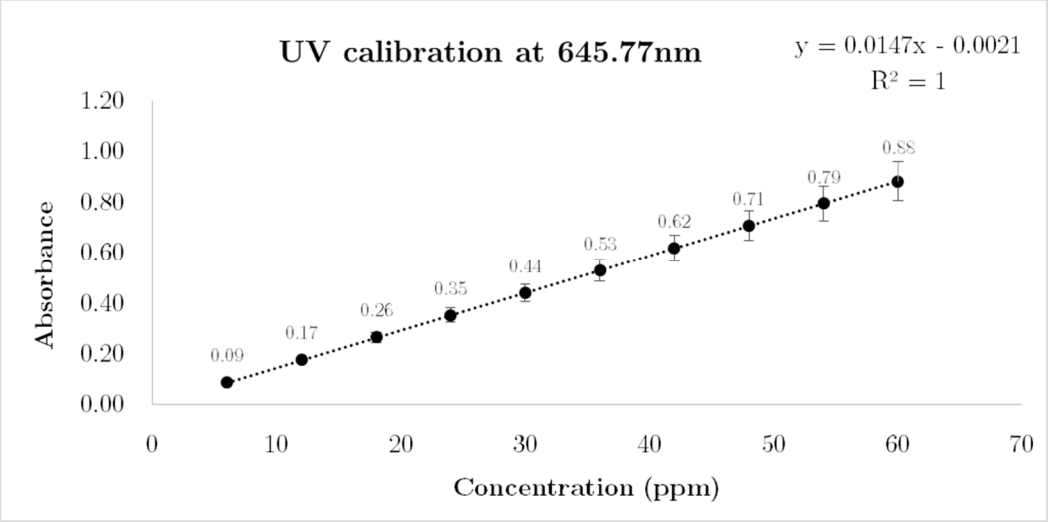

Figure 6.3. UV calibration of the dye

6.2.4.2 Dye recovery from the granules

To control the formulation interference in the measurement of released dye, the recovery of dye from both the blend and individual components of the blend was determined, by mixing 10 ml of a 60 ppm by weight dye-IPA solutions with the blend and each individual component in the same proportion as the formulation. Filtration was performed using a sample processing manifold (Biotage® VacMaster™ 10, Biotage, Uppsala, Sweden) using syringe isolute single fritter reservoir filter 70 ml 5µm (Biotage, Uppsala, Sweden) with smaller pore diameter than the d10 of the individual component's particle size. Afterwards, monitored vacuum was applied by a vacuum controller (BUCHI™ V-850, BÜCHI Labortechnik AG, Flawil, Switzerland). The dye solution recovered was analysed measuring the absorbance at the same wavelength of the UV calibration (645.77 nm).

After filtration dye recovery was between 98-101% which is inside of the variance range of the UV spectrometer and let us conclude that released dye can be fully recovered from the materials.

6.2.4.3 Breakage of the microencapsulated stress sensors

The shear stress which produces sensor rupture is calibrated for each lot by the manufacturer and the relationship between the shear stress and the percentage of rupture was shown to be linear. The proportional rupture under certain shear stress was qualitatively confirmed by the use of shear cell rotor-stator integrated with a microscopic stage (Leica Microsystems (UK) Ltd, Milton Keynes, United Kingdom) visualising the rupture of the microencapsulated sensors with <44 μm. The stage was adjusted to a gap distance between the rotor and stator discs to match the mean size of the sensors and spinning speeds range of 0.01 to 5 rad / sec. In figure 6.4, the shear stress over the sensors was increased by the increment of the velocity of the rotor. As was expected, the microencapsulated sensors break as the shear stress increases.

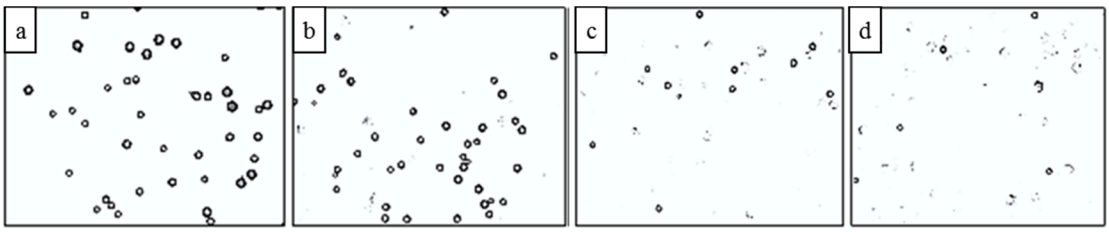

Figure 6.4. Microscopic images of the microencapsulated sensors breakage in the shear cell. a) 0.01 b) 0.1 c) 1 d) 5 rad/sec.

In addition to determine quantitatively the absorbance of 100% sensor rupture the sensors were mixed with the blend in 0.53% w/w proportion and compressed in a manual hydraulic press (Specac Ltd., Orpington, United Kingdom) with a die of 0.8 cm applying a force over 7000 kPa, which is higher than the maximum value indicated by the manufacturer. The fully broken capsules and the released dye were dissolved in IPA, filtered and their absorbance was analysed in UV. Five samples from different batches were analysed providing a concentration of 547.38 ± 69.73 ppm_w for the fully broken microencapsulated sensors.

The granules obtained from the TSG were dissolved in 4-10 ml of IPA, filtered and the absorbance was measured in the UV. The amount of IPA varied in order to optimise the washing of the filter. The concentration was calculated using the dye-IPA calibration. Concentrations were standardised using equation 6.3 depending of the exact amount of IPA and filtered solid. Afterwards, stand-

ardised concentration was divided by the concentration given from a 100% rupture according to equation 6.4. From that value is possible to calculate the shear stress using equation 6.5 which was provided by the manufacturer (MACH I Inc, Pensilvania, United States).

$$C_{eq} = C_i * \frac{1}{m_i} * \frac{1}{V_i} \quad \text{Eq. 6.3}$$

$$B\ (\%) = \frac{C_e}{C_{100\%}} \quad \text{Eq.6.4}$$

$$\sigma_{CAMES}(kPa) = 9.925 * B\ (\%) + 231.75 \quad \text{Eq. 6.5}$$

where C_{eq} is the standardised concentration (ppm), C_i is the concentration calculated from the absorbance (ppm), m_i is the mass of the sample (g), V_i is the volume of the sample (ml), B is the percentage of broken sensors (%), $C_{100\%}$ is the concentration when 100% of the sensors are broken, σ_{CAMES} (kPa) is the shear stress calculated by the CAMES..

6.2.5 Relationship between shear forces and channel fill in granulation

Eight replicate granulations with microencapsulated sensors and ten replicate granulations without them were carried out in the 11 mm TSG with a constant feed rate and L/S ratio but by varying the screw velocity between 40-400 rpm (Table 6.1) in order to vary the torque as calculated by the equipment software. In addition, the same conditions were reproduced without liquid addition to

study the effect of the granulation process on the torque. The results were compared with both torque and specific mechanical energy for the granulations without the microencapsulated sensors. Three repetitions were carried out for all the experiments with only formulation and one repetition carried out with microencapsulated sensors. In addition, three different conditions at the same high channel fill were studied to investigate the variability of the specific mechanical energy at same channel fill.

Table 6.1 Summary of channel fill and shear stress relationship experiments with (w/) and without (w/o) microencapsulated sensors.

Torque velocity (rpm)	Feed rate (kg/hr)	L/S	Φ	Microencapsulated sensors
400	0.5	0.175	0.068	w/-w/o
350	0.5	0.175	0.078	w/-w/o
300	0.5	0.175	0.091	w/o
250	0.5	0.175	0.110	w/-w/o
200	0.4	0.175	0.137	w/o
150	0.5	0.175	0.183	w/-w/o
100	0.5	0.175	0.274	w/-w/o

80	0.5	0.175	0.342	w/-w/o
60	0.5	0.175	0.457	w/-w/o
40	0.5	0.175	0.685	w/-w/o

In addition, the granulations with microencapsulated sensors were used to compare the specific mechanical energy with total shear forces experienced by the granules. Samples of 0.5 g after reaching steady state were taken and analysed by the method explained in the previous section. The specific mechanical energy of the granulation was calculated by applying equation 6.6. (Dhenge et al., 2013, Godavarti and Karwe, 1997).

$$\text{SME} = \frac{\text{T} * N}{F} \qquad \text{Eq.6.6}$$

where SME is the specific mechanical energy (kJ/kg), T is the motor torque of the TSG ($\text{N} \cdot \text{m}$), N is the screws velocity (rpm) and F is the feed rate of the powder (kg/min).

To study the relationship between local stress and channel fill, three channel fills were selected (low: 0.073, medium: 0.146 and high: 0.270) at two different velocities: 150 and 400 rpm (Table 6.2). In order to isolate the impact of granulation from the conveyor transport of the powder, samples of 2 grams were taken for

each run at the solid feeder exit and compared with the outlet of twin-screw granulation before and after the binder addition.

Table 6.2 Summary of experiments of channel fill at two different levels and shear stress relationship.

Φ	Screws velocity (rpm)	Feed rate (kg/hr)	L/S
0.073	150	0.2	0.175
0.073	400	0.53	0.175
0.146	150	0.4	0.175
0.146	400	1.06	0.175
0.270	150	0.74	0.175
0.270	400	1.98	0.175

6.3. Results

6.3.1 Demonstration of 11mm TSG channel fill scalability

The potential of using channel fill to scale up feed rate was investigated verifying if this parameter can be used to predict PSDs in the 11-mm TSG. In figure 6.5, six different channel fills were investigated showing high similarity between their density distributions along a channel fill line independent of the screw velocity. The equivalence between the shapes of the PSDs is remarkable at low ($\Phi = 0.046$ and $\Phi = 0.073$) and high ($\Phi = 0.194$ and $\Phi = 0.271$) channel fills where at low channel fills fines are more prevalent than at high channel fills. One explanation for this behaviour is that the mean residence time and material hold-up increased for the same feed rate as function of the channel fill (Gorringe et al., 2017, Lee et al., 2012) which could reduce the contact between powder and therefore, the granulation rate.

However, the middle channels show more discrepancies between them. In both cases ($\Phi = 0.108$ and $\Phi = 0.147$), two of the conditions presented very similar shapes and one of them was different. In order to compare statistically if the curves were significantly different, F-test and one way Anova with O'Brien homogeneity of variance assumption were performed depending on the number of experiments carried out for channel fill. In all the cases, it was concluded that

at 0.05 level of tolerance, there were no significant differences between PSDs at the same channel fill (Table 6.3).

Table 6.3. Statistical analysis performed to the PSDs at different channel fill.

	F-test		Anova One-way-HOV			
Channel fill	F	p-value	B-F statistic	df	p-value	Significantly different
0.046	0.749	0.693	-	-	-	No
0.073	0.755	0.700	-	-	-	No
0.108	-	-	0.491	7	0.827	No
0.147	-	-	0.855	7	0.560	No
0.194	1.396	0.608	-	-	-	No
0.271	-	-	1.3	8	0.304	No

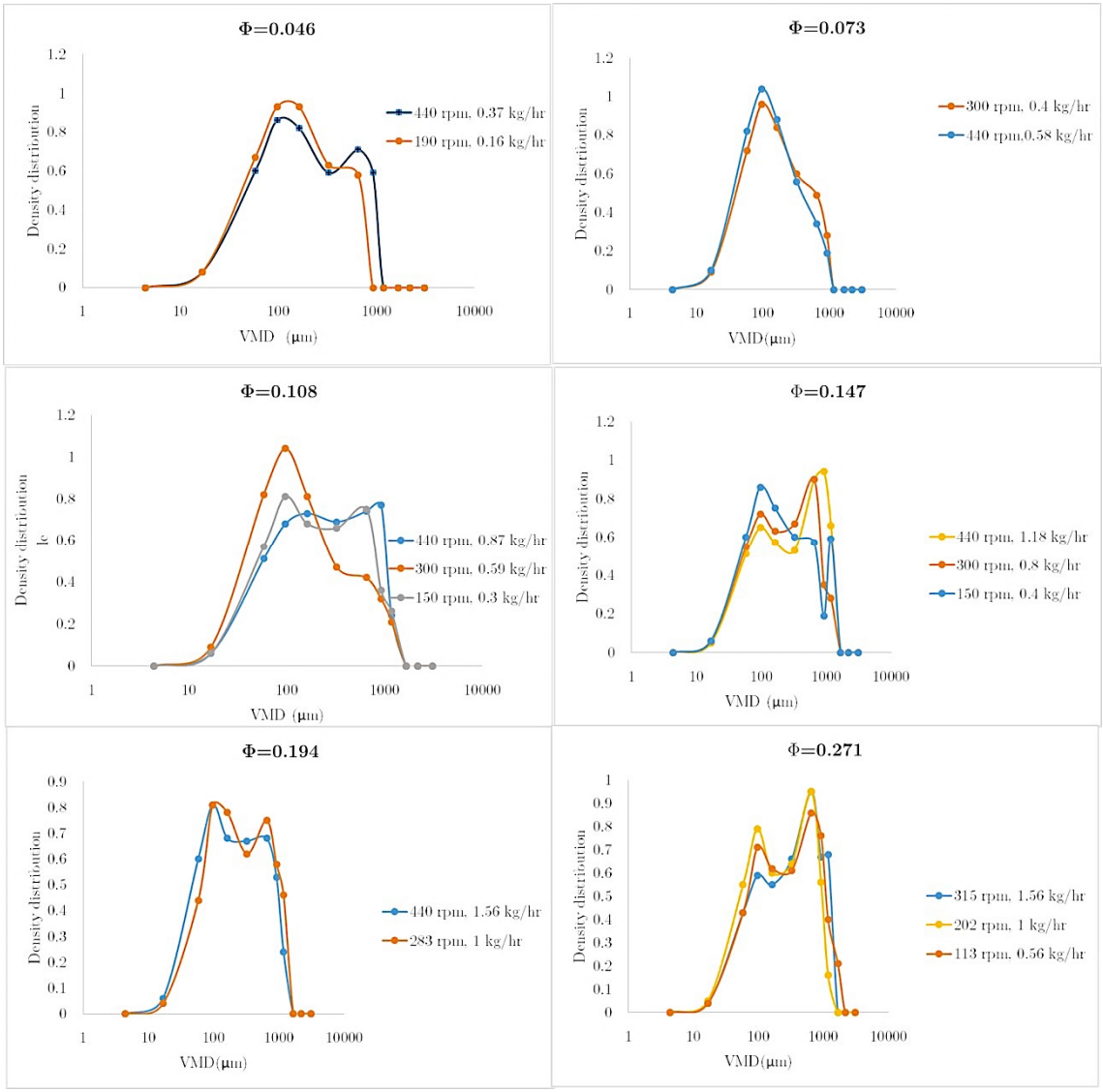

Figure 6.5 PSDs depending on the channel fill in the 11mm-TSG

In figure 6.6, the PSDs were compared depending of the screw speed at three levels of difference of channel fill ($\Delta\Phi$): low (0.039), medium (0.121) and high (0.225). In this case, it is possible to observe that PSDs appeared significantly different at high level of difference of channel fill but this difference was not that significant when $\Delta\Phi$ was small. F-test statistical analysis was carried out (Table

6.4) for the PSDs and it confirmed that at low channel fill differences, the variation of channel fill is not significant. However as $\Delta\Phi$ increases, the difference in the PSDs increases too reaching a point at high levels of channel fill where the PSDs are not statistically equivalent anymore. This suggests the inadequacy of using screw velocity as a design tool to predict PSDs this formulation.

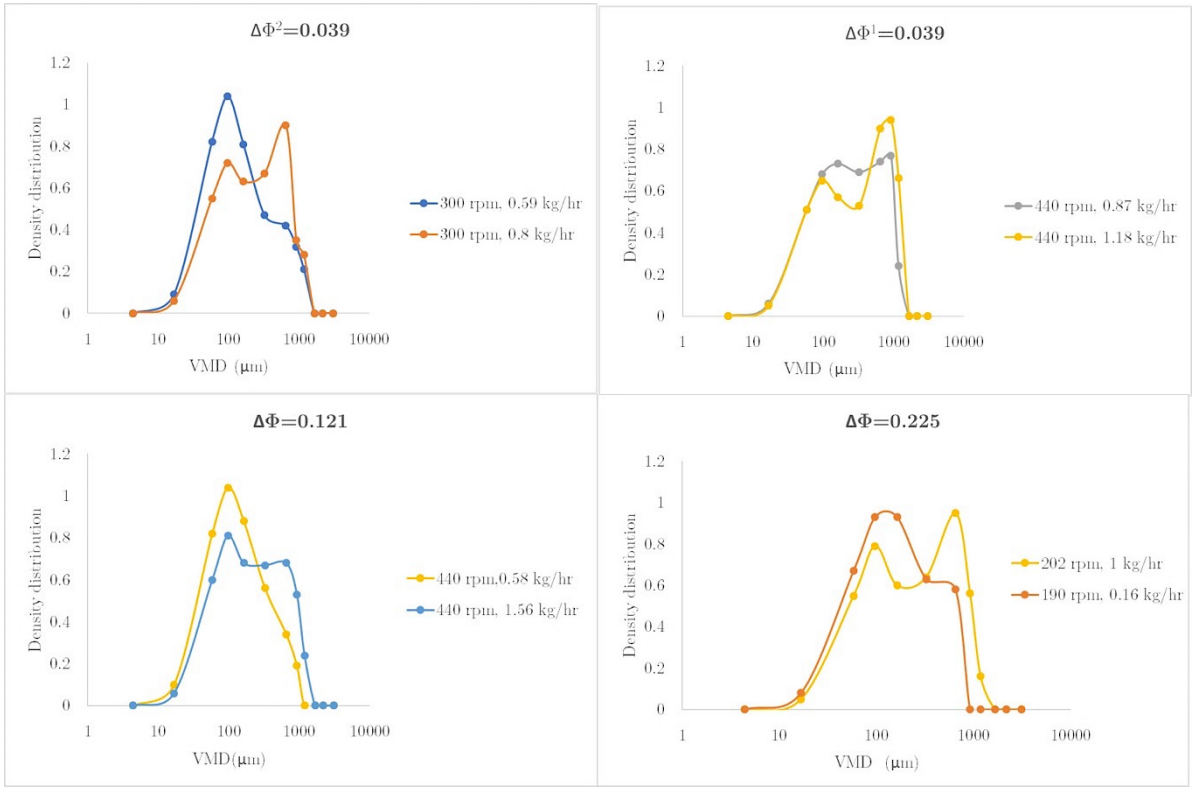

Figure 6.6. Comparison of PSDs at different screw velocity at three levels of $\Delta\Phi$.

Table 6.4.Statistical analysis performed to the PSDs at different screw velocity.

		F-test		
$\Delta\Phi$	Screw speed	F	p-value	Significantly different
0.039[1]	440	0.93	9.27E-1	No
0.039[2]	300	0.67	6.05E-1	No
0.121	440	2.40	2.71E-1	No
0.225	196 ± 6	34.52	4.57E-6	Yes

6.3.2 Comparison between 11 mm TSG and 16 mm TSG channel fill

In order to compare both scales 11mm and 16 mm, the same conditions were reproduced in the 11 mm and 16 mm and analysed both in QICPIC and sieving. Although they are statically equivalent (Table 6.5), figure 6.6 only shows similarities between both scales at low channel fills and higher discrepancies at high channel fills. Therefore, further higher channel fills should be analysed before it can be extrapolated between equipment. These phenomena can be related with the equipment size difference. In the 11 mm TSG, the barrel depth is 2.2 mm and in the 16 mm TSG is 3.3 mm which is a physical limitation to the maximum

possible growth of the granules. Therefore, this parameter requires further investigation to scale-up.

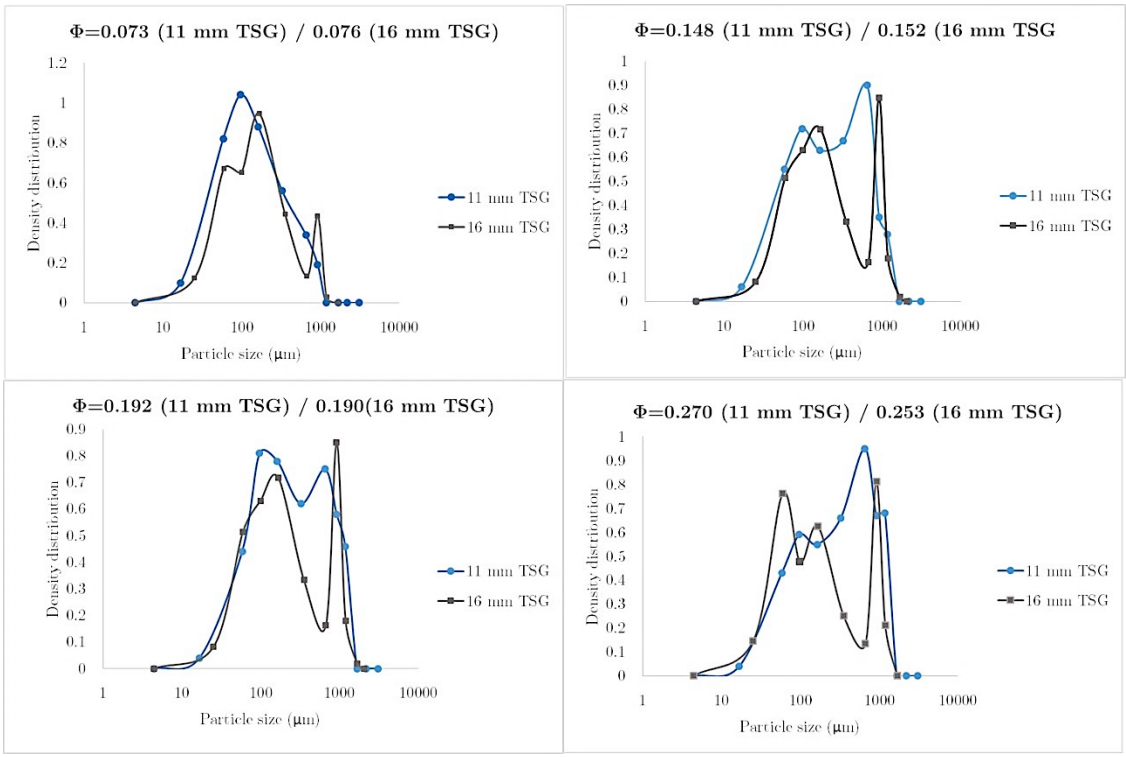

Figure 6.7. Comparison between 11 mm and 16 mm TSGs at low, medium and high channel fills

Table 6.5. Statistical analysis performed to the PSDs at different scale

	F-test		
Φ	**F**	**p-value**	**Significantly different**
0.076	1.12	8.83E-1	No
0.150	0.812	8.04E-1	No

0.190	1.00	9.99E-1	No
0.26	0.87	8.67E-1	No

6.3.4 Relationship between channel fill and torque force

The channel fill effect on the torque required was studied at a constant feed rate of 0.5 kg/h and L/S ratio and varying the screw velocity from 40 to 400 rpm (Table 6.1). In Fig. 6.8, the force required to both transport the powder with and without the addition of granulation fluid are presented. The torque necessary to move the powder when granulation and wet transport take place is nearly double than when only dry powder is transported. This phenomena can be associated with the changes of density due to the increased presence of formed granules and the resulting change in powder physical properties interacting with downstream elements. As well, the torque required at channel fills lower than 0.271 is relatively low in all the cases ($<1.5\,\mathrm{N \cdot m}$) increasing slowly (green area). However, after channel fill 0.271, the torque increases sharply (red-coloured area). Gorringe et al. demonstrated that the material hold-up and the mean residence time inside the granulator are linear functions of the channel fill and increases considerably at low screw speeds (Gorringe et al., 2017). Therefore,

this change in trend could be an indication that after reaching a certain point, the material hold-up within the equipment increased sharply at small variations.

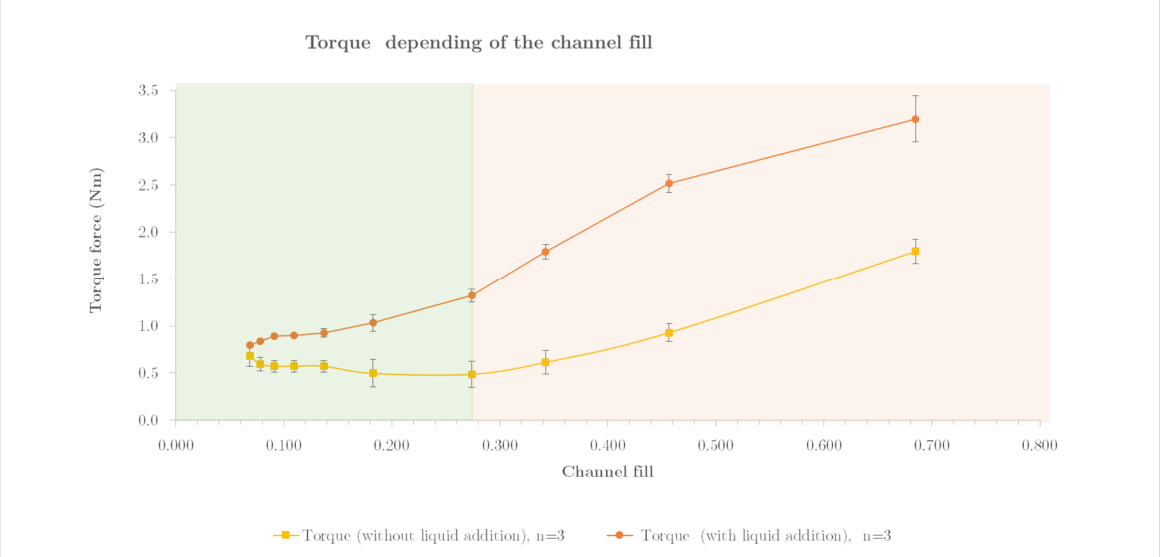

Figure 6.7. Torque depending of channel fill with and without liquid addition (n=number of repetitions, points=arithmetic mean, error bar= standard deviations)

The specific mechanical energy spent in granulation and wet powder transport was estimated subtracting the values used for transport of the dry powder from the values used when liquid was added to the system. Although the transport of dry and wet powder has not the same efficiency, the SME does not consider this difference since it is calculated as function of the total amount of material introduced into the equipment which is constant in this case. Figure 6.9a suggests that initially the specific mechanical energy value used for transport of the dry powder is higher than the one used for wet powder until it equalises around a channel fill of 0.18. After that point energy used for wet powder becomes

predominant until the last channel fill value. This value which corresponds with the last value possible without producing equipment damage, transport became predominant again over granulation. The specific mechanical energy used in granulation does not vary as much as the one required from transport that varies from 36.8 to 206 kJ/kg. Furthermore, comparing Figure 6.9a and 6.9b shows that after 0.27 channel fill, although the torque required increases dramatically, the specific mechanical energy used in granulation is almost constant.

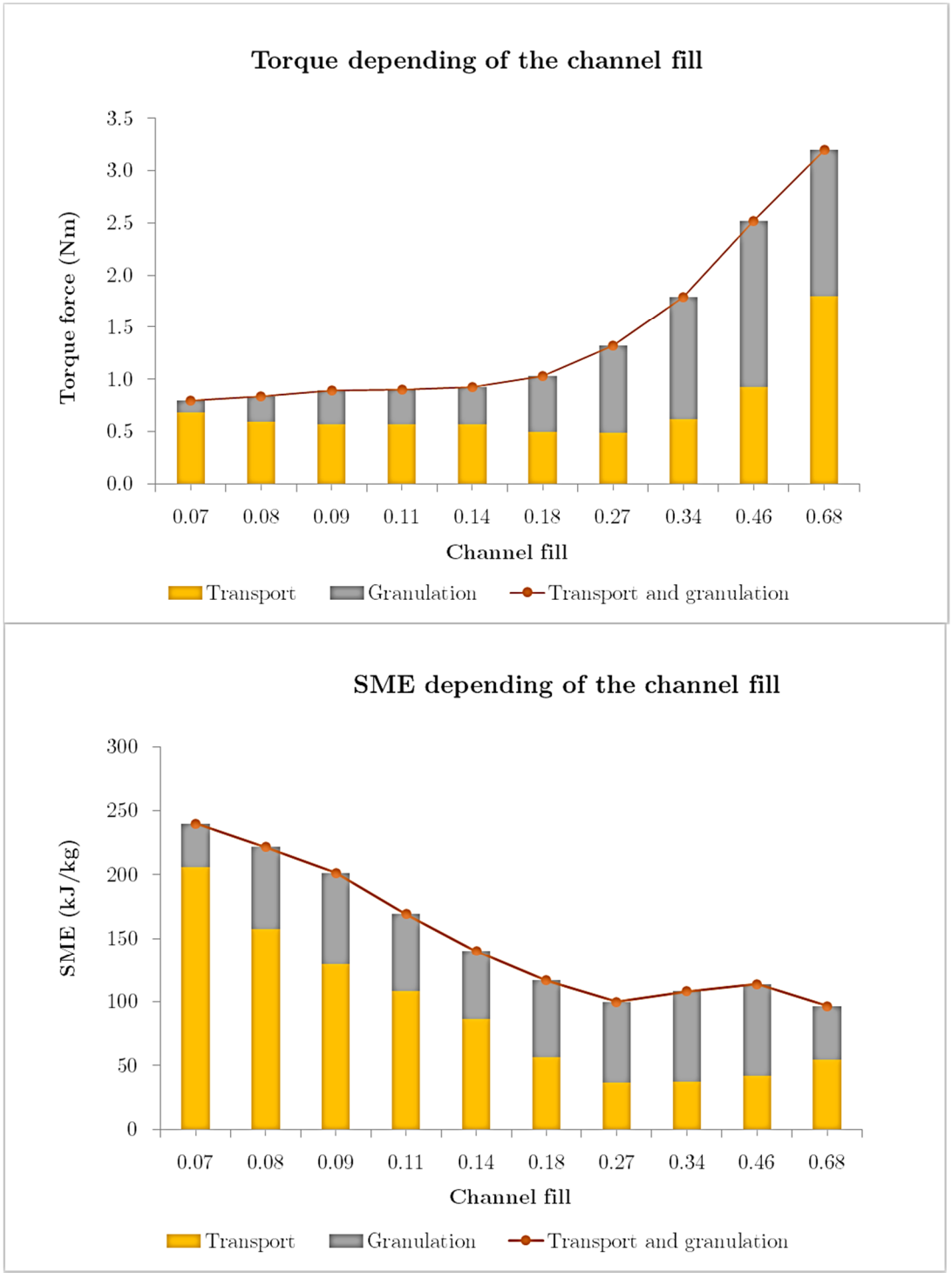

Figure 6.9. Predominant event depending on a) Torque and b) Specific mechanical energy

In addition, the specific mechanical energy was studied at channel fill of 0.27 produced by three different conditions (Figure 6.10). It was found that this

value was not constant depending on the channel fill and it varied highly depending on the torque requirements. However, the large size of the error bars seems to indicate that the specific mechanical energy has not a constant value along the same conditions of feed rate and screw velocity. The range variation of this parameter reduces highly its potential as process design parameter.

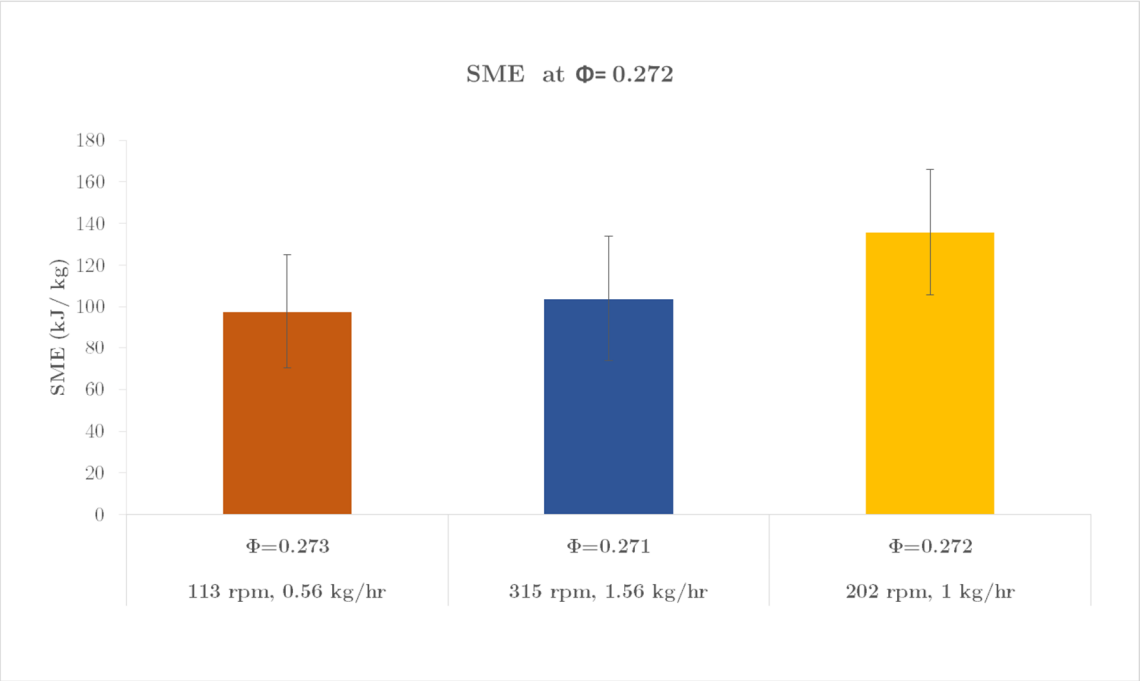

Figure 6.10. Specific mechanical energy at channel fill fraction of 0.272 (n> 90, Error bars = Standard deviation calculated as function of the standard deviation of the torque).

6.3.5 Effect of the increase of channel fill and torque in the shear stress.

The microencapsulated sensors were used to measure the stress experienced by the powder at different channel fills. In figure 6.11, three different levels of

channel fill at two different sets of conditions each (Table 6.2) are presented. The local stress produced by the transport of the powder through the granulator without liquid addition was consistently in the range 360-490 kPa which corresponds for 55-70% of the total shear experienced by the formulation during granulation conditions. This result is consistent with the results obtained in figure 6.7 for no liquid addition where at channel fills up to 0.270, the torque required did not have great variations (0.49-0.68 Nm) and did not present a linear trend with channel fill. The breakage of the microsensors in this case is due only to the transport of the powder through the equipment since no liquid addition was done at that point. In addition, figure 6.11 suggests that the local stress experienced in the combined granulation and transport process increases when channel fill increases within the channel fill range in figure 6.11. As the transport only data suggest this is not due to transport, this increase would be due only to granulation which is consistent with the increment in size observed in the PSDs in figure 6.5. However, with the variability obtained it is not possible to confirm this trend and it is only possible to conclude that there is a significant increase in stress due to addition of water to drive the granulation process.

Granulation using a constant feedrate of 0.5 kg/hr and L/S=0.175 and varying the screws velocity between 40-400 rpm (Table 6.1) are presented in figure 6.12

with the local stress plotted against the channel fill with the specific mechanical energy as labeled. Interestingly the results suggest that granules experience higher local stresses at a specific range of channel fills and this is not directly related to overall SME input. The points with highest local stresses align to transition to exponential torque rise with increased granulation energy but prior to fully filled barrel.

Nonetheless, it is possible to conclude that all the formulations or powder introduced into the twin screw granulator experienced a total stress between 360 and 1000 kPa. Direct comparisons with the literature is not possible due to the change of scale and formulation. However, these values are significantly higher than those found in literature which could be due to the lack of equivalence in size between the formulation and the sensors (Pradhan et al., 2017a) or the underestimation of some of the internal forces experienced by the granules from global estimates (Dhenge et al., 2011).

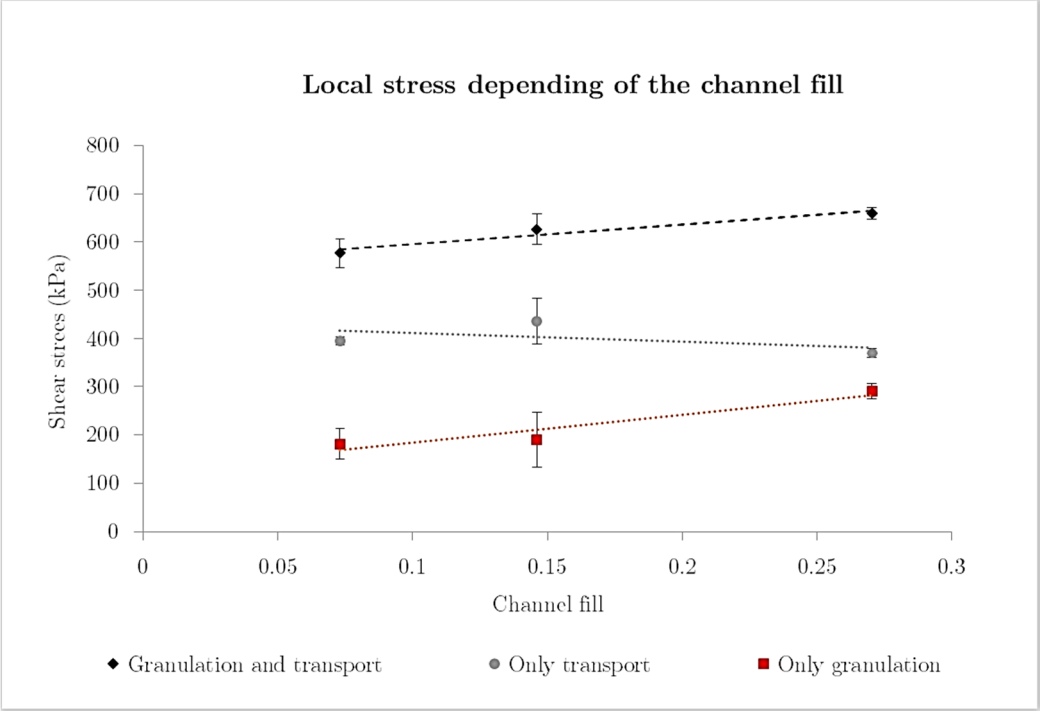

Figure 6.11. Local shear stress depending of the channel fill produced (points= arithmetic mean of the two different channel fills, error bars= standard deviation).

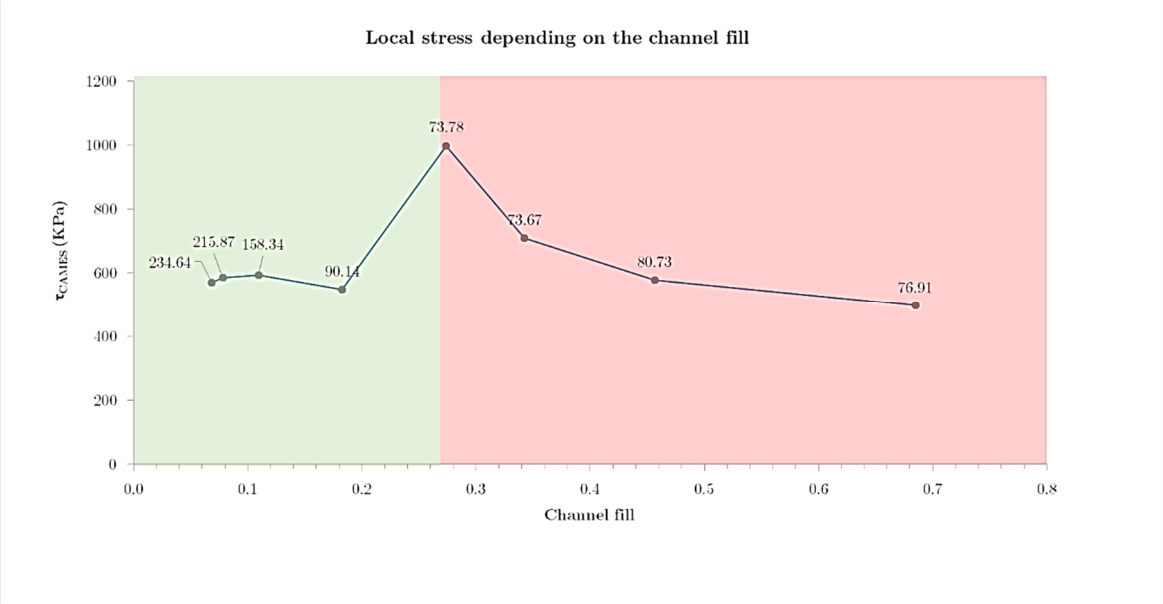

Figure 6.12. Local stress at steady state depending on the channel fill data labels= specific mechanical energy).

6.4. Conclusions

This chapter verified the applicability of the channel fill fraction to the 11 mm TSG. Also, it was established that it cannot be applied directly to exchanges in scale between the 11mm and 16 mm TSG. The similarities between low channel fills but discrepancies at higher channel fills suggested that the reason is probably the difference of available space allowing the granules grow bigger in the 16 mm than in the 11mm. As well as the same channel fills, the stress experienced by the granules was similar confirming the expectation that granules would have similar morphological properties. In addition, the applicability of the CAMES microparticles in granulation was demonstrated offering a novel way to measure TSG internal stress at a particle scale of scrutiny. It was verified that during granulation, the powder experienced total stresses in a 360-1000 kPa range which was relatively higher than expected.

A potential local maximum in local stress was observed that doesn't align to high SME input but instead with torque transition caused by channel fill. Transport of the granules without liquid addition suggested that up to 70% of the total breakage of the microencapsulated sensors and up to 86% of the required torque may not be created by granulation process. Furthermore, it was

found that the twin screw granulator does not present a linear relationship between channel fill and torque increasing sharply after a certain point and becoming sensitive to small variations in speed and or fill. Understanding this interplay of local and global behaviour can be critical in both implementation and control of the technology.

Since Thompson and Sun identified the machinery variables as one of the most immediate hurdles to adopt twin screw granulation (Thompson and Sun, 2010), the results of this chapter could potentially have a direct impact in industry. As industrial and mechanical engineering have increased their trend of using modelling and simulation tools to produce their designs, identifying the range of forces experienced by the granules could be directly applied for subsequent operations (e.g. tableting or transport) or equipment design (e.g. screw elements).

Chapter 7

General Conclusions and future work

This thesis has attempted to increase the current knowledge of continuous wet granulation focusing the majority of the research in twin screw granulation.

Two computational tools where developed allowing an increased scrutiny of granule properties. In chapter three, the homogeneity factor was developed allowing a simpler definition of workspaces without the issues associated with other metrics like span or d_{10} and d_{90}. In general, the parameter showed the potential as a design factor for two different materials and it helped to select the L/S as the parameter which required further investigation.

In chapter four, an algorithm was developed to reveal the internal structure of a continuous granule. Despite the limitations in the methods to evaluate objectively the segmentation and the tracking, the results in batch were equivalent in size and morphology to the ones found in the literature (Hapgood, 2000). However, further work will be required to find an objective method to compare the continuous results. Also, the code was found to be computationally expensive when larger amounts of particles were analysed and further optimisation is necessary to reduce the processing time required. In addition, it will be recommended to remove the hard-code parameters and substitute them for a calculated value based on the geometric properties of the image. It was found that these don't produce any differences at similar pixel size (0.8 μm-1.4 μm) but they start to give some issues when the pixel size varies significantly (0.8 μm-4 μm). In addition, Hapgood produced an experimental analysis of a full range of nuclei morphology with different materials (Hapgood, 2000) that will be very interesting to reproduce by this method. This will allow research into the differences between continuous and batch and different configurations to incorporate into further simulation models.

Chapter five was based on the use of drying temperature and liquid-to-solid ratio to control the granules liquid bonding. As it was expected from the literature,

liquid availability played a fundamental role in twin screw granulation in the formation of the granules. The results suggested that drying has a direct effect in how the internal granule is packed but not in the size. The size was determined by the initial liquid availability which defined the number of nuclei. The nuclei were, for all the liquid to solid ratios, similar in size i.e. when the number increased, the size of the final granule increased as well. Due to time availability, the internal analysis of the granules was limited to one change of L/S ratio at one drying temperature. It would have been very interesting to pursue further analysis in the effect of the drying in the internal morphology at all the temperatures incorporating drying methods.

In chapter six experiments demonstrated that the internal forces experienced by the powder are larger than expected and referenced in the literature. Also, limitations of the equipment were discovered and indicated that there exists a limit where the torque required starts to increase exponentially with very small variances on the process parameters, this needs to be known and avoided to provide safer operation. Further work in this area will be very relevant to understand the relationship between torque and internal forces at other scales and configurations.

To sum up, this thesis covered some of the required knowledge of granulation which an extensive literature review disclosed as a gap. Although this topic has been extensively studied during the past two decades, these hurdles need to be addressed which was specifically made in this thesis by three main contributions: the quantification of the stresses range within the granulator, the important of the capillary force and drying temperature in the inner structure of the granule and the isolation of specific clusters from X-Ray CT. Whilst the implications of each of these contributions have been already discussed, altogether allow to give a step forward in the overall challenge of safely implementing twin screw granulation.

References

AGRAWAL, R. & NAVEEN, Y. 2011. Pharmaceutical processing–A review on wet granulation technology. *International J Pharmaceutical Frontier Research,* 1, 65-83.

AKTIENGESELLSCHAFT, G. G. 2015. Available: http://www.gea-ps.com/npsportal/cmsdoc.nsf/WebDoc/ndkw73ej59 [Accessed 02/04/2015.

AULTON, M. E. & TAYLOR, K. M. 2017. *Aulton's Pharmaceutics E-Book: The Design and Manufacture of Medicines*, Elsevier Health Sciences.

AUNGST, B. J. 2017. Optimizing Oral Bioavailability in Drug Discovery: An Overview of Design and Testing Strategies and Formulation Options. *Journal of Pharmaceutical Sciences,* 106, 921-929.

BARRASSO, D., EL HAGRASY, A., LITSTER, J. D. & RAMACHANDRAN, R. 2015a. Multi-dimensional population balance model development and validation for a twin screw granulation process. *Powder Technology,* 270, 612-621.

BARRASSO, D., EPPINGER, T., PEREIRA, F. E., AGLAVE, R., DEBUS, K., BERMINGHAM, S. K. & RAMACHANDRAN, R. 2015b. A multi-scale, mechanistic model of a wet granulation process using a novel bi-directional PBM–DEM coupling algorithm. *Chemical Engineering Science,* 123, 500-513.

BARRASSO, D. & RAMACHANDRAN, R. 2012. A comparison of model order reduction techniques for a four-dimensional population balance model describing multi-component wet granulation processes. *Chemical Engineering Science,* 80, 380-392.

BARRASSO, D. & RAMACHANDRAN, R. 2016. Qualitative assessment of a multi-scale, compartmental PBM-DEM model of a continuous twin-screw wet granulation process. *Journal of Pharmaceutical Innovation,* 11, 231-249.

BARRASSO, D., TAMRAKAR, A. & RAMACHANDRAN, R. 2014. A reduced order PBM–ANN model of a multi-scale PBM–DEM description of a wet granulation process. *Chemical Engineering Science,* 119, 319-329.

BARRASSO, D., WALIA, S. & RAMACHANDRAN, R. 2013. Multi-component population balance modeling of continuous granulation processes: A parametric study and comparison with experimental trends. *Powder Technology,* 241, 85-97.

BERGGREN, J. & ALDERBORN, G. 2001. Effect of drying rate on porosity and tabletting behaviour of cellulose pellets. *International journal of pharmaceutics,* 227, 81-96.

BEUCHER, S. 1992. The watershed transformation applied to image segmentation. *SCANNING MICROSCOPY-SUPPLEMENT-*, 299-299.

BIGIO, D., PAPPAS, W., BROWN II, H., DEBEBE, B. & DUNHAM, W. Residence stress distributions in a twin screw extruder. SPE ANTEC Proceedings, 2011.

BLAKE, T. & DE CONINCK, J. 2002. The influence of solid–liquid interactions on dynamic wetting. *Advances in colloid and interface science,* 96, 21-36.

BRANDT, S. & BRANDT, S. 2014. *Data analysis*, Springer.

BRAUMANN, A., KRAFT, M. & WAGNER, W. 2010. Numerical study of a stochastic particle algorithm solving a multidimensional population balance model for high shear granulation. *Journal of Computational Physics,* 229, 7672-7691.

BUENESTADO, P. & ACHO, L. 2018. Image Segmentation Based on Statistical Confidence Intervals. *Entropy,* 20**,** 46.

CARDONA, J., FERREIRA, C., MCGINTY, J., HAMILTON, A., AGIMELEN, O. S., CLEARY, A., ATKINSON, R., MICHIE, C., MARSHALL, S., CHEN, Y.-C., SEFCIK, J., ANDONOVIC, I. & TACHTATZIS, C. 2018. Image analysis framework with focus evaluation for in situ characterisation of particle size and shape attributes. *Chemical Engineering Science,* 191**,** 208-231.

CAPPELLI, S., XIE, Q., HARTING, J., DE JONG, A. & PRINS, M. 2015. Dynamic wetting: status and prospective of single particle based experiments and simulations. *New biotechnology,* 32**,** 420-432.

CONDON, J. B. 2006. *Surface area and porosity determinations by physisorption: measurements and theory*, Elsevier.

DE SOETE, W., DEWULF, J., CAPPUYNS, P., VAN DER VORST, G., HEIRMAN, B., AELTERMAN, W., SCHOETERS, K. & VAN LANGENHOVE, H. 2013. Exergetic sustainability assessment of batch versus continuous wet granulation based pharmaceutical tablet manufacturing: a cohesive analysis at three different levels. *Green Chemistry,* 15**,** 3039-3048.

DHENGE, R. M., CARTWRIGHT, J. J., DOUGHTY, D. G., HOUNSLOW, M. J. & SALMAN, A. D. 2011. Twin screw wet granulation: Effect of powder feed rate. *Advanced Powder Technology,* 22**,** 162-166.

DHENGE, R. M., CARTWRIGHT, J. J., HOUNSLOW, M. J. & SALMAN, A. D. 2012a. Twin screw granulation: Steps in granule growth. *International Journal of Pharmaceutics,* 438**,** 20-32.

DHENGE, R. M., CARTWRIGHT, J. J., HOUNSLOW, M. J. & SALMAN, A. D. 2012b. Twin screw wet granulation: Effects of properties of granulation liquid. *Powder Technology,* 229, 126-136.

DHENGE, R. M., FYLES, R. S., CARTWRIGHT, J. J., DOUGHTY, D. G., HOUNSLOW, M. J. & SALMAN, A. D. 2010. Twin screw wet granulation: Granule properties. *Chemical Engineering Journal,* 164, 322-329.

DHENGE, R. M., WASHINO, K., CARTWRIGHT, J. J., HOUNSLOW, M. J. & SALMAN, A. D. 2013. Twin screw granulation using conveying screws: Effects of viscosity of granulation liquids and flow of powders. *Powder technology,* 238, 77-90.

DJURIC, D. & KLEINEBUDDE, P. 2008. Impact of screw elements on continuous granulation with a twin-screw extruder. *Journal of pharmaceutical sciences,* 97, 4934-4942.

DJURIC, D., VAN MELKEBEKE, B., KLEINEBUDDE, P., REMON, J. P. & VERVAET, C. 2009. Comparison of two twin-screw extruders for continuous granulation. *European Journal of Pharmaceutics and Biopharmaceutics,* 71, 155-160.

DURGIN, J. M. & HANAN, Z. I. 2004. *Thomson Delmar Learning's Pharmacy Practice for Technicians*, Cengage Learning.

DUSSAN, E. 1979. On the spreading of liquids on solid surfaces: static and dynamic contact lines. *Annual Review of Fluid Mechanics,* 11, 371-400.

EL HAGRASY, A., HENNENKAMP, J., BURKE, M., CARTWRIGHT, J. & LITSTER, J. 2013a. Twin screw wet granulation: influence of formulation parameters on granule properties and growth behavior. *Powder Technology,* 238, 108-115.

EL HAGRASY, A. & LITSTER, J. 2013. Granulation rate processes in the kneading elements of a twin screw granulator. *AIChE Journal,* 59, 4100-4115.

EL HAGRASY, A. S., HENNENKAMP, J. R., BURKE, M. D., CARTWRIGHT, J. J. & LITSTER, J. D. 2013b. Twin screw wet granulation: Influence of formulation parameters on granule properties and growth behavior. *Powder Technology,* 238, 108-115.

ENNIS, B. & LITSTER, J. 1997. Particle size enlargement. *Perry's Chemical Engineers' Handbook, 7th edn, McGraw-Hill, New York*, 20-56.

ENNIS, B. J., LI, J., GABRIEL I, T. & ROBERT, P. 1990. The influence of viscosity on the strength of an axially strained pendular liquid bridge. *Chemical Engineering Science,* 45, 3071-3088.

ERIKSSON, L., BYRNE, T., JOHANSSON, E., TRYGG, J. & VIKSTRÖM, C. 2013. *Multi-and megavariate data analysis basic principles and applications*, Umetrics Academy.

FARBER, L., TARDOS, G. I. & MICHAELS, J. N. 2003. Evolution and structure of drying material bridges of pharmaceutical excipients: studies on a microscope slide. *Chemical Engineering Science,* 58, 4515-4525.

FARBER, L., TARDOS, G. I. & MICHAELS, J. N. 2005. Micro-mechanical properties of drying material bridges of pharmaceutical excipients. *International journal of pharmaceutics,* 306, 41-55.

FEDERSEL, H.-J. 2009. Chemical Process Research and Development in the 21st Century: Challenges, Strategies, and Solutions from a Pharmaceutical Industry Perspective. *Accounts of Chemical Research,* 42, 671-680.

FELL, J. & NEWTON, J. 1970. Determination of tablet strength by the diametral-compression test. *Journal of pharmaceutical sciences,* 59, 688-691.

FIELDEN, K., NEWTON, J. M., O'BRIEN, P. & ROWE, R. C. 1988. Thermal studies on the interaction of water and microcrystalline cellulose. *Journal of pharmacy and pharmacology,* 40, 674-678.

FLORENCE, A. T. & SIEPMANN, J. 2009. *Modern Pharmaceutics Volume 1: Basic Principles and Systems*, CRC Press.

FONTEYNE, M., VERCRUYSSE, J., DÍAZ, D. C., GILDEMYN, D., VERVAET, C., REMON, J. P. & BEER, T. D. 2013. Real-time assessment of critical quality attributes of a continuous granulation process. *Pharmaceutical development and technology,* 18, 85-97.

FOOD & ADMINISTRATION, D. 2004. Guidance for industry: PAT—A framework for innovative pharmaceutical development, manufacturing, and quality assurance. *DHHS, Rockville, MD.*

GHEBRE-SELASSIE, I., MARTIN, C. E., ZHANG, F. & DINUNZIO, J. 2018. *Pharmaceutical extrusion technology*, CRC Press.

GIBSON, M. 2009. *Pharmaceutical preformulation and formulation: a practical guide from candidate drug selection to commercial dosage form*, CRC Press.

GODAVARTI, S. & KARWE, M. V. 1997. Determination of Specific Mechanical Energy Distribution on a Twin-Screw Extruder. *Journal of Agricultural Engineering Research,* 67, 277-287.

GOMBAS, A., SZABÓ-RÉVÉSZ, P., KATA, M., REGDON, G. & ERŐS, I. 2002. Quantitative determination of crystallinity of α-lactose

monohydrate by DSC. *Journal of Thermal Analysis and Calorimetry,* 68, 503-510.

GORRINGE, L., KEE, G., SALEH, M., FA, N. & ELKES, R. 2017. Use of the channel fill level in defining a design space for twin screw wet granulation. *International journal of pharmaceutics,* 519, 165-177.

GUIDELINE, I. H. T. 2009. Q8 (R2) Pharmaceutical Development. *Step 4 Version.*

HAPGOOD, K. P. 2000. Nucleation and binder dispersion in wet granulation.

HAPGOOD, K. P., LITSTER, J. D. & SMITH, R. 2003. Nucleation regime map for liquid bound granules. *AIChE Journal,* 49, 350-361.

HUH, C. & SCRIVEN, L. 1971. Hydrodynamic model of steady movement of a solid/liquid/fluid contact line. *Journal of colloid and interface science,* 35, 85-101.

ICH Q8 (R2) 2009. ICH HARMONISED TRIPARTITE GUIDELINE. *Step 4 Version.*

ISO 13322-1:2014 2014. Particle size analysis – Image analysis methods – Part 1: Static image analysis methods.

IVESON, S. M. 2002. Limitations of one-dimensional population balance models of wet granulation processes. *Powder Technology,* 124, 219-229.

IVESON, S. M., LITSTER, J. D., HAPGOOD, K. & ENNIS, B. J. 2001. Nucleation, growth and breakage phenomena in agitated wet granulation processes: a review. *Powder Technology,* 117, 3-39.

IVESON, S. & LITSTER, J. 1998. Growth regime map for liquid-bound granules. *AIChE journal,* 44, 1510-1518.

JACOBS, P., SEVENS, E. & KUNNEN, M. 1995. Principles of computerised X-ray tomography and applications to building materials. *Science of the total environment,* 167, 161-170.

JACOBZONE, S. 2000. *Pharmaceutical Policies in OECD Countries*, OECD Publishing.

JIMÉNEZ-GONZÁLEZ, C., POECHLAUER, P., BROXTERMAN, Q. B., YANG, B.-S., AM ENDE, D., BAIRD, J., BERTSCH, C., HANNAH, R. E., DELL'ORCO, P., NOORMAN, H., YEE, S., REINTJENS, R., WELLS, A., MASSONNEAU, V. & MANLEY, J. 2011. Key Green Engineering Research Areas for Sustainable Manufacturing: A Perspective from Pharmaceutical and Fine Chemicals Manufacturers. *Organic Process Research & Development,* 15, 900-911.

KAN, H., NAKAMURA, H. & WATANO, S. 2015. Numerical simulation of particle–particle adhesion by dynamic liquid bridge. *Chemical Engineering Science,* 138, 607-615.

KAN, H., NAKAMURA, H. & WATANO, S. 2017. Effect of droplet size on particle-particle adhesion of colliding particles through droplet. *Powder Technology,* 321, 318-325.

KELEB, E. I., VERMEIRE, A., VERVAET, C. & REMON, J. P. 2004. Twin screw granulation as a simple and efficient tool for continuous wet granulation. *International Journal of Pharmaceutics,* 273, 183-194.

KLEINEBUDDE, P., KHINAST, J. & RANTANEN, J. 2017. *Continuous manufacturing of pharmaceuticals*, John Wiley & Sons.

KLEINEBUDDE, P. & LINDNER, H. 1993. Experiments with an instrumented twin-screw extruder using a single-step granulation/extrusion process. *International journal of pharmaceutics,* 94, 49-58.

KORHONEN, O. 2017. Continuous Line Roller Compaction. *Continuous Manufacturing of Pharmaceuticals,* 7703.

KUMAR, A., ALAKARJULA, M., VANHOORNE, V., TOIVIAINEN, M., DE LEERSNYDER, F., VERCRUYSSE, J., JUUTI, M., KETOLAINEN, J., VERVAET, C., REMON, J. P., GERNAEY, K. V., DE BEER, T. & NOPENS, I. 2016a. Linking granulation performance with residence time and granulation liquid distributions in twin-screw granulation: An experimental investigation. *European Journal of Pharmaceutical Sciences,* 90, 25-37.

KUMAR, A., GERNAEY, K., NOPENS, I. & DE BEER, T. 2017. Twin-screw Granulation Process Development: Present Approaches, Understanding and Needs. *Continuous Manufacturing of Pharmaceuticals*, 283-311.

KUMAR, A., VERCRUYSSE, J., MORTIER, S. T. F. C., VERVAET, C., REMON, J. P., GERNAEY, K. V., DE BEER, T. & NOPENS, I. 2016b. Model-based analysis of a twin-screw wet granulation system for continuous solid dosage manufacturing. *Computers & Chemical Engineering,* 89, 62-70.

KUMAR, A., VERCRUYSSE, J., VANHOORNE, V., TOIVIAINEN, M., PANOUILLOT, P.-E., JUUTI, M., VERVAET, C., REMON, J. P., GERNAEY, K. V. & DE BEER, T. 2015. Conceptual framework for model-based analysis of residence time distribution in twin-screw granulation. *European Journal of Pharmaceutical Sciences,* 71, 25-34.

LAMBERT, P., CHAU, A., DELCHAMBRE, A. & RÉGNIER, S. 2008. Comparison between two capillary forces models. *Langmuir,* 24, 3157-3163.

LEE, K. F., PATTERSON, R. I. A., WAGNER, W. & KRAFT, M. 2015. Stochastic weighted particle methods for population balance equations with coagulation, fragmentation and spatial inhomogeneity. *Journal of Computational Physics,* 303, 1-18.

LEE, K. T., INGRAM, A. & ROWSON, N. A. 2012. Twin screw wet granulation: The study of a continuous twin screw granulator using Positron Emission Particle Tracking (PEPT) technique. *European Journal of Pharmaceutics and Biopharmaceutics,* 81, 666-673.

LEHMANN, G. & LEGLAND, D. 2012. Efficient N-Dimensional surface estimation using Crofton formula and run-length encoding. *Efficient N-Dimensional surface estimation using Crofton formula and run-length encoding, Kitware INC (2012).*

LEUENBERGER, H. 2001a. New trends in the production of pharmaceutical granules: batch versus continuous processing. *European Journal of Pharmaceutics and Biopharmaceutics,* 52, 289-296.

LEUENBERGER, H. 2001b. New trends in the production of pharmaceutical granules: the classical batch concept and the problem of scale-up. *European Journal of Pharmaceutics and Biopharmaceutics,* 52, 279-288.

LI, H., THOMPSON, M. R. & O'DONNELL, K. P. 2014. Understanding wet granulation in the kneading block of twin screw extruders. *Chemical Engineering Science,* 113, 11-21.

LI, H., THOMPSON, M. R. & O'DONNELL, K. P. 2015. Examining drug hydrophobicity in continuous wet granulation within a twin screw extruder. *International Journal of Pharmaceutics,* 496, 3-11.

LINDBERG, N.-O., MYRENAS, M., TUFVESSON, C. & OLBJER, L. 1988. Extrusion of an effervescent granulation with a twin screw extruder,

Baker Perkins MPF 50D. Determination of mean residence time. *Drug Development and Industrial Pharmacy,* 14, 649-655.

LITSTER, J., ENNIS, B. & LIAN, L. 2004. *The science and engineering of granulation processes*, Springer.

LIU, D. & YU, J. Otsu method and K-means. Hybrid Intelligent Systems, 2009. HIS'09. Ninth International Conference on, 2009. IEEE, 344-349.

LOCKE, R. M. & WELLHAUSEN, R. L. 2014. *Production in the innovation economy*, MIT Press.

LUTE, S. V., DHENGE, R. M. & SALMAN, A. D. 2018. Twin Screw Granulation: An Investigation of the Effect of Barrel Fill Level. *Pharmaceutics,* 10.

MACLEOD, C. S. & MULLER, F. L. 2012. On the fracture of pharmaceutical needle-shaped crystals during pressure filtration: case studies and mechanistic understanding. *Organic Process Research & Development,* 16, 425-434.

MALFLIET, W. 2004. The tanh method: a tool for solving certain classes of nonlinear evolution and wave equations. *Journal of computational and applied mathematics,* 164, 529-541.

MASCIA, S., HEIDER, P. L., ZHANG, H., LAKERVELD, R., BENYAHIA, B., BARTON, P. I., BRAATZ, R. D., COONEY, C. L., EVANS, J. & JAMISON, T. F. 2013. End-to-End Continuous Manufacturing of Pharmaceuticals: Integrated Synthesis, Purification, and Final Dosage Formation. *Angewandte Chemie International Edition,* 52, 12359-12363.

MATHWORKS, T. 2018. *Image Processing Toolbox User's Guide* [Online]. Release. Available: https://uk.mathworks.com.

MCGUIRE, A. D., MOSBACH, S., LEE, K. F., REYNOLDS, G. & KRAFT, M. 2018. A high-dimensional, stochastic model for twin-screw granulation – Part 1: Model description. *Chemical Engineering Science,* 188, 221-237.

MILLER, D. 1995. Remington-The Science and Practice of Pharmacy. Pennsylvania: MACK Publishing Company.

NGUYEN, T. H., MORTON, D. A. & HAPGOOD, K. P. 2013. Application of the unified compaction curve to link wet granulation and tablet compaction behaviour. *Powder technology,* 240, 103-115.

NIEUWMEYER, F. J., DAMEN, M., GERICH, A., RUSMINI, F., VAN DER VOORT MAARSCHALK, K. & VROMANS, H. 2007a. Granule characterization during fluid bed drying by development of a near infrared method to determine water content and median granule size. *Pharmaceutical Research,* 24, 1854-1861.

NIEUWMEYER, F. J. S., VAN DER VOORT MAARSCHALK, K. & VROMANS, H. 2007b. Granule breakage during drying processes. *International Journal of Pharmaceutics,* 329, 81-87.

NOLTE, E. 2010. *Advanced Granulating Technology Improves Process Efficiencies* [Online]. Pharmaceutical Processing. Available: http://www.pharmpro.com/articles/2010/08/advanced-granulating-technology-improves-process-efficiencies [Accessed 03/12/2014.

OKA, S., KAŠPAR, O., TOKÁROVÁ, V., SOWRIRAJAN, K., WU, H., KHAN, M., MUZZIO, F., ŠTĚPÁNEK, F. & RAMACHANDRAN, R. 2015. A quantitative study of the effect of process parameters on key granule characteristics in a high shear wet granulation process involving a two component pharmaceutical blend. *Advanced Powder Technology,* 26, 315-322.

OSORIO, J. G., SAYIN, R., KALBAG, A. V., LITSTER, J. D., MARTINEZ-MARCOS, L., LAMPROU, D. A. & HALBERT, G. W. 2017. Scaling of continuous twin screw wet granulation. *AIChE Journal,* 63, 921-932.

OTSU, N. 1979. A threshold selection method from gray-level histograms. *IEEE transactions on systems, man, and cybernetics,* 9, 62-66.

PAGLIERONI, D. W. 1992. Distance transforms: Properties and machine vision applications. *CVGIP: Graphical Models and Image Processing,* 54, 56-74.

PAPPAS, W., BROWN II, H., FUKUDA, G., ADNEW, R. & BIGIO, D. 2012. Variable strength stress bead analysis in a twin screw extruder. *SPE ANTEC Tech. Papers*.

PARIKH, D. M. 2009. *Handbook of pharmaceutical granulation technology*, Taylor and Francis.

PASSE, T. 1997. Grain size distribution expressed as tanh-functions. *Sedimentology,* 44, 1011-1014.

PERRY, J. H. 1950. Chemical engineers' handbook. *Journal of Chemical Education,* 27, 533.

PIZER, S. M., AMBURN, E. P., AUSTIN, J. D., CROMARTIE, R., GESELOWITZ, A., GREER, T., TER HAAR ROMENY, B., ZIMMERMAN, J. B. & ZUIDERVELD, K. 1987. Adaptive histogram equalization and its variations. *Computer vision, graphics, and image processing,* 39, 355-368.

PLUMB, K. 2005. Continuous Processing in the Pharmaceutical Industry: Changing the Mind Set. *Chemical Engineering Research and Design,* 83, 730-738.

POECHLAUER, P., MANLEY, J., BROXTERMAN, R., GREGERTSEN, B. & RIDEMARK, M. 2012. Continuous Processing in the Manufacture of

Active Pharmaceutical Ingredients and Finished Dosage Forms: An Industry Perspective. *Organic Process Research & Development,* 16, 1586-1590.

PRADHAN, S. U., SEN, M., LI, J., LITSTER, J. D. & WASSGREN, C. R. 2017a. Granule breakage in twin screw granulation: Effect of material properties and screw element geometry. *Powder Technology,* 315, 290-299.

PRADHAN, S. U., ZHANG, Y., LI, J., LITSTER, J. D. & WASSGREN, C. R. 2017b. Tailored granule properties using 3D printed screw geometries in twin screw granulation. *Powder Technology.*

PROFILES, I. 1995. Chemical works pharmaceuticals manufacturing works. *In:* UK, D. O. E. O. (ed.).

QUANTACHROME INSTRUMENTS 2009. autosorb iQ and ASiQwin operating manual.

REIN, M. 1993. Phenomena of liquid drop impact on solid and liquid surfaces. *Fluid Dynamics Research,* 12, 61.

REMINGTON, J. P., TROY, D. B. & BERINGER, P. 2006. *Remington: The science and practice of pharmacy*, Lippincott Williams & Wilkins.

RHODES, M. 2013. Introduction to particle technology. Wiley & Sons.

RIAZ, M. N. 2000. *Extruders in food applications*, CRC Press.

RICHARDSON, J. & COULSON, J. 2002. *Chemical Engineering: Particle Technology and Seraration Processes*, Elsevier Engineering Information, Incorporated.

ROBINSON, H. B. Z. P., OLIVIER, M. P. P. & SHIH, H. S. T. K. 2009. Visual Informatics: Bridging Research and Practice. Springer.

SAFFOON, N., UDDIN, R., HUDA, N. H. & SUTRADHAR, K. B. 2011. Enhancement of oral bioavailability and solid dispersion: a review. *Journal of Applied Pharmaceutical Science,* 1, 13-20.

ŠANTL, M., ILIĆ, I., VREČER, F. & BAUMGARTNER, S. 2011. A compressibility and compactibility study of real tableting mixtures: The impact of wet and dry granulation versus a direct tableting mixture. *International Journal of Pharmaceutics,* 414, 131-139.

SASTRY, K. V. & FUERSTENAU, D. 1973. Mechanisms of agglomerate growth in green pelletization. *Powder Technology,* 7, 97-105.

SAYIN, R., MARTINEZ-MARCOS, L., OSORIO, J. G., CRUISE, P., JONES, I., HALBERT, G. W., LAMPROU, D. A. & LITSTER, J. D. 2015. Investigation of an 11 mm diameter twin screw granulator: Screw element performance and in-line monitoring via image analysis. *International Journal of Pharmaceutics,* 496, 24-32.

SEEM, T. C., ROWSON, N. A., INGRAM, A., HUANG, Z., YU, S., DE MATAS, M., GABBOTT, I. & REYNOLDS, G. K. 2015. Twin screw granulation—A literature review. *Powder Technology,* 276, 89-102.

SHI, L., FENG, Y. & SUN, C. C. 2011. Origin of profound changes in powder properties during wetting and nucleation stages of high-shear wet granulation of microcrystalline cellulose. *Powder technology,* 208, 663-668.

SHIRAZIAN, S., KUHS, M., DARWISH, S., CROKER, D. & WALKER, G. M. 2017. Artificial neural network modelling of continuous wet granulation using a twin-screw extruder. *International Journal of Pharmaceutics,* 521, 102-109.

SING, K. S. 1985. Reporting physisorption data for gas/solid systems with special reference to the determination of surface area and porosity (Recommendations 1984). *Pure and applied chemistry,* 57, 603-619.

SURESH, P., SREEDHAR, I., VAIDHISWARAN, R. & VENUGOPAL, A. 2017. A comprehensive review on process and engineering aspects of pharmaceutical wet granulation. *Chemical Engineering Journal,* 328, 785-815.

TAYLOR, D. 2015. The pharmaceutical industry and the future of drug development.

THE MATHWORKS INC 2013. Release, Matlab. *Inc., Natick, Massachusetts, United States,* 488.

THOMPSON, M. 2014. Twin screw granulation-review of current progress. *Drug development and industrial pharmacy*, 1-9.

THOMPSON, M. R. & SUN, J. 2010. Wet Granulation in a Twin-Screw Extruder: Implications of Screw Design. *Journal of Pharmaceutical Sciences,* 99, 2090-2103.

TREIMAN, J. S. 2014. *Calculus with Vectors*, Springer.

VAN HAUWERMEIREN, D., VERSTRAETEN, M., DE BEER, T. & NOPENS, I. 2017. Methodology and Pitfalls when Calibrating a PBM: the Case of Twin-Screw Wet Granulation. *In:* ESPUÑA, A., GRAELLS, M. & PUIGJANER, L. (eds.) *Computer Aided Chemical Engineering.* Elsevier.

VAN HAUWERMEIREN, D., VERSTRAETEN, M., DOSHI, P., AM ENDE, M. T., TURNBULL, N., LEE, K., DE BEER, T. & NOPENS, I. 2018. On the modelling of granule size distributions in twin-screw wet

granulation: Calibration of a novel compartmental population balance model. *Powder Technology.*

VERCRUYSSE, J., BURGGRAEVE, A., FONTEYNE, M., CAPPUYNS, P., DELAET, U., VAN ASSCHE, I., DE BEER, T., REMON, J. P. & VERVAET, C. 2015. Impact of screw configuration on the particle size distribution of granules produced by twin screw granulation. *International journal of pharmaceutics,* 479, 171-180.

VERCRUYSSE, J., CÓRDOBA DÍAZ, D., PEETERS, E., FONTEYNE, M., DELAET, U., VAN ASSCHE, I., DE BEER, T., REMON, J. P. & VERVAET, C. 2012. Continuous twin screw granulation: Influence of process variables on granule and tablet quality. *European Journal of Pharmaceutics and Biopharmaceutics,* 82, 205-211.

VERSTRAETEN, M., VAN HAUWERMEIREN, D., LEE, K., TURNBULL, N., WILSDON, D., AM ENDE, M., DOSHI, P., VERVAET, C., BROUCKAERT, D. & MORTIER, S. T. 2017. In-depth experimental analysis of pharmaceutical twin-screw wet granulation in view of detailed process understanding. *International journal of pharmaceutics,* 529, 678-693.

VERVAET, C. & REMON, J. P. 2005. Continuous granulation in the pharmaceutical industry. *Chemical Engineering Science,* 60, 3949-3957.

WANG, Y., RODRÍGUEZ DE GIL, P., CHEN, Y.-H., KROMREY, J. D., KIM, E. S., PHAM, T., NGUYEN, D. & ROMANO, J. L. 2017. Comparing the performance of approaches for testing the homogeneity of variance assumption in one-factor ANOVA models. *Educational and psychological measurement,* 77, 305-329.

WEINBERG, S. 2011. *Cost-contained Regulatory Compliance: For the Pharmaceutical, Biologics, and Medical Device Industries*, John Wiley & Sons.

WILLECKE, N., SZEPES, A., WUNDERLICH, M., REMON, J. P., VERVAET, C. & DE BEER, T. 2018. A novel approach to support formulation design on twin screw wet granulation technology: Understanding the impact of overarching excipient properties on drug product quality attributes. *International Journal of Pharmaceutics,* 545, 128-143.

WILLETT, C. D., ADAMS, M. J., JOHNSON, S. A. & SEVILLE, J. P. 2000. Capillary bridges between two spherical bodies. *Langmuir,* 16, 9396-9405.

WONG, J., D'SA, D., FOLEY, M., CHAN, J. G. Y. & CHAN, H.-K. 2014. NanoXCT: a novel technique to probe the internal architecture of pharmaceutical particles. *Pharmaceutical research,* 31, 3085-3094.

WU, H., KHAN, M. A. & HUSSAIN, A. S. 2007. Process control perspective for process analytical technology: integration of chemical engineering practice into semiconductor and pharmaceutical industries. *Chemical Engineering Communications,* 194, 760-779.

YERRAMILLI, L. & KARWE, M. V. 2004. Velocity Distributions and Mixing in the Translational Region of a Kneading Section in a Co-rotating Twin-screw Extruder. *Food and Bioproducts Processing,* 82, 5-12.

ZHANG, H., FRITTS, J. E. & GOLDMAN, S. A. 2008. Image segmentation evaluation: A survey of unsupervised methods. *Computer Vision and Image Understanding,* 110, 260-280.

ZHANG, Y.-J. 2006. *Advances in image and video segmentation*, IGI Global.

Appendices

Appendices: List of contents

Appendix a: Previously Published Work

Chapter 3 has been published in International Journal of Pharmaceutics as research article: *A novel methodology to study polymodal particle size distributions produced during continuous wet granulation.*

https://doi.org/10.1016/j.ijpharm.2017.01.023

My contribution to the article included:

- Conceptualization, methodology, software development, formal analysis, investigation, validation and writing of the original draft.

Chapter 6 has been published in International Journal of Pharmaceutics as research article: *The impact of channel fill level on internal forces during continuous twin screw wet granulation.*

https://doi.org/10.1016/j.ijpharm.2018.12.052

My contribution to the article included:

- Methodology, formal analysis, investigation, validation and writing of the original draft.

Appendix b: Tracking diagram

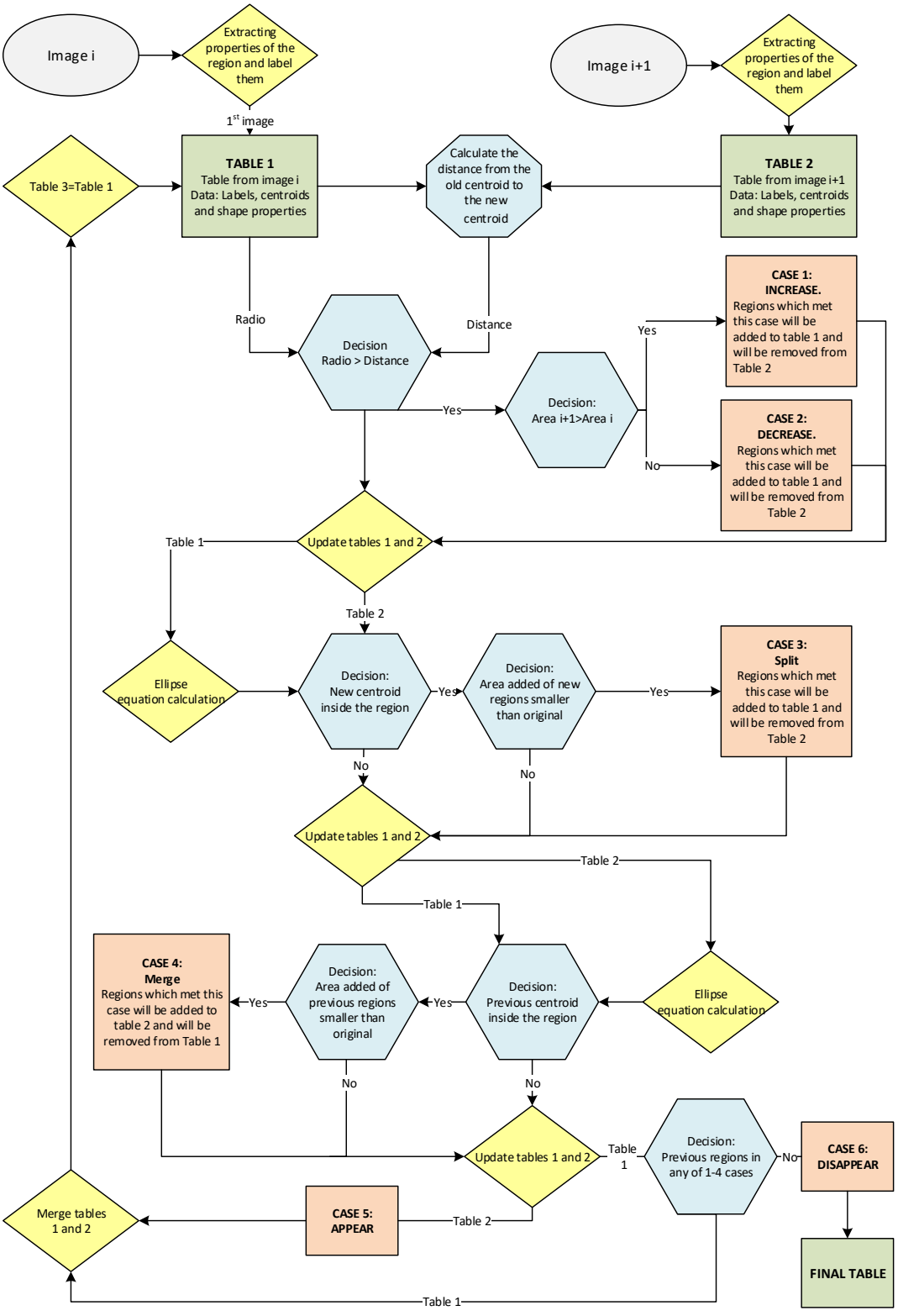

Appendix c: ANOVA analysis of PSDs

L/S=0.10

	DF	Sum of squares	Mean square	F value	P value	Significantly different
T12	4	0.4605	0.1151	1.136	0.3423	No
T62	5	0.1475	0.0295	0.4543	0.8097	No
T72	5	0.45504	0.09101	1.0948	0.36557	No
T82	6	0.42526	0.07088	0.9503	0.46054	No
All	23	2.26765	0.09859	1.22058	0.2188	No

L/S=0.13

	DF	Sum of squares	Mean square	F value	P value	Significantly different
T23	5	0.0219	0.00438	0.0531	0.9982	No
T63	5	0.1394	0.0279	0.3473	0.8834	No
T73	5	0.1419	0.0284	0.2799	0.9236	No

T93	4	0.2154	0.0539	1.0621	0.3778	No
All	22	1.09544	0.04979	0.62499	0.90779	No

L/S=0.16

	DF	**Sum of squares**	**Mean square**	**F value**	**P value**	**Significantly different**
T24	4	0.0119	0.00297	0.0221	0.999	No
T64	6	0.0878	0.0146	0.1337	0.9918	No
T74	6	0.15598	0.026	0.2126	0.9725	No
T84	5	0.00168	3.36207E-4	0.00313	1	No
All	24	0.4578	0.0191	0.1615	1	No

Appendix d: Physisorption isotherms

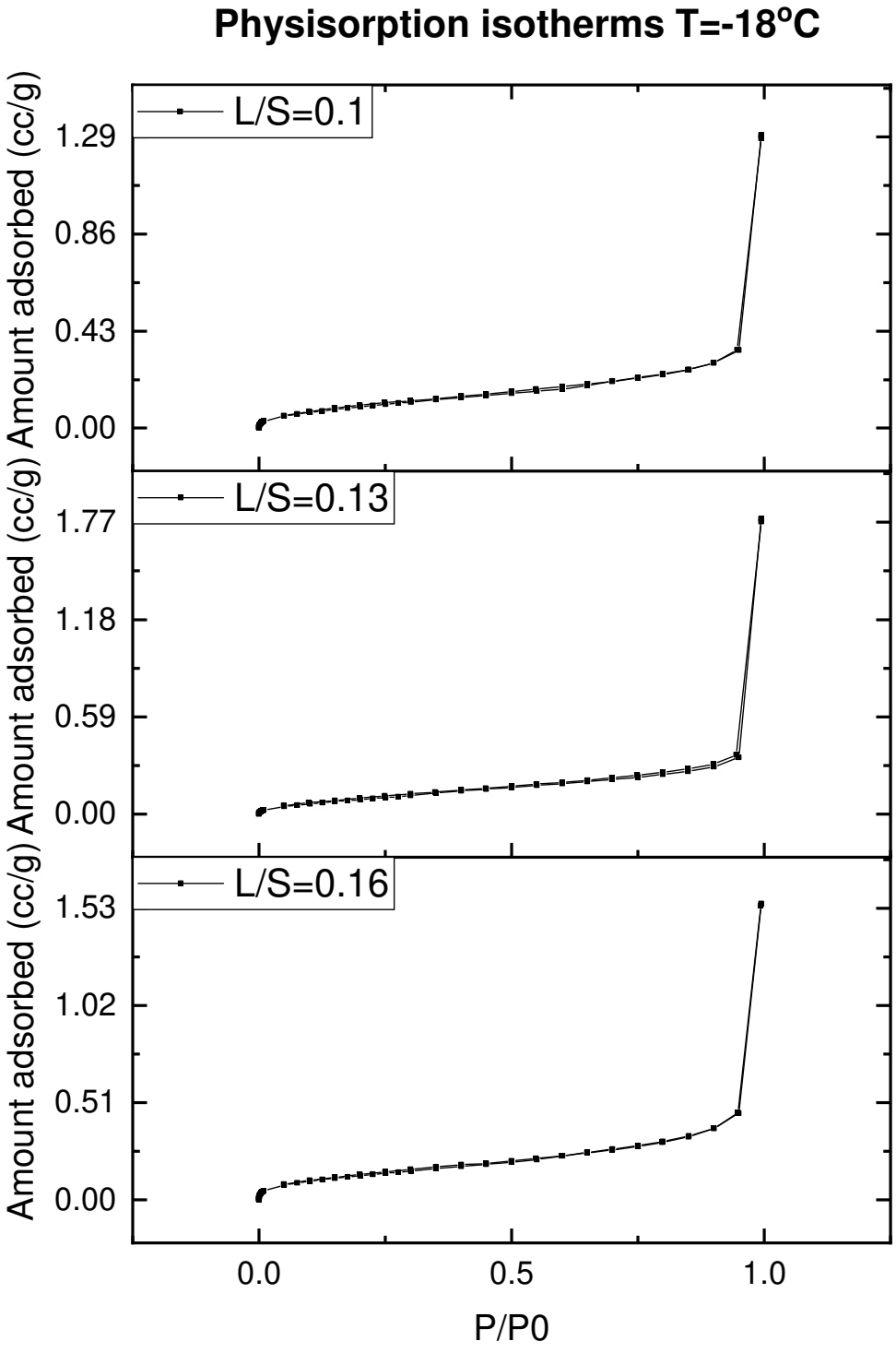

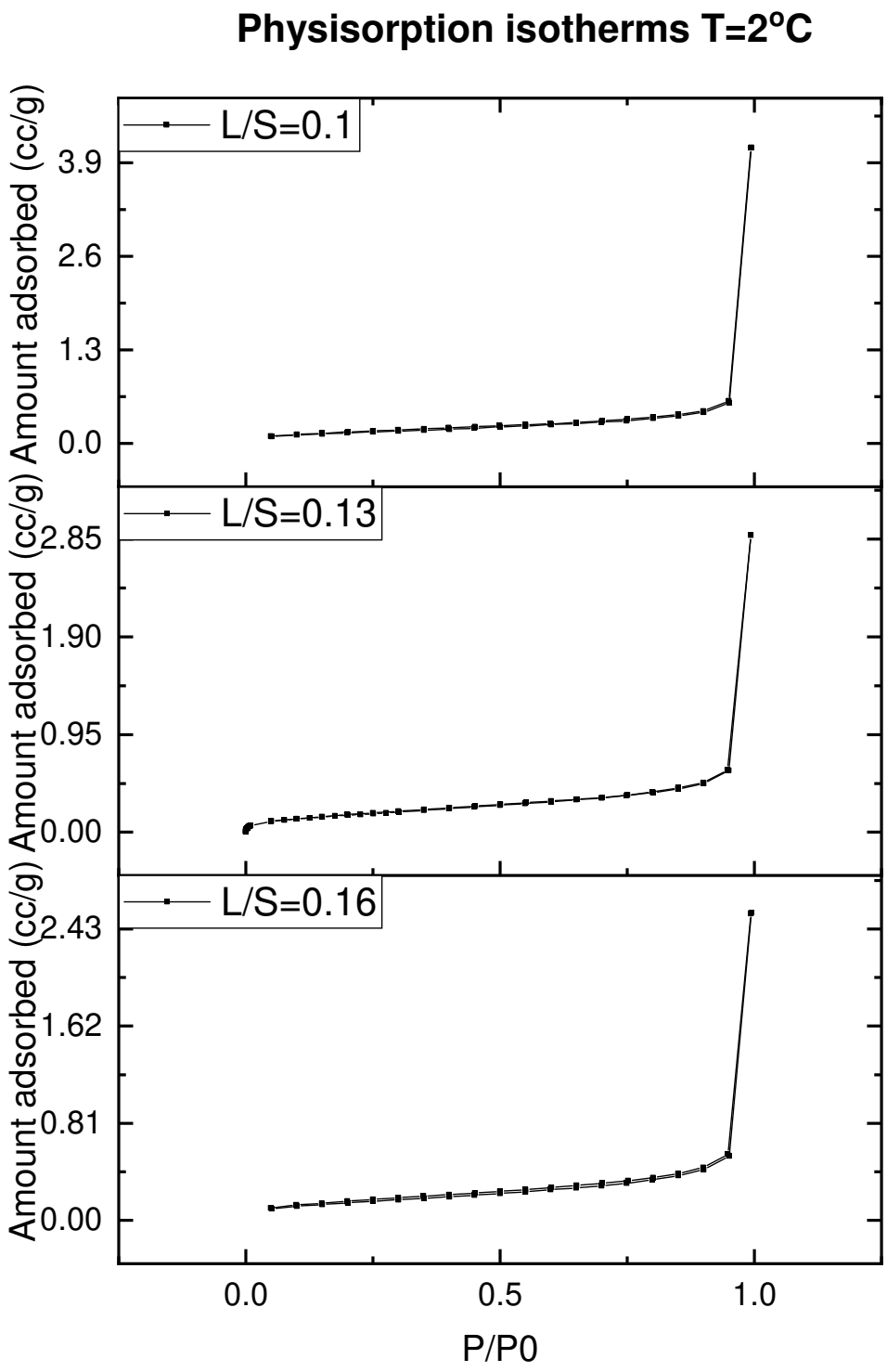
Physisorption isotherms T=2°C
L/S=0.1
L/S=0.13
L/S=0.16
Amount adsorbed (cc/g)
Amount adsorbed (cc/g)
Amount adsorbed (cc/g)
3.9
2.6
1.3
0.0
2.85
1.90
0.95
0.00
2.43
1.62
0.81
0.00
0.0
0.5
1.0
P/P0

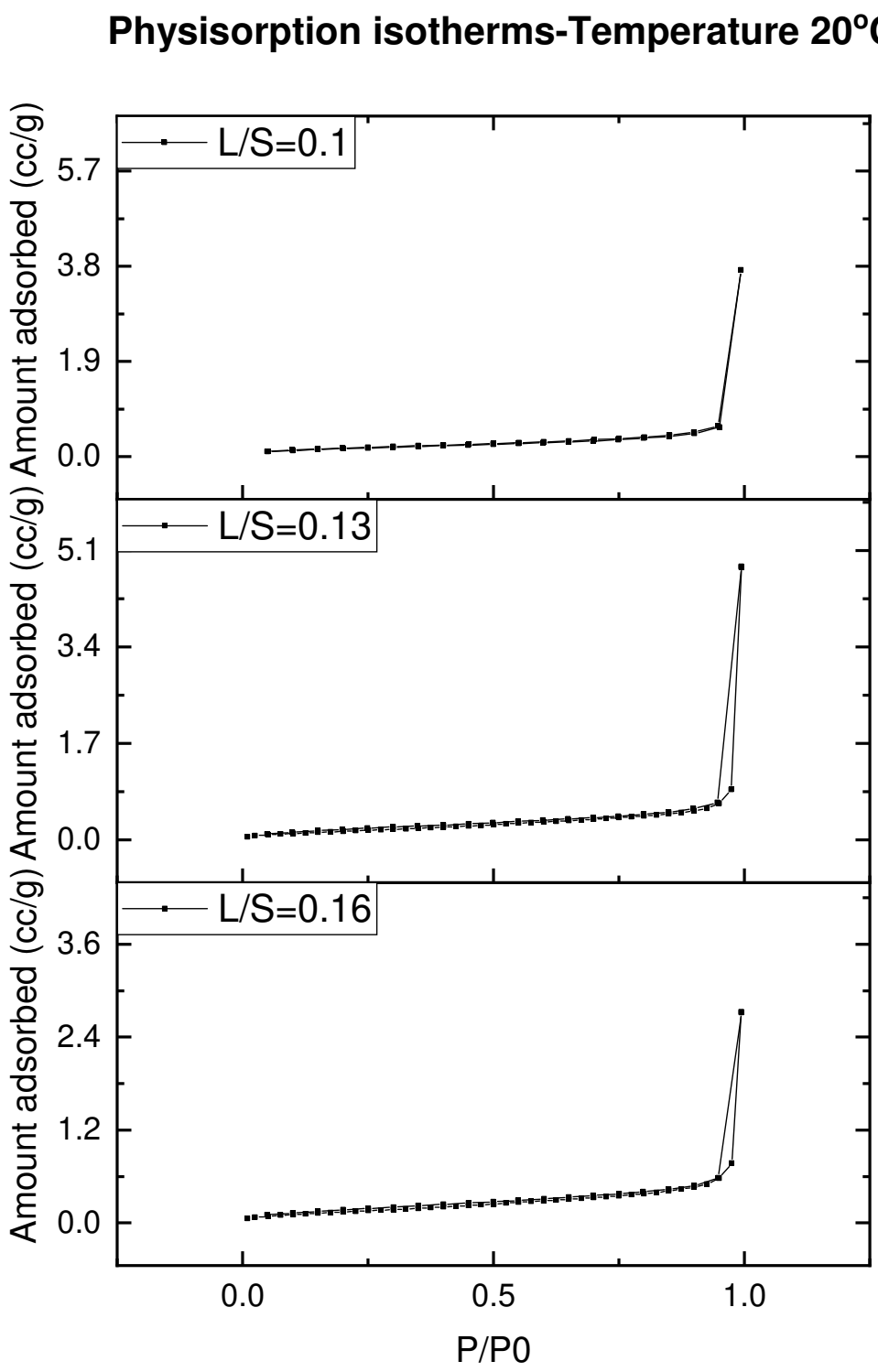
Physisorption isotherms-Temperature 20°C
L/S=0.1
L/S=0.13
L/S=0.16
Amount adsorbed (cc/g) Amount adsorbed (cc/g) Amount adsorbed (cc/g)
5.7
3.8
1.9
0.0
5.1
3.4
1.7
0.0
3.6
2.4
1.2
0.0
0.0
0.5
1.0
P/P0

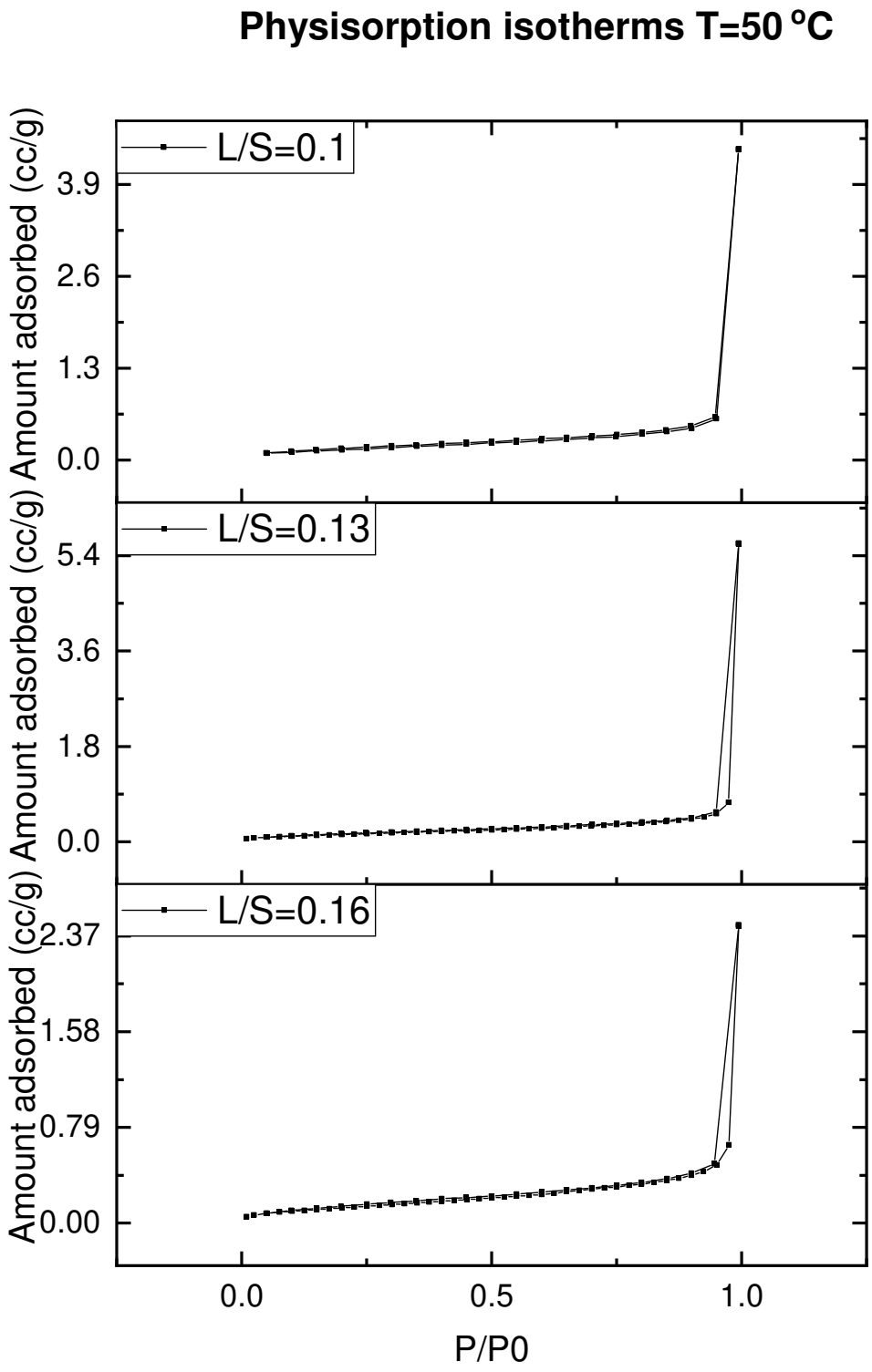
Physisorption isotherms T=50 °C
L/S=0.1
L/S=0.13
L/S=0.16
Amount adsorbed (cc/g)
Amount adsorbed (cc/g)
Amount adsorbed (cc/g)
3.9
2.6
1.3
0.0
5.4
3.6
1.8
0.0
2.37
1.58
0.79
0.00
0.0
0.5
1.0
P/P0

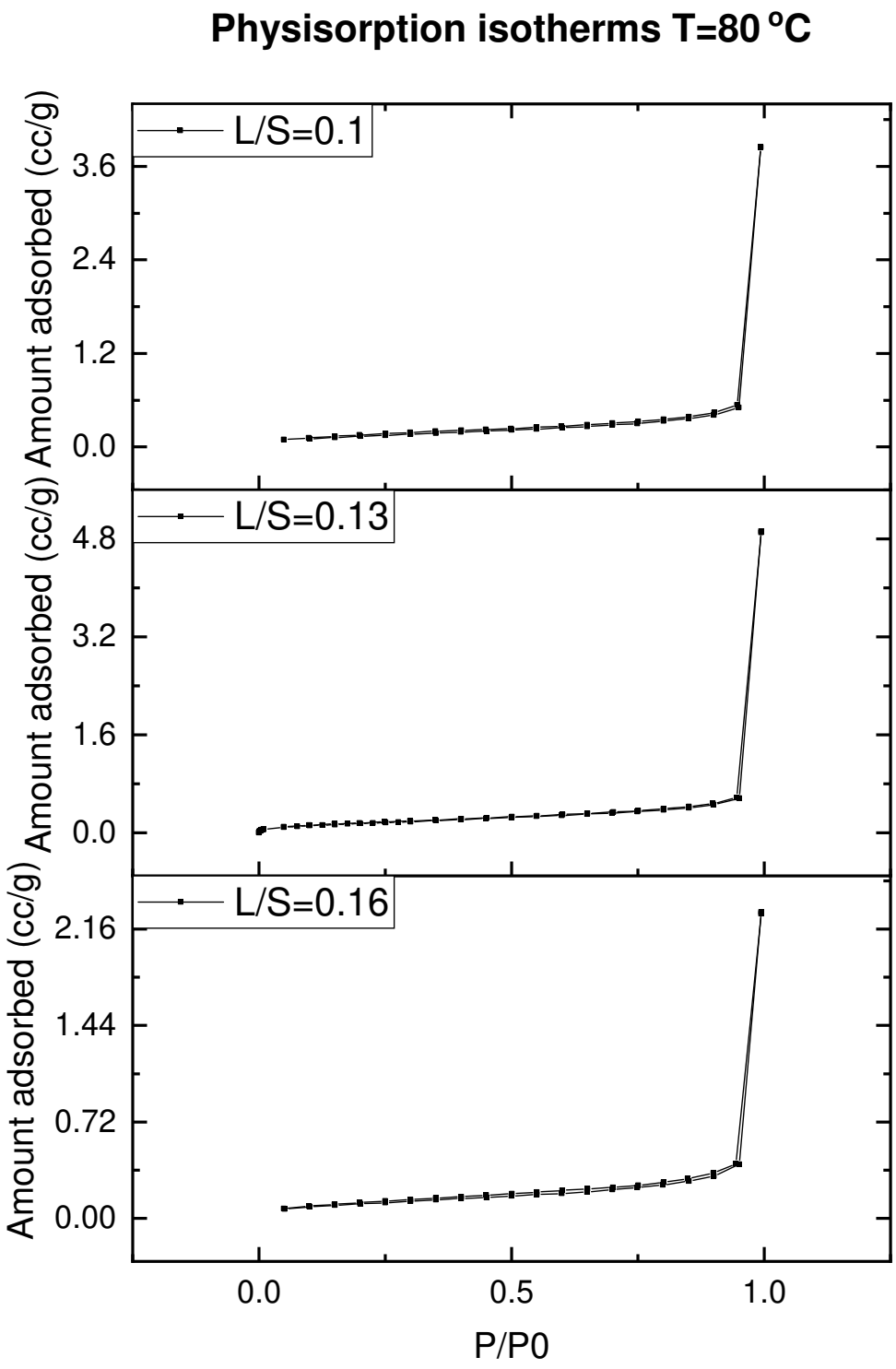
Physisorption isotherms T=80 °C
L/S=0.1
L/S=0.13
L/S=0.16
Amount adsorbed (cc/g)
Amount adsorbed (cc/g)
Amount adsorbed (cc/g)
3.6
2.4
1.2
0.0
4.8
3.2
1.6
0.0
2.16
1.44
0.72
0.00
0.0
0.5
1.0
P/P0

Appendix e: One Sample Wilcoxon Signed Rank Test

	Temperature (°C)				
	-18.5	2	20	50	80
L/S=0.10	TBn2	TFCn2	TAn2	TOWn2	TORn2
L/S=0.13	TBn3	TFCn3	TAn3	TOWn3	TORn3
L/S=0.16	TBn4	TFCn4	TAn4	TOWn4	TORn4

L/S=0.10 // Temperature -18.5 °C

	N	Min	Q1	Me-dian	Q3	Max	SD*
TB12	4	0.02279	0.02406	0.06587	0.10931	0.11112	No
TB42	4	0.1114	0.11313	0.1776	0.24556	0.24845	No
TB72	4	0.1776	0.17935	0.2696	0.38278	0.39218	No
TB82	4	0.20113	0.20438	0.29983	0.42003	0.43153	No

L/S=0.10 // Temperature 2°C

	N	Min	Q1	Me-dian	Q3	Max	SD*
TFC12	4	0.11937	0.12153	0.13249	0.14484	0.14746	No
TFC42	4	0.20671	0.20806	0.23471	0.26103	0.26228	No
TFC72	4	0.29318	0.31323	0.37553	0.38005	0.38084	No
TFC82	4	0.40184	0.40341	0.41058	0.41394	0.41423	No

L/S=0.10 // Temperature 20°C

	N	Min	Q1	Me-dian	Q3	Max	SD*
TA12	4	0.10669	0.10911	0.11789	0.12831	0.13127	No
TA42	4	0.22009	0.22247	0.2331	0.25026	0.25481	No
TA72	4	0.31783	0.32326	0.34659	0.37642	0.38401	No
TA82	4	0.37625	0.37982	0.40751	0.42746	0.42844	No

L/S=0.10 // Temperature 50°C

	N	Min	Q1	Me-dian	Q3	Max	SD*
TOW12	4	0.07947	0.08364	0.09659	0.10496	0.1076	No
TOW42	4	0.19743	0.1984	0.21354	0.23028	0.23178	No
TOW72	4	0.28607	0.29083	0.3203	0.3558	0.36258	No
TOW82	4	0.33303	0.34075	0.37977	0.41652	0.42348	No

L/S=0.10 // Temperature 80°C

	N	Min	Q1	Me-dian	Q3	Max	SD*
TOR12	4	0.06868	0.07476	0.0961	0.10734	0.11004	No
TOR42	4	0.1798	0.18463	0.21386	0.22904	0.22918	No
TOR72	4	0.25816	0.27026	0.32906	0.35242	0.3527	No
TOR82	4	0.33355	0.3448	0.38116	0.39432	0.39783	No

L/S=0.13 // Temperature -18.5 °C

	N	Min	Q1	Me-dian	Q3	Max	SD*
TB23	4	0.00341	0.01917	0.06688	0.08516	0.09111	No
TB43	4	0.09952	0.11888	0.19217	0.21978	0.22392	No
TB73	4	0.1645	0.19042	0.29153	0.33203	0.33774	No
TB93	4	0.22185	0.23877	0.31326	0.35742	0.36424	No

L/S=0.13 // Temperature 2°C

	N	Min	Q1	Me-dian	Q3	Max	SD*
TFC23	4	0.05978	0.07476	0.12714	0.13724	0.13813	No
TFC43	4	0.18665	0.20271	0.2529	0.26268	0.26527	No
TFC73	4	0.28611	0.30708	0.37268	0.3821	0.38434	No
TFC93	4	0.40184	0.40341	0.41058	0.41394	0.41423	No

L/S=0.13 // Temperature 20°C

	N	Min	Q1	Me-dian	Q3	Max	SD*
TA23	4	0.08775	0.08866	0.09657	0.1127	0.11636	No
TA43	4	0.18377	0.1896	0.21248	0.22665	0.22959	No
TA73	4	0.26794	0.27989	0.32244	0.33695	0.33955	No
TA93	4	0.34935	0.35286	0.36983	0.41094	0.4225	No

L/S=0.13 // Temperature 50°C

	N	Min	Q1	Me-dian	Q3	Max	SD*
TOW23	0.04399	0.05591	0.09771	0.1118	0.11448	0.04399	No
TOW43	0.13037	0.1491	0.20939	0.22587	0.23	0.13037	No
TOW73	0.20549	0.23084	0.30984	0.31384	0.31419	0.20549	No
TOW93	0.328	0.32938	0.33388	0.35725	0.36493	0.328	No

L/S=0.13 // Temperature 80°C

	N	Min	Q1	Median	Q3	Max	SD*
TOR23	0.02552	0.04092	0.08912	0.09329	0.09402	0.02552	No
TOR43	0.13154	0.14584	0.19317	0.20068	0.20169	0.13154	No
TOR73	0.2078	0.22627	0.28828	0.29604	0.29642	0.2078	No
TOR93	0.30134	0.30414	0.31288	0.35979	0.37531	0.30134	No

L/S=0.16// Temperature -18.5 °C

	N	Min	Q1	Me-dian	Q3	Max	SD*
TB24	4	0.04337	0.04519	0.05239	0.06058	0.06273	No
TB44	4	0.1432	0.14637	0.15969	0.16498	0.16548	No
TB74	4	0.20198	0.20495	0.22861	0.25322	0.25651	No
TB94	4	0.21933	0.22056	0.24838	0.28095	0.28375	No

L/S=0.16// Temperature 2°C

	N	Min	Q1	Me-dian	Q3	Max	SD*
TFC24	4	0.07784	0.08288	0.10807	0.13839	0.14513	No
TFC44	4	0.22408	0.2257	0.23142	0.24088	0.24375	No
TFC74	4	0.32627	0.33198	0.35378	0.36705	0.36991	No
TFC94	4	0.36685	0.37003	0.3872	0.39796	0.39901	No

L/S=0.16// Temperature 20°C

	N	Min	Q1	Me-dian	Q3	Max	SD*
TA24	4	0.04364	0.04918	0.07097	0.08128	0.08299	No
TA44	4	0.16734	0.16975	0.18942	0.20271	0.20299	No
TA74	4	0.27779	0.27974	0.29616	0.31386	0.31624	No
TA94	4	0.30218	0.30372	0.32314	0.37096	0.38197	No

L/S=0.16// Temperature 50°C

	N	Min	Q1	Me-dian	Q3	Max	SD*
TOW24	4	0.05643	0.05908	0.06916	0.07825	0.08057	No
TOW44	4	0.156	0.15934	0.17272	0.20913	0.22014	No
TOW74	4	0.24262	0.24794	0.26608	0.31132	0.32567	No
TOW94	4	0.27979	0.28114	0.30284	0.33615	0.34137	No

L/S=0.16// Temperature 80°C

	N	Min	Q1	Median	Q3	Max	SD*
TOR24	4	0	0.01605	0.06779	0.10553	0.11691	No
TOR44	4	0.13634	0.14097	0.17334	0.19696	0.19867	No
TOR74	4	0.24253	0.2466	0.27306	0.29281	0.29465	No
TOR94	4	0.25862	0.26261	0.28187	0.30275	0.30728	No